Coastal Marine Institute

Wave-Bottom Interaction and Bottom Boundary Layer Dynamics in Evaluating Sand Mining at Sabine Bank for Coastal Restoration, Southwest Louisiana

U.S. Department of the Interior

Bureau of Ocean Energy Management

Gulf of Mexico OCS Region

Cooperative Agreement

Coastal Marine Institute

Louisiana State University

Coastal Marine Institute

Wave-Bottom Interaction and Bottom Boundary Layer Dynamics in Evaluating Sand Mining at Sabine Bank for Coastal Restoration, Southwest Louisiana

Authors

Gregory W. Stone
Daijito Kobashi
Felix Jose
Baozhu Liu
Seyed Mostafa Siadatmousavi
Amy Spaziani

November 2013

DISCLAIMER

This report was prepared under cooperative agreement between the Bureau of Ocean Energy Management (BOEM) and Louisiana State University, Coastal Studies Institute. This report has been technically reviewed by BOEM, and it has been approved for publication. Approval does not necessarily signify that the contents reflect the views and policies of BOEM, nor does mention of trade names or commercial products constitute endorsement or recommendation for use.

REPORT AVAILABILITY

To download a PDF file of this Gulf of Mexico OCS Region report, go to the U.S. Department of the Interior, Bureau of Ocean Energy Management, Environmental Studies Program Information System website and search on OCS Study BOEM 2013-209.

This report can be viewed at select Federal Depository Libraries. It can also be obtained from the National Technical Information Service; the contact information is below.

> U.S. Department of Commerce
> National Technical Information Service
> 5301 Shawnee Rd.
> Springfield, Virginia 22312
> Phone: (703) 605-6000, 1(800)553-6847
> Fax: (703) 605-6900
> Website: http://www.ntis.gov/

CITATION

Stone, Gregory W., Daijiro Kobashi, Felix Jose, Baozhu Liu, Seyed Mostafa Siadatmousavi, Amy Spaziani. **2013**. Wave-bottom interaction and bottom boundary layer dynamics in evaluating sand mining at Sabine Bank for coastal restoration, Southwest Louisiana. U.S. Dept. of the Interior, Bureau of Ocean Energy Management, Gulf of Mexico OCS Region, New Orleans, LA. OCS Study BOEM 2013-209. 139 pp.

ACKNOWLEDGEMENTS

ABSTRACT

Sabine Bank, a transgressive shoal located in the Gulf of Mexico, 30 km (18.64 mi) off the Louisiana-Texas border, has been considered one of the potentially plausible sand resources for re-nourishment of the adjacent barrier islands and beaches due to the available sand volume and proximity to target restoration areas. However, little has been reported on the bottom boundary layer dynamics and sediment transport from this shallow coastal environment.

A comprehensive field investigation, coupled with numerical modeling, has been completed for Sabine Bank and is presented in this report. Three bottom boundary layer arrays were deployed on the crest, as well as on the nearshore and offshore flanks of the shoal, during spring 2004, winter 2006, and summer 2008. Time series observations of waves, currents, water level, suspended sediment concentration, temperature and salinity were measured for 30–40 days each, during these deployments. Bottom boundary layer parameters, viz., wave and current induced shear stress and shear velocity, were computed. The *in situ* observations showed that waves were low amplitude and did not re-suspend sediment during fair weather conditions. Currents were sufficiently strong to re-suspend sediment during the entire period except during fair weather conditions. Wave and bottom boundary layer interactions were strongly associated with the passage of cold fronts across the region. Strong southerly/southeasterly wind regimes also affected the wave and the bottom boundary layer interactions during the observation period. During summer 2008, bottom boundary layer dynamics were significantly influenced by the high wind regime associated with a high pressure system that prevailed over the eastern Gulf and U.S. East Coast. The high wind regime, during fair weather, forced high wave height and relatively strong currents over the bank. Frequencies of this high wind regime were approximately every two to three weeks. During the summer, except for the periods of the high wind regime, waves and currents were weak, and therefore bottom sediment re-suspension was insignificant.

The MIKE 21 Spectral wave model (SW) and MIKE 3 Hydrodynamic model were implemented for the coast. Modification in bulk wave parameters due to two mining scenarios was computed using modified bathymetries. It has been observed that alteration in the significant wave height, peak period and dominant direction were insignificant with the modified bathymetries. Sediment re-suspension intensity (RI) was high over the inner shelf and shoal during severe and strong storms. During moderate storm conditions, the RI decreases from the shallowest western shoal to the deeper eastern shoal; the RI off the shoal was significantly lower than on the shoal. The computation of wave fields generated by Hurricanes Gustav and Ike showed that the shoal acts as a submerged breakwater against hurricane generated waves and effectively protects the coast from substantial erosion. No significant modification in wave pattern was observed when it comes to the partial removal of the shoal crests. Variation in wave heights along the coast, due to partial removal of the shoal crests was remarkably insignificant, of the order of less than 2%. Among the five stations that were selected for coastal monitoring, the highest variability was observed for the eastern-most station, which, in fact, was not sheltered by the offshore bank.

CONTENTS

LIST OF FIGURES

LIST OF TABLES

LIST OF ABBREVIATIONS

mg O_2/L	milligram of Oxygen in 1 liter of sea water
ADV	Acoustic Doppler Velocimeter
PC ADP	Pulse coherent Acoustic Doppler Profiler
ADCP	Acoustic Doppler Current Profiler
Hz	unit of frequency (number of cycles per second)
Hs	Significant wave height, unit (meters)
T_p	Peak wave period, unit (second)
U_b	wave orbital velocity at the bottom
f_p	peak frequency
u_{*w}	Shear velocity at the bed due to waves
τ_w	Shear stress at the bottom due to waves
ν	Kinematic viscosity
OBS	Optical backscatter intensity, measured in NTU units
NTU	Nephelometric turbidity units
ϕ	unit of sediment size

CHAPTER 1: EXECUTIVE SUMMARY

The coastal zone spanning the Louisiana-Texas border has been exposed to extensive erosion due to a myriad of factors, including the landfall of devastating hurricanes viz., Lili in 2002, Rita in 2005, and Ike in 2008. The entire Holly Beach community in southwest Louisiana was devastated by the destruction of Hurricane Rita's landfall in September 2005. In addition, extensive coastal erosion and infrastructure damage was reported after the landfall of Hurricane Ike in September 2008. Federal and state agencies have embarked on ambitious coastal restoration projects to rebuild and re-nourish this rapidly deteriorating coast in Louisiana. Given the deltaic nature of this coast, offshore sand bodies are of considerable importance as viable sand resources to execute these multi-million dollar restoration projects. However, before initiating a large-scale extraction of sand from these transgressive offshore shoals along the northern Gulf of Mexico, the Minerals Management Service (MMS) commissioned physical and biological environmental impact studies for these shoals.

This report summarizes the studies conducted in terms of wave bottom interaction and bottom boundary layer dynamics for Sabine Bank, a transgressive sand body located approximately 30 km (18.64 mi) offshore, encompassing an area of 600 km^2 (231.66 mi$^{2)}$. This study also includes output from a suite of hydrodynamic models that were implemented to quantify the wave transformation over the shoal, as well as alteration that may occur due to targeted sand mining from the crest of the shoal. Detailed work, encompassing the physical, geological and biological aspect of the shoal, has been completed by Stone et al. (2009) and the work focuses on Ship Shoal, situated farther east.

Previous studies have indicated that Sabine Bank has an important effect on shoreward propagating waves during fair weather conditions; the bank mitigates the wave field during storms. To fully understand the wave characteristics and bottom boundary layer dynamics of the bank, three extensive field deployments were conducted during spring 2004, winter 2006, and summer 2008; the *in situ* measurements from these deployments include time series of waves, currents (horizontal and vertical), water level, suspended sediment concentration, bottom elevation change, and time series of temperature and salinity at the bottom. In addition, surface sediments were collected during the deployment and retrieval of the tripods. The computed parameters, based on *in situ* observations, were wave and current induced shear stress at the bottom, shear velocity, re-suspension intensity, and sedimentological parameters of the bottom sediments.

Based on our extensive *in situ* observations, encompassing much of the weather conditions of the coast, it is summarized that waves were generally weak and did not re-suspend sediment during fair weather conditions. Currents were sufficiently strong to re-suspend sediments during the entire observation period except during fair weather conditions. Wave and bottom boundary layer interactions were strongly associated with the passage of cold fronts across the region. Strong southerly/southeasterly wind regimes also affected wave and bottom boundary layer interactions during the observation period.

During summer 2008, bottom boundary layer dynamics were significantly influenced by the high wind regime associated with high pressure covering the eastern Gulf of Mexico and U.S. East Coast. The high wind regime during fair weather accompanied high wave height and relatively strong currents over the bank. Frequencies of this high wind regime were approximately every two to three weeks. During the summer, except for periods of the high wind regime, waves and currents were weak, and, therefore, bottom sediment re-suspension was insignificant. Turbidity data captured during the 2008 summer deployment imply that bottom boundary layer dynamics may be influenced by sediment supply from outside Sabine Bank, perhaps by fluvial sediment from the Atchafalaya River or Sabine Pass.

In summary, it is evident that while waves are not an important factor for sediment transport during fair weather conditions, waves generated during cold fronts and strong southerly/southeasterly wind regimes affect sediment transport significantly. Currents are strong enough to re-suspend sediment for the entire period, except during fair-weather. Cold fronts and strong wind regimes are important to the bottom boundary layer dynamics of Sabine Bank. In summer, the strong wind regime seems to be a dominant force for affecting the bottom boundary layer dynamics and sediment transport.

We have also implemented a suit of numerical models to quantify the modifications of wave, currents, and sediment re-suspension parameters at Sabine Bank, as associated with the proposed sand mining projects for the nourishment of beaches and barrier islands along the Louisiana coast. The MIKE 21 Spectral Wave (SW) model and MIKE 3 Hydrodynamic models were implemented to examine the wave and current regime over the shoal and its modifications due to targeted mining. The SWAN model, coupled with WAVEWATCH III, was implemented to quantify the hurricane generated wave fields along the Louisiana and Texas coast and implications due to partial removal of sand from the shoal. The MIKE 3 model could not be calibrated well and it is assumed that the inaccuracy in the bathymetry may be a plausible reason.

The wave and hydrodynamic modeling studies have allowed us to make the the following conclusions: The spectral wave model (MIKE 21 SW) performed well for the study area. Variations in bulk wave parameters, due to modified bathymetry from two mining scenarios (cumulative and Holly Beach restoration), were not significant. Sediment re-suspension intensity (RI) was high over the inner shelf and shoal during severe and strong storms. During moderate storm conditions, RI decreases from the shallowest western shoal to the deeper eastern shoal; RI off the shoal was significantly lower than on the shoal. RI with partial mining was insignificantly lower than with the shoal present.

The following conclusions were drawn from this study as they pertain to simulating the wave field associated with Hurricanes Gustav and Ike. The shoal acts as a submerged breakwater against hurricane-generated waves and effectively protects the coast from destructive wave erosion. The level of energy dissipation over the shoal depends on the height and wavelength of incident waves. It is important to note that no significant modification in wave energy transformation was observed when the shoal crests have been partially removed. The wave field, on modeling complete shoal removal, has not yet been computed. However, Kobashi et al. (2008b) completed a similar study for Ship Shoal, with scenarios of complete and partial shoal removal. In that case, the removal of the shoal profoundly altered the incident wave field and

bottom boundary layer parameters. In the case of Sabine Bank, variation in wave height along the coast, due to partial removal of the shoal crests, was remarkably insignificant, and in the order of less than 2%. Among the five stations that were selected for coastal monitoring, the highest variability was observed for the eastern-most station, which was not sheltered by Sabine Bank.

Large-scale sand mining (entire removal of the shoal) could significantly change hydrodynamics over the shoal, particularly waves and associated wave-induced sediment re-suspension. Therefore, large-scale dredging is not recommended without more detailed analyses. However, smaller-scale dredging should have minimal impacts, and those impacts are expected to be analagous to Hurricane events, from which the physical system generally shows recovery within several years. Post-Rita side scan sonar survey by Dellapenna et al. (2006) confirmed the shoal's rapid recovery from an extremely energetic event. Depth changes were a significant factor for changes in waves and wave-induced sediment re-suspension, but did not yield abrupt changes in current distribution. More details on the hydrodynamics will be discussed later in this report and are based on the MIKE 3 model implementation.

CHAPTER 2: GENERAL INTRODUCTION

2.1. INTRODUCTION

During the past half century, the Louisiana coast has experienced severe land loss (Penland et al. 2005) which is considered the highest in the nation. Each year, Louisiana's 3 million acres of wetlands are lost at the rate of approximately 75 square kilometers (29 suare miles) (USGS 1995).This loss can be attributed to various natural and anthropogenic processes. The former includes land subsidence and deltaic processes of the Mississippi River, eustatic sea-level rise, and the landfall of severe hurricanes and tropical storms. Anthropogenic components are mainly the control of river sediment discharge and interactions with engineering structures (National Research Council 2006). Artificial levees and dams prevent natural sediment supply from the rivers creating disequilibrium of the sediment budget which further exacerbates land loss problems. Dredging navigation channels across the low-lying marshes and the withdrawal of fluids (i.e., oil and gas) from the inner shelf and offshore also contribute to wetland loss along the coast (Chan and Zoback 2007).

During extreme weather conditions, viz. severe hurricanes, tropical storms, and extra-tropical storms, barrier islands and the adjoining marsh are severely damaged by the combined action of storm surge and energetic waves (Figure 2.1). Long stretches of the barrier islands were either breached or severely eroded during the landfall of Hurricanes Lili and Isidore in 2002, Ivan in 2004, Katrina and Rita in 2005, Gustav and Ike in 2008. Many of the barrier island chains have either disappeared completely or are stripped of their coarser, surface sediment layers by these hurricanes. The northern Gulf Coast is hurricane-prone, with a return rate of approximately once every 3.0 years (Keim et al. 2007). In addition, approximately 30–40 extra-tropical storms, associated with cold fronts, cross the coast each year during October–May (Roberts et al. 1989; Kobashi et al. 2005). During the post-frontal phase of these storms, the bay side of the barrier islands is undergoing erosion, and consequently affects the adjacent marsh in terms of wave-induced erosion.

The Louisiana-Texas inner shelf is characterized by the following: (1) a shallow and broad shelf, (2) a predominantly muddy seabed with transgressive sand bodies and shallow reefs (Penland et al. 1988; Roberts 1997; Kjerfve 2003), (3) high discharge of freshwater and sediments from the Mississippi, Atchafalaya, and Sabine Rivers (Roberts 1997), (4) a low-energy micro-tidal environment, (5) frequent passage of winter storms and occasional tropical storm/hurricane landfalls (Hsu 1988; Stone et al. 2004), (6) the largest surface area of wetlands in the contiguous lower 48 states, and (7) a wide variety of wildlife habitats and nationally important commercial and recreational fisheries (O'Connel et al. 2005).

2.2. CONCEPTUAL FRAMEWORK

In an effort to control the rapid retreat of the shoreline along the Louisiana-Texas Coast, federal and state agencies have helped develop ambitious projects for the restoration of the region.

Given the geological evolution of the Louisiana deltaic plain, quality sand resources are scarce for implementing these projects in a cost-effective manner. The U.S Department of the Interior's Bureau of Ocean Energy Management (BOEM, formerly the Minerals Management Service [MMS]), which administers mineral leases within U.S. federal waters and conducts environmental studies under the National Environmental Policy Act, is actively involved in pursuing potential sand resources for re-building the coasts along the Louisiana and Texas (Drucker et al. 2004).

Sand resources from buried channels, abandoned islands and offshore transgressive sand shoals have been considered for these massive restoration efforts. The former two sources may not be economically viable given the costs associated with dredging and transferring material to the targeted restoration site. However, the sand resources from the outer continental shelf (OCS) have been considered as one of the potentially plausible resources for re-nourishment of the barrier islands and beaches due to the available sand volume, proximity to target restoration areas, and sand quality (Drucker et al. 2004; Khalil et al. 2007). Among the prospective sand shoals along the northern Gulf coast, Sabine Bank (hereafter referred to by name or as "the shoal") is a large transgressive sand body located off the Louisiana-Texas border, approximately located on the 10 m isobath (Figure 2.2). The shoal has been identified as a viable borrow site for restoring the beaches along the western Louisiana and eastern Texas coast. Sabine Bank encompasses an area of 600 km^2 (231.66 mi$^{2)}$, is situated 30 km (18.6 mi) offshore, and is divided into two sections, viz. western and eastern bank, by Sabine Pass. Numerical models have demonstrated that extraction of sediment from a similar transgressive sand body located to the east (Ship Shoal), has the potential to significantly impact the local wave current processes (Stone and Xu 1996; Stone 2000; Kobashi et al. 2007a, b; Kobashi and Stone 2008a, b). Preliminary findings by Underwood et al. (1999) showed that Sabine Bank has an important effect on shoreward propagation of fair weather waves and mitigate the wave field during storms. The stretch of the coast directly sheltered by the shoal would be exposed to high-energy waves if the shoal is dredged substantially without any prior environmental impact assessment. As presented here, target areas have been identified by MMS and integrated into our computational grid. However, additional sand mining scenarios will require further investigation regarding potential hydrodynamic and environmental changes.

2.2.1. Brief Literature Review

Many studies have already been reported from the region, concerning the shoal's physical, geomorphological, sedimentological, and biological characteristics. Sedimentological studies were conducted by (Morton and Gibeaut 1995; Rodriguez et al. 1999) Dellapenna et al. (2006) conducted a preliminary side scan sonar investigation over Sabine Bank. Based on a multi-beam bathymetry survey they estimated that Sabine Bank is 35 km (21.7 mi) long and 6 km (3.7 mi) wide at the eastern end and decreases to 2 km (1.24 mi) along the western end. On the western side, the bank decreases in water depth to approximately 9 m (29.5 ft) and eastward it attains a depth of 5 m (16.4 ft). Based on the side scan sonar surveys conducted before and after the passage of Hurricane Rita, the authors concluded that Sabine Bank has a very short recovery period, as far as bottom geomorphology is concerned. The same study also identified two bottom types at the shoal. Facies A is composed of a shell hash made up of of gravel- to sand-sized fragments of shell and which appears as shell ridges. These shell ridges sit on Facies B, which is

a layer of fine to very fine siliclastic sand. The flanks of these shell ridges are covered by a thin veneer of Facies B.

Cochrane and Kelly (1986) attributed the circulation over the inner shelf of this region, where water depth is less than 50 m (164 ft), principally to the effects of wind stress. Based on extensive field experiments, they proposed that when the wind is directed alongshore and down-coast, nearshore currents also flow downcoast (i.e., from the Mississippi River mouth to Brownsville, Texas). Likewise, currents flow upcoast in response to upcoast wind, which prevails during summer (Figure 2.3). The along-shore component of surface wind is generally down-coast except during a brief period (July–August) when it reverses. BOEM (then MMS) sponsored a Louisiana-Texas Shelf Physical Oceanography Program (LATEX), the largest physical oceanography project yet undertaken for this region. As a component of this program, mean currents and wind stress over the study area and contour plots of surface salinity, on a monthly basis, were generated. The study also observed that above the 27.5°N latitude line and during non-summer months the average wind stress over the inner shelf had a downcoast component. Hence currents over the inner shelf, likewise, were directed downcoast during the non-summer months. During the summer months the opposite wind conditions prevails and hence the currents follow the same trend as wind.

Brooks et al. (2003) conducted an assessment of fish communities associated with offshore sand banks and shoals in the northwestern Gulf of Mexico. They have estimated that fish abundance was over two times greater on the east side of Sabine Pass than on the west side. However, the average fish abundance per trawl was greatest in the off-bank samples and demersal fish were low in abundance in the shoal environment. The study also demonstrated that the sandy areas of the shoal were not hypoxic at the time of the cruise, and had a mean oxygen level of 4.4 mg O_2/L recorded at the bottom. Condrey and Gelpi (2008) also reported a hypoxia refuge for Ship Shoal, to the east, based on their 2007 summer and fall cruises. However, Harper et al. (1981) and Rabalais et al. (2002) reported hypoxic areas off the Texas coast.

Coastal Planning and Engineering (CP&E) conducted a study in 2002 to estimate the borrow area impacts for a proposed mining of 12.54 million cubic meters of beach compatible sand from Sabine Bank for the restoration of Holly Beach. The study employed the Ref/Dif Model (Dalrymple and Kirby 1991) to estimate the wave transformation over the shoal and its alteration due to mining. It was estimated that, due to the proposed mining, along the coastal stretch, maximum alteration in wave height would be 0.30 m (.98 ft) along the coast. The model estimated that the wave height behind the borrow pits, which were designed on the crest of the shoal, increases while along the flanks of the pit, the wave height decreases. The study concluded that the greatest difference between existing and post-excavation wave conditions lie within 2.5 km (1.55 mi) of the borrow area wave shadow, well offshore from the adjacent beaches. The study also affirmed that dredging Sabine Bank is not expected to disrupt the long-term or short-term pattern of the beach morphology near Holly Beach, Louisiana.

2.3. OBJECTIVES

Little data exists on *in situ* observations of waves, currents, and suspended sediment concentration that have been reported regarding Sabine Bank. Available data are confined to the TABS buoys (Guinasso et al. 2001) and a NDBC buoy (42035) off Galveston. No studies were reported from Sabine Bank region concerning bottom boundary layer dynamics and associated sediment transport processes. Also, the shoal's complex response in mitigating hurricane- and tropical storm-induced waves is poorly understood. Considering the above, and within the context of sand mining, we developed the following objectives in this research:

1. Quantify regional hydrodynamic responses, including waves, currents, and bottom boundary layer parameters, to various statistically significant meteorological conditions on Sabine Bank and landward on the inner shelf,
2. Initialize numerical wave models in deep water and spatially-integrated comparisons of output to *in situ* measurements for skill assessment and fine-tuning of various parameterization schemes,
3. Compare numericallyderived hydrodynamic scenarios for respective pre- and post-dredging bathymetries/scenarios, and
4. Quantify potential impacts of sand extraction from the shoal on inner shelf and hydrodynamic processes.

This report includes six chapters, including the general introduction. Chapter 3 discusses detailed, waves, currents and other hydrodynamic parameters observed from the shoal based on three separate deployments. The chapter also elaborates on the bottom boundary layer physics and their impact on sediment transport in the shoal environment. Chapter 4 discusses the various numerical models employed in the study and their implementation over the shoal and model validation. This chapter also discusses the effects of cumulative and targeted dredging, on the hydrodynamics of the near-shoal and off-shoal environments. Chapter 5 discusses the response of Sabine Bank to the wave field generated by Hurricanes Gustav and Ike. Chapter 6 provides a summary and conclusion of the research carried out.

Figure 2.1   The Louisiana coast was ravaged by Hurricanes Gustav and Ike in September 2008.

The grey area along the coast is decaying marsh due to salt water intrusion from storm surge. Photo credit: Jeff Schmaltz, NASA, GSFC.
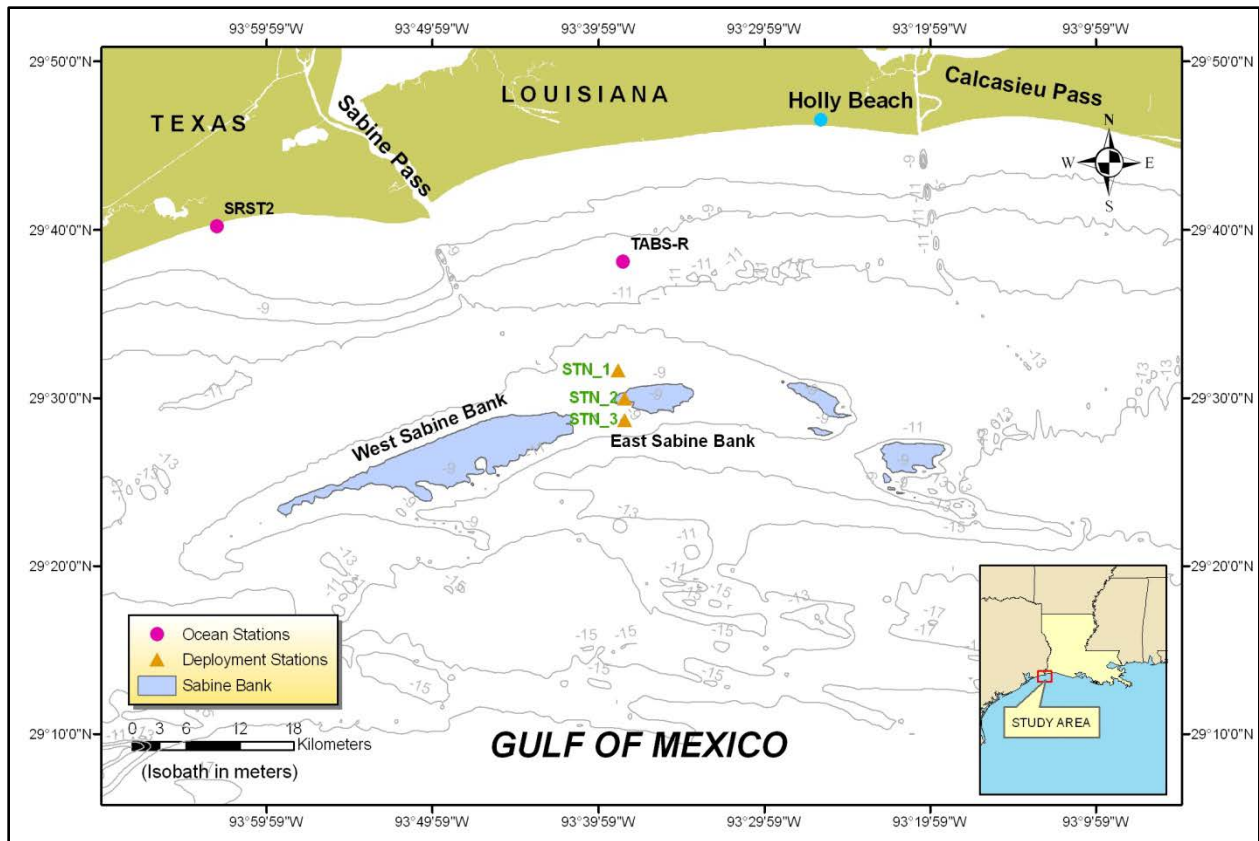
Figure 2.2   Location map. Sabine Bank and the adjoining shoals are demarcated along the 9 m isobaths.

Also shown in the figure are the three sites (stn1, stn2 and stn3) where bottom boundary layer arrays were deployed in 2004, 2006 and 2008.
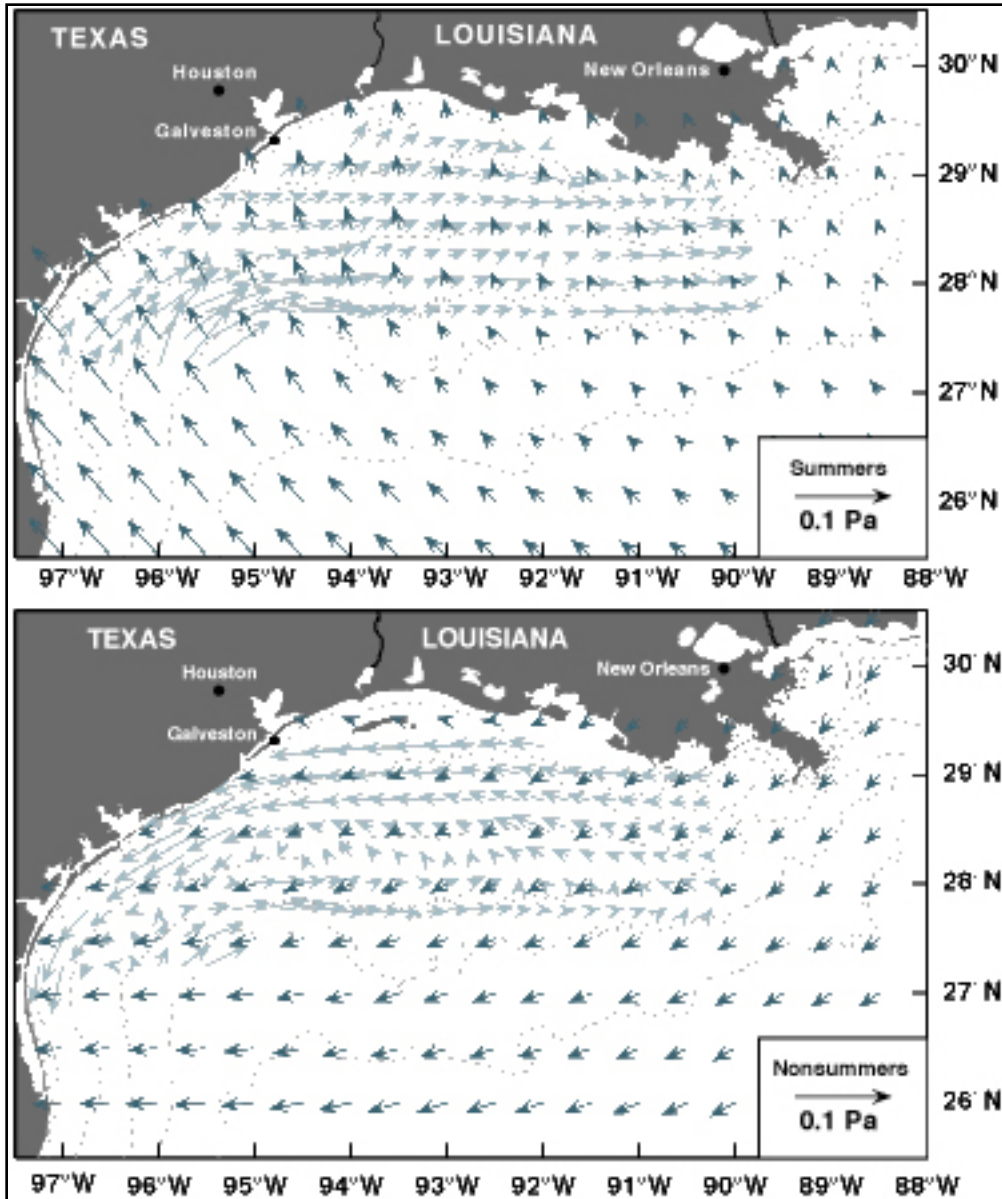
Figure 2.3   Wind direction and intensity (dark arrows) plots with shelf currents 10 m below the surface (light arrows), along the Louisiana-Texas coast.

Upcoast winds in the summer (top) generate upcoast currents, while downcoast wind in non-summer periods (bottom) cause downcoast currents. Modified from Cochrane and Kelly (1986).

CHAPTER 3: HYDRODYNAMICS AND BOTTOM BOUNDARY LAYER DYNAMICS OVER SABINE BANK

3.1. INTRODUCTION

This chapter addresses bottom boundary layer dynamics and sediment transport based on results from deployments of bottom boundary layer arrays on the eastern flank of Sabine Bank in 2004, 2006, and 2008.

3.2. METHODOLOGY

3.2.1. Survey Locations

Three stations were set up along the study site: an offshore station (29°28.666'N, 93°38.375'W), a middle station (29°29.942'N, 93°38.414'W), and an onshore station (29°31.640'N, 93°38.826'W) (Figure 3.1). The middle station is located at the crest of Sabine Bank; both offshore and onshore stations were situated along the lateral edges of the bank.

3.2.2. Instrument Arrays

Three oceanographic instrument tripods were deployed in this study, consisting of WADMAS, ADV, and PCADP systems, in 2004, 2006, and 2008.

Acoustic Doppler Velocimeter (ADV) System

The Acoustic Doppler Velocimeter (ADV) is a single-point, high resolution acoustic Doppler current meter characterized by three dimensional velocity measurements in a small sampling volume. No regular factory calibration is required for this instrument and direct calculation of turbulence such as Reynolds stress (SonTek Inc. 1996; Voulgaris and Trowbridge 1997) is possible. Such characteristics enabled us to use the ADV to investiage bottom boundary layer dynamics, which has been widely used for similar studies (see Voulgaris and Trowbridge 1997; Kim et al. 2000; Stone 2000, to name a few). The SonTek^{TM} ADV is characterized by one transmitter and three acoustic scattering receivers tilted by 30 degrees; it is capable of measuring velocity with a minimum 1.0 mm/s and up to over 5.0 m/s. Sampling frequency can be selected for as high as 25 Hz (i.e., 0.04 second interval).
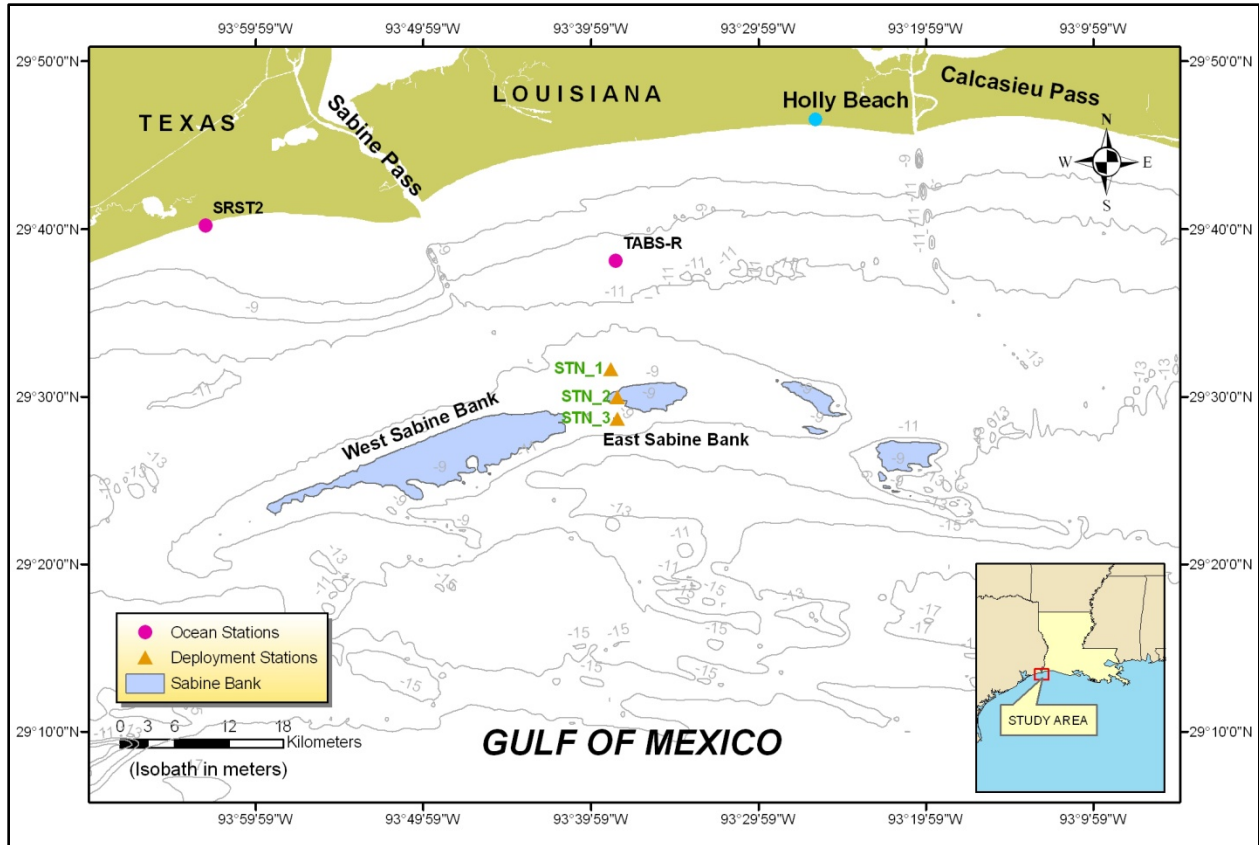
Figure 3.1   Map of Sabine Bank (shaded), off southwest Louisiana.

Station locations are indicated by green dots (isobaths in meters).

The ADV measures velocity by Doppler shift; therefore, a minimum amount of scattering materials are required in the medium, such as suspended sediments, for an optimized operation. The ADV acoustic backscatter signal amplitude (ABS) is related to suspended sediment concentration (hereafter SSC), particle type, and size so that sediment concentration can be estimated as a first order approximation with proper calibration.

Two ADV systems were used in the study: one with an ADV and a pressure sensor (hereafter referred to as ADV1 system) and the other with an ADV, a pressure sensor, and two turbidity sensors (i.e., optical backscatter sensor) (hereafter referred to as ADV2 system) (Figure 3.2). The ADVs were both deployed downward-looking with the distance between the transducer and a sampling volume set to approximately 18 cm and with the sampling frequency of 4 Hz and 10 Hz and 2048 burst data for every 30 or 60 minute burst duration (Table 3.1).
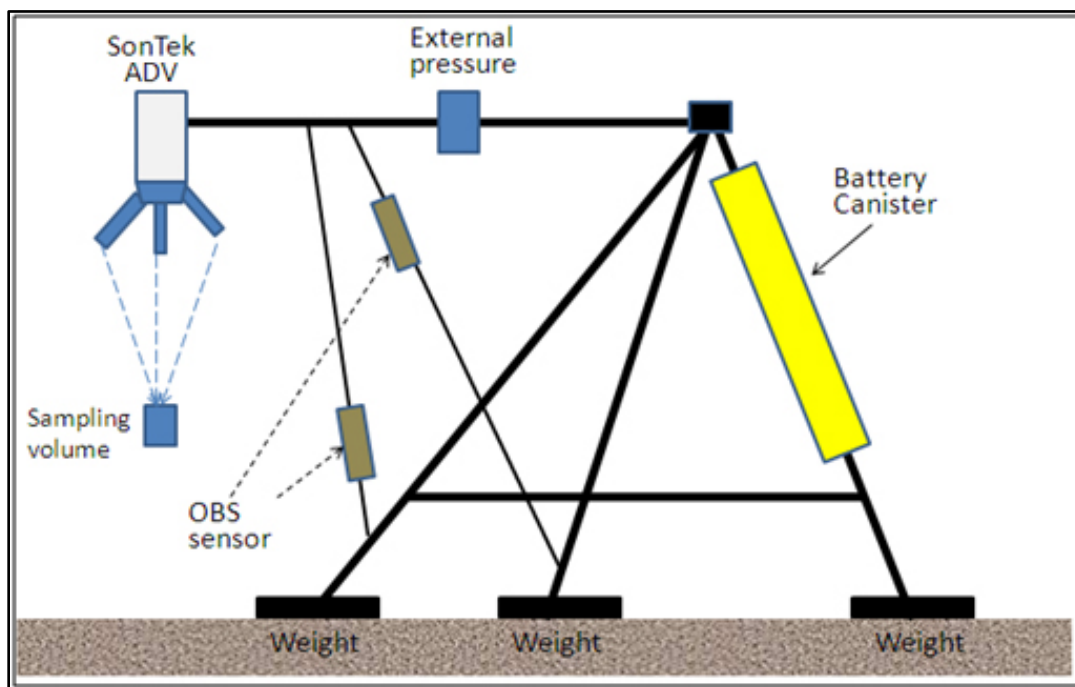
Figure 3.2   ADV tripod (upper) and its tripod design (lower).

Table 3.1

Sampling Schemes for All Deployments

System (Year)	Instrument	Burst hour	Sampling frequency (Hz)	Sampling number per burst
ADV onshore (2004)	ADV	3 hours	4 Hz	2048
	Pressure	3 hours	4 Hz	2048
	OBS	3 hours	4 Hz	2048
WADMAS (2004)	ECM	1 hour	4 Hz	2048
	OBS	1 hour	-	1
	Pressure	1 hour	4 Hz	2048
ADV offshore (2004)	ADV	3 hours	4 Hz	2048
	Pressure	3 hours	4 Hz	1024
ADV Onshore (2006)	ADV	30 min	4 Hz	2048
	Pressure	30 min	4 Hz	2048
	OBS	30 min	4 Hz	2048
ADV Offshore (2006)	ADV	30 min	4 Hz	2048
	Pressure	30 min	4 Hz	2048
PCADP (2006)	PCADP	1 hour	2 Hz	2048
	OBS	1 hour	2 Hz	2048
	Pressure	1 hour	2 Hz	2048
ADV Onshore (2008)	ADV	30 minute	10 Hz	2048
	Pressure	30 minute	10 Hz	2048
	OBS	30 minute	10 Hz	2048
ADV Crest (2008)	ADV	30 minute	4 Hz	2048
	Pressure	30 minute	4 Hz	2048
PCADP (2008)	PCADP	1 hour	2 Hz	2048
	ADCP	20 minute	2 Hz	1 (average)
	OBS	1 hour	2 Hz	2048
	CTD	1 hour	-	1

Pulse-Coherent Acoustic Doppler profiler (PCADP) System

The Pulse-Coherent Acoustic Doppler Profiler (PCADP1) is a current profiler which measures high-resolution three dimensional current profiles using a pulse coherent technique (SonTek Inc. 1997a; Lacy and Sherwood 2004; SonTek Inc. 2004) This pulse-coherent mechanism records data when the PCADP transmits two sets of coherent pulses and the change in phase between the pulse-pair is measured by the PCADP instead of determining Doppler shift of the return signals of the ADCP (Lhermitte and Serafin 1984; Lacy and Sherwood 2004; SonTek Inc. 2004). Acoustic wave length and frequency are known so that three dimensional currents can be simply computed by the following equation (SonTek Inc. 1997a).

$$U = \frac{\lambda(\varphi_2 - \varphi_1)}{4\pi T_1}$$
(2-1)

Where λ is wavelength of acoustic pulse, φ_1 and φ_2 are the phases of return signals for 1st and 2nd pulses, respectively, and T_1 is time.

This method is capable of measuring three-dimensional velocity profile resolution as fine as every 1.6 cm. However, as the pulse-coherent technique cannot resolve phase shifts larger than 2π, resulting in velocity ambiguity, there is a limitation on the velocity range. SonTek developed an algorithm to resolve this velocity ambiguity and improve the accuracy of current measurement for higher current fields (Lacy and Sherwood 2004; SonTek Inc. 2004). In spite of such a limitation, this pulse-coherent method has been widely examined (e.g., Lacy and Sherwood 2004) and has been used for several bottom boundary layer studies (e.g., Lacy and Sherwood 2004; Kobashi et al. 2007b). In addition, similar to the ADV, acoustic backscatter signal amplitude, a parameter associated with flow measurement, can be used to monitor suspended sediment concentration (SSC) (SonTek Inc. 1997b).

The PCADP1 instrumentation measures water level, directional wave parameters (coupled with an external pressure sensor), seabed elevation, and the current profile within the bottom boundary layer (Figure 3.3). The PCADP was deployed downward-looking with an external pressure sensor, two optical backscatter sensors (OBS), and two sediment traps at the bottom and the top. For the 2008 deployment, two CTD (Conductivity, Temperature, Depth) sensors at the bottom and the top layers and upward-looking ADCP were also mounted. Cell size of each bin was selected as 5 cm (1.97 in) for the 2006 deployment and 3.0 cm (1.18 in) for the 2008 deployments, respectively.

3.2.3. Deployment Protocols

Field deployments were undertaken during winter (to capture the passage of cold fronts), spring, and early summer. Since similar surveys were also conducted in 1998 and 2000 on the western flank of the shoal, the deployment locations were focused on the east and middle of the shoal (Figure 3.1). In 2005, 2006, and 2008, the bottom boundary layer arrays were deployed on the eastern and middle shoal (Figure 3.1) using the R/V Tiger-1 and R/V Coastal Profiler both owned by the Coastal Studies Institute, Louisiana State University (Figure 3.4). The instrument arrays were tethered to oil platforms (Figure 3.5) for secure installation and for easy recovery (Figure 3.6). When weather permitted, sediment samples were taken during the deployment and retrieval cruises.
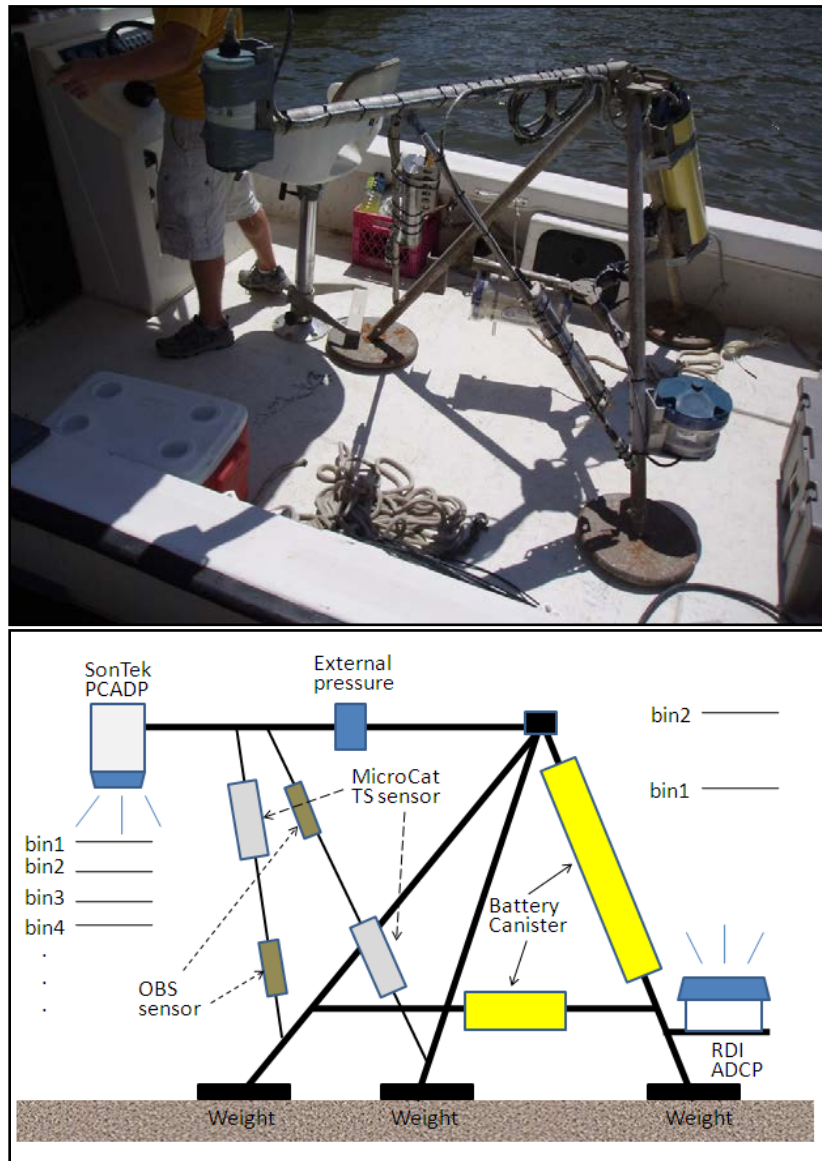
Figure 3.3   PCADP (upper) and its tripod configuration (lower).

Figure 3.4   R/V *Coastal Profiler* (upper) and R/V *Tiger* 1 (lower).

Figure 3.5   Sabine Bank crest platform.
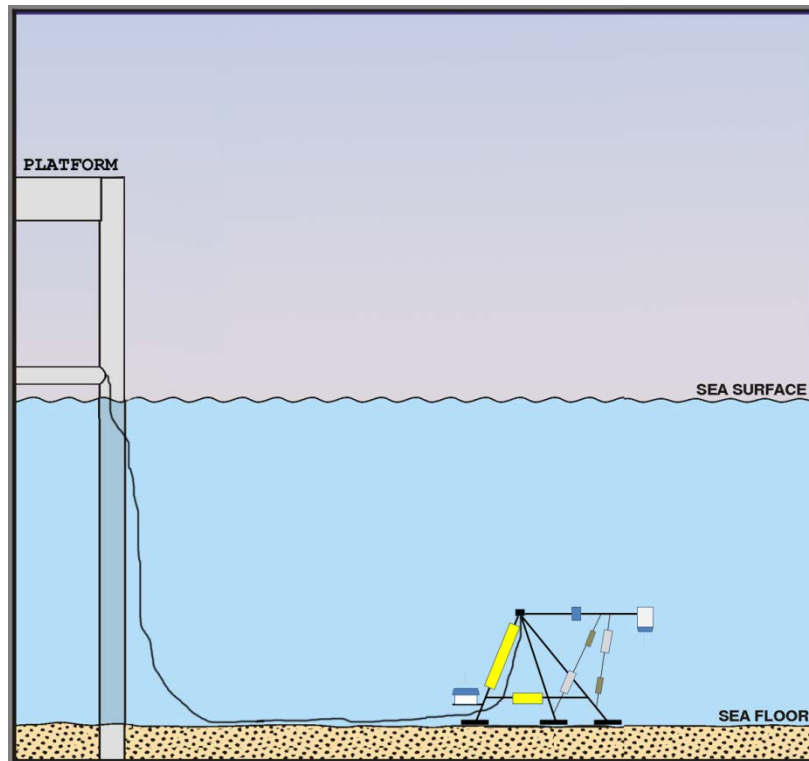
Figure 3.6   Schematic illustration of instrument deployment.

All of the systems measured discontinuous data to maximize survey duration. Data were recorded in bursts of 2048 data with a burst interval of 30 minutes or 1 hour, and sampling frequencies of 2 Hz, 4 Hz, or 10 Hz, depending on instrument configurations, as recorded in Table 3.1.

On December 7, 2006, ADV1, ADV2, and PCADP1 were deployed on the north and south banks (SB06_1 and SB06_3), and on the crest of the bank (SB06_2), individually over a period of 44 days (Table 3.2). Bottom sediments were also collected from all stations during both pre- and post-deployment trips by a diver and a ponar grab sampler (Figure 3.7). Data from all instruments except one pressure sensor at SB06_1 were successfully recovered. The PCADP system and onshore ADV did not work because of a mechanical malfunction (Charlie Sibley, personal communication, 2007).

In 2008, three bottom boundary layer arrays were deployed along a transect across the middle of the shoal on May 29, for a period of 48 days (Figure 3.1; Table 3.3); The ADV1 tripod was deployed on the north bank of the shoal (SB08_1). The ADV2 and PCADP systems were deployed on the crest of the shoal (SB08_2) (Figure 3.1). Bottom sediments were successfully sampled for all stations during both pre- and post-deployments. Data from all instruments were successfully recovered. For unknown reasons, the PCADP raw data could not be recovered; however, all hourly-processed data were successfully recovered (Sibley, C., personal communication 2008).

Table 3.2

System Description for Sabine Bank 2004 Deployment (3/11/04-4/23/04)

System	Instruments	Locations	Sensor height(cm)
ADV (Onshore)	Druck[TM] Pressure Sensor	29° 31.640'N	63.6
	SonTek[TM] Acoustic Doppler Velocimeter	93° 38.826'W	40.6
WADMAS (Crest)	MarshMcBirney Electromagnetic current meter	29° 29.942'N 93° 38.414'W	29.3, 66.1, 105.5
	McVan[TM] Optical Backscatter		30.0, 61.5, 103.8
	ParoScientific[TM] Pressure Sensor		132.8
ADV (Offshore)	SeaGauge[TM] Pressure Sensor	29° 28.666'N	73.0
	SonTek[TM] Acoustic Doppler Velocimeter	93° 38.375'W	43.1

Table 3.3

Instrument Design for Sabine Bank 2006 Deployment (12/7/06-1/20/07)

System	Instruments	Locations	Sensor height (cm)
ADV (Onshore)	Druck[TM] Pressure Sensor	29º 31.620'N	46
	D&A[TM] Optical Backscatter	93 º 38.814'W	25, 50
	SonTek[TM] Acoustic Doppler Velocimeter		
PCADP (Crest)	SonTek[TM] Pulse-Coherent Doppler Profiler	29 º 29.926'N	115
	D&A[TM] Optical Backscatter	93 º 23.840'W	25, 50
	Druck[TM] Pressure Sensor		
	RDI Workhorse ADCP 1200kHz		
	Microcat CTD sensor		
ADV (Crest)	ParoScientific[TM] Pressure Sensor	29 º 28.693'N	70.5
	SonTek[TM] Acoustic Doppler Velocimeter	93 º 38.293'W	47

Table 3.4

Instrument Design for Sabine Bank 2008 Deployment (5/29/08-7/8/08)

System	Instruments	Locations	Sensor height (cm)
PCADP (Crest)	SonTek^{TM} Pulse-Coherent Doppler Profiler D&A^{TM} Optical Backscatter Druck^{TM} Pressure Sensor RDI Workhorse ADCP 1200kHz Microcat CTD sensor	29 º 29.9926'N 93 º 38.40'W	112 25, 50 112 64 38, 97
ADV (Onshore)	Druck^{TM} Pressure Sensor D&A^{TM} Optical Backscatter SonTek^{TM} Acoustic Doppler Velocimeter	29 º 31.620'N 93 º 38.814'W	50 25, 50 50
ADV (Offshore)	ParoScientific^{TM} Pressure Sensor SonTek^{TM} Acoustic Doppler Velocimeter	29 º 28.693'N 93 º 38.293'W	70 50

Bottom sediments were successfully sampled during pre- and post-deployments indicating sandy sediments for both pre- and post-deployments (Table 3.1).

3.2.4. Sediment Sampling

In order to examine the shoal bed characteristics, bottom sediments were collected by both a diver and a ponar grab sampler (see Figure 3.7) during the 2008 deployment only, due to rough weather. The sampled sediments were then properly labeled and kept in the refrigerator for further sediment analysis. The ponar grab allowed capturing unconsolidated mud as well as sand from the surface bottom, which is often blown away and therefore not able to be sampled by box cores (Winans, personal communication 2007).

Sampled sediments were analyzed for grain size by means of granulometry and SediGraph.

Figure 3.7   Ponar grab.

3.2.5. Data Analysis

Meteorological Data

Meteorological data (wind speed, wind direction, barometric pressure, and air temperature) were obtained from the National Data Buoy center (NDBC) (NOAA 2004). Station SRST2 (29°40'12''N, 94°03'00''W) is the nearest station to the bank and was used in this study (Figure 3.1). In addition, weather charts were obtained from the National Visual data system to check the synoptic weather patterns of the Gulf region during the survey period (NOAA/NCDC).

Wave Characteristics

Wave characteristics of significant wave height, peak direction, and peak period were calculated from the velocity and pressure data using spectral analysis the following equations (Green 1992; Earle 1996; Stone 2000), where wave number (k) and wave length (L) were calculated from the dispersion relation (Hunt 1979; Dean and Dalrymple 2000):

$$H_S = 4.0\sqrt{m_0} \qquad \text{.................. (1)}$$

$$T_P = \frac{1}{f_P} \qquad \text{.................. (2)}$$

$$u_b = \frac{\pi H}{T \sinh \dfrac{2\pi h}{L}} \qquad \text{.................. (3)}$$

22

$$d_0 = \frac{H}{\sinh\dfrac{2\pi h}{L}}$$ ….……………….. (4)

where H_s is significant wave height, f_P is peak frequency, H is wave height, m_0 is zero moment of non-directional spectrum, T is wave period, h is depth, ν is molecular viscosity, u_b is orbital velocity, and d_0 is orbital diameter.

Bottom Boundary Parameters

Bottom boundary layer parameters (shear velocity and shear stress) were calculated using the following methods:

(I) Log-Linear method

The Log-Linear method was used to calculate the shear velocity and shear stress due to currents. However, in order to use this method two conditions must generally be satisfied: (1) the correlation coefficient (r^2) has to be equal to or higher than 0.994 (Drake and Cacchione 1992; Stone 2000) and (2) variation in average directions between velocity in meters must be less than 20 degrees (Stone 2000). On the other hand, Wright et al. (1997) calculated the shear velocity and shear stress using the log-linear method with $r^2 \geqq 0.98$ for the Louisiana inner shelf. In our case, almost all of the data did not satisfy either condition. Therefore, although we estimated the shear velocity and shear stress using the log-linear profile, the values are not reliable. We omitted the values where r^2 is less than 0.98 (Wright et al. 1997).

(II) Quadratic stress law using mean velocity 100 cm above the bottom

Shear velocity and shear stress was estimated using the mean velocity 100 cm above the bottom from the following equation (Sternberg 1972; Komar 1976).

$$U_* = 5.47*10^{-2}*\bar{u}_{100}$$

$$\tau = C_{100}*\rho_f*(\bar{u}_{100})^2$$ ….…… (5)

where U_* is shear velocity, C_{100} is a constant value (=0.003), ρ_f is a fluid density (=1025 kg/m^3), and $\bar{u}_{100}$ is mean velocity 100 cm above the bottom.

(III) Shear velocity and shear stress from Reynolds stress

Shear velocity and shear stress are calculated using Reynolds stress (Green 1992; Pepper 2000; Stone 2000).

$$u_{*_c} = -\rho\sqrt{\overline{u'*v'}}$$ ….…………… (6)

$$\tau_c = \rho*(u_{*_c})^2$$

where u_{*c} is shear velocity and τ_C is shear stress.

23

(IV) Linear Wave Theory (Madsen 1976)

Shear velocity and shear stress due to waves were calculated from spectral analysis using pressure data and Eqs.(3), (4), (7) and (8) (Madsen 1976).

$$\tau_W = \rho u_{ob} \left(v \frac{2\pi}{T} \right)^{1/2}$$ ……………… (7)

$$u_{*w} = \left(\frac{\tau_w}{\rho} \right)^{1/2}$$ ……………….. (8)

where u_{ob} is near bottom wave orbital velocity, u_{*w} is shear velocity due to waves and τ_W is shear stress due to waves.

Sediment transport modeling (Grant and Madsen model)

We have also implemented a bottom boundary layer/sediment transport model (Grant and Madsen 1986) using observed conditions as input to get a qualitative estimation of the sediment transport characteristics of the bank.

3.3. RESULTS

3.3.1. 2004 Deployment

Meteorology

Figure 3.8 shows the time series plots of wind speed, wind direction, barometric pressure, and air temperature collected from the nearby NDBC station. Winds were usually from south-east, except during the cold front passages. Maximum wind speed during the survey was 11.5 m/s on April 21 and at least 10 cold fronts passed over the area during the survey period, according to a criterion set up based on the prevailing wind direction, wind speed, and air temperature data.
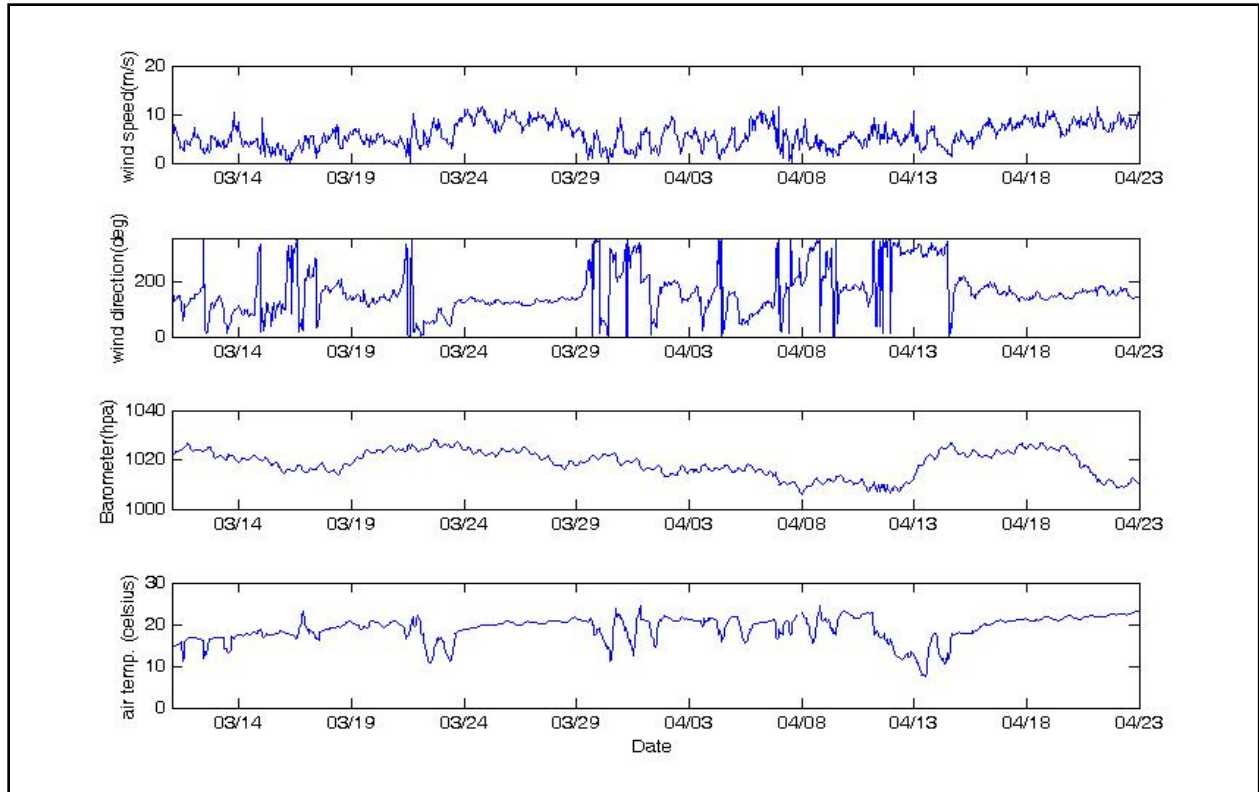
Figure 3.8   Time series plots of meteorological data.

Current Velocity

ECM (Electromagnetic Current Meter) Figure 3.9 shows time series plots of a stick diagram of current velocity and significant wave height. Unrealistically high frequency spikes were cut off from the final outputs. Velocity at the upper layer shows diurnal variations due to tide. Conversely, velocities at the middle and bottom layers always were directed north. Mean velocity was 7.0 cm/s. Northward dominant peak velocity appeared mostly during the cold fronts and high wind regime.
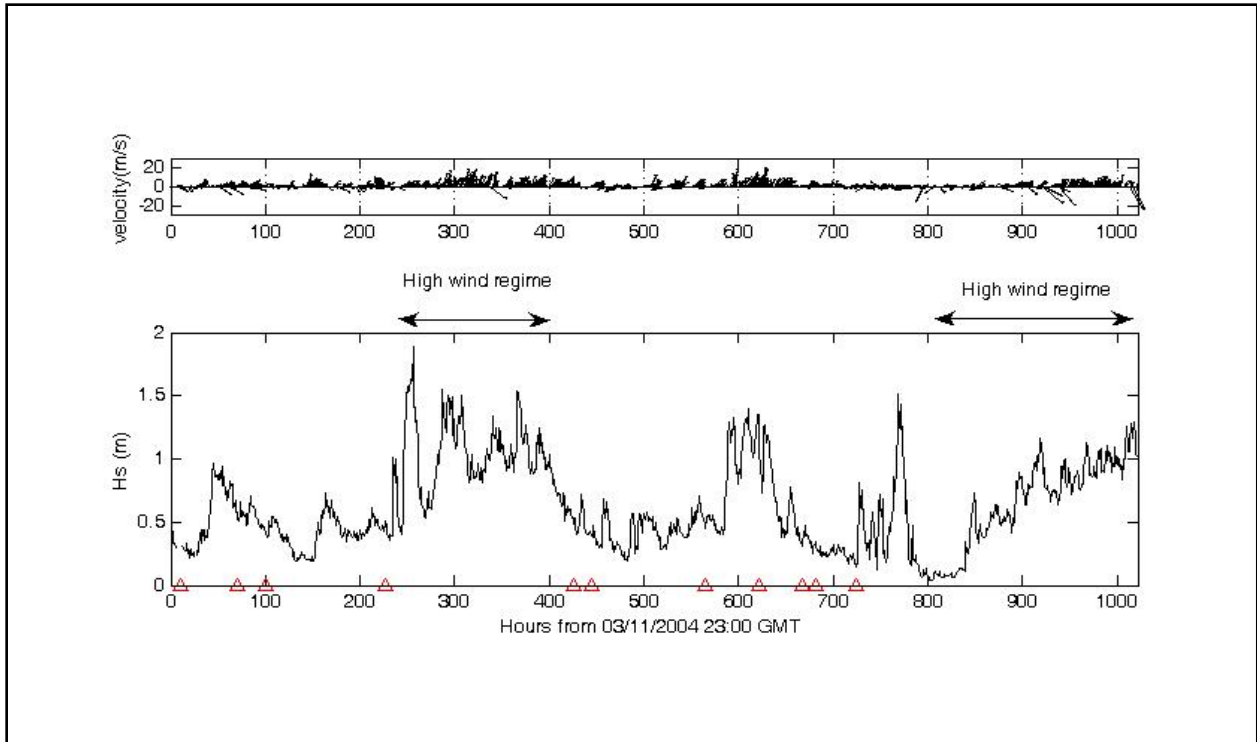
Figure 3.9   Time series stick plots of current velocity and significant wave height at the middle station.

Red triangles indicate the passage of cold fronts.

ADV (Acoustic Doppler Velocimeter)

Figure 3.10 shows the time series stick plot of current velocity and significant wave height. Velocity profile is controlled by the diurnal variations due to tides. Dominant southward velocity did appear during cold fronts and high winds. Mean and maximum velocities were 24.6 cm/s and 6.3 cm/s, respectively.
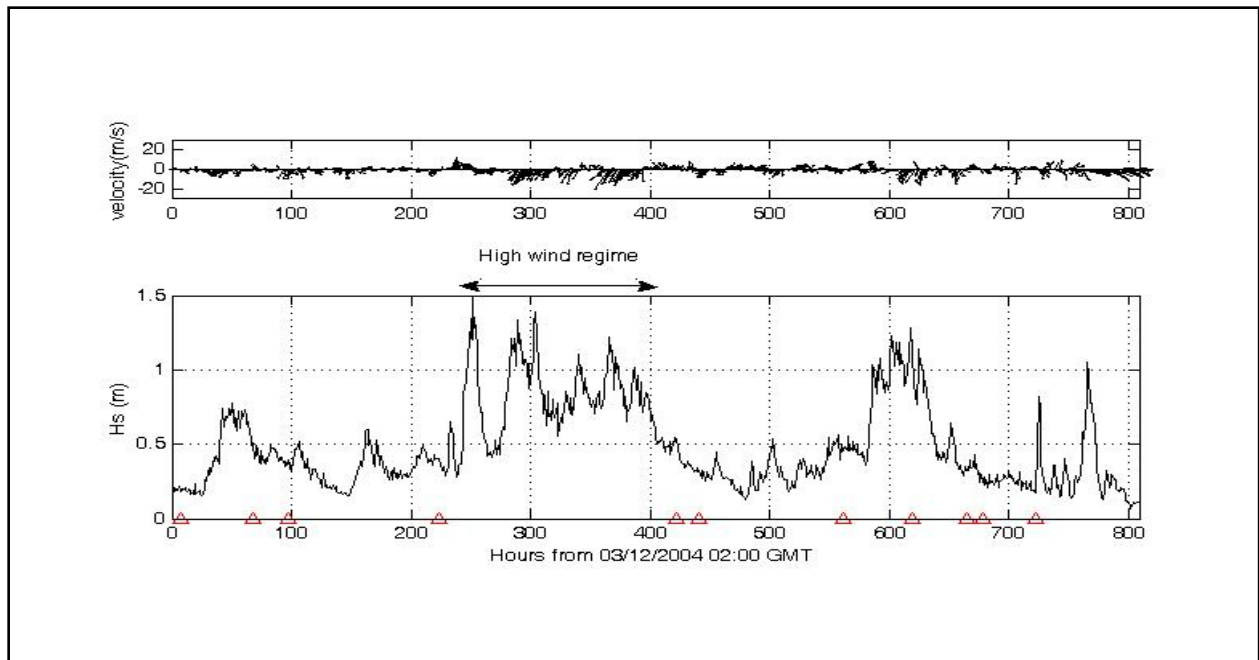
Figure 3.10   Time series plots of stick diagram of velocity and significant wave height at the onshore station.

Red triangles indicate the passage of the cold fronts.

Optical Backscatter (OBS)

Figure 3.11 shows the time series plots of OBS data from the crest of the bank. All three sensors recorded what may be unrealistically high values during the second half of the observation period. It is possible that algae or other marine disturbances may have blocked the sensors and hence caused these erroneous recordings. Therefore we omitted this portion of the data.

A few peaks were recorded on March 12 and March 14, which corresponds to a cold front passage, and on March 24 and March 28, which corresponds to a high wind regime. OBS data between March 24 and March 28 recorded the maximum peak during the entire period. Due to a lack of water samples, the OBS sensors were not calibrated and the SSC were not computed from the OBS data. However, it is inferred from the data that during the cold fronts and high wind regimes the SSC in the water column is higher than during fair weather conditions.
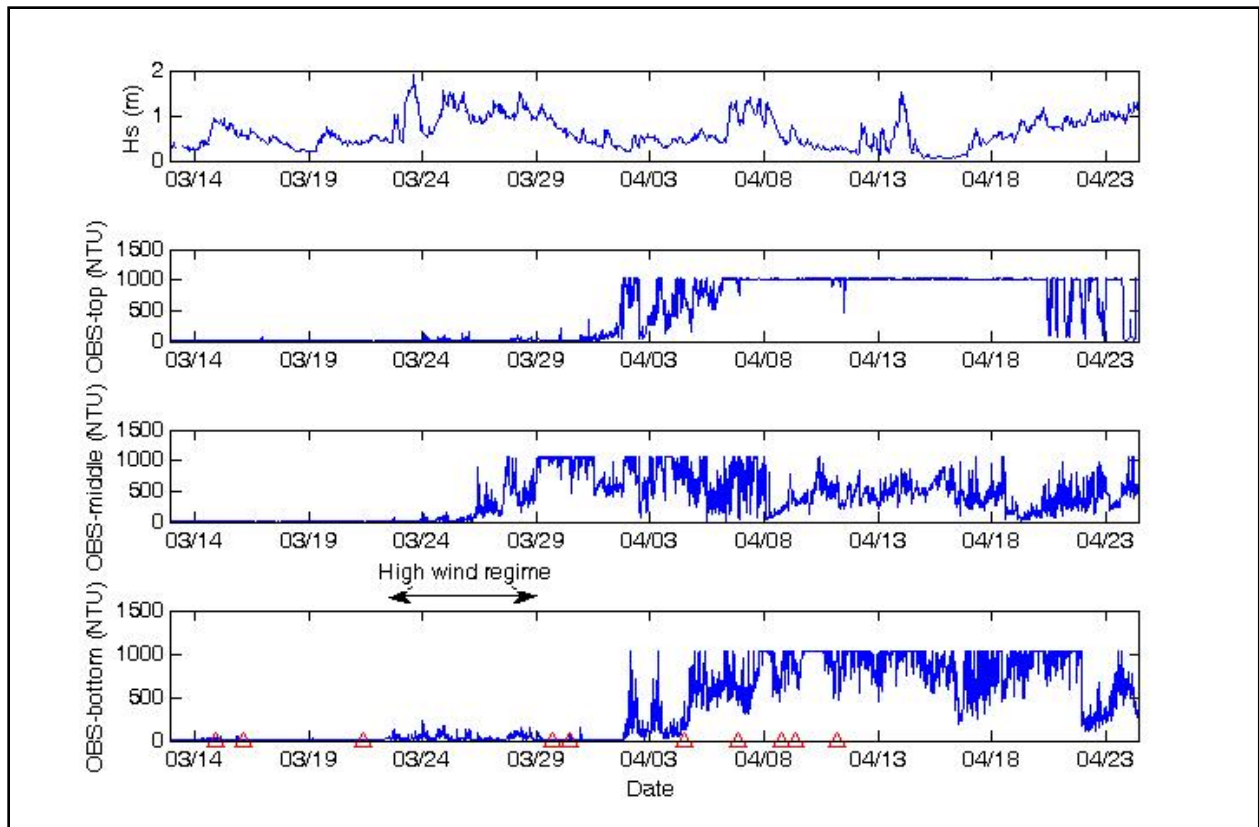
Figure 3.11   Time series plots of OBS and significant wave height at the middle station.

Red triangles indicate the passage of cold fronts.

Wave Characteristics

Wave characteristics at all three stations are similar. Figure 3.12 shows time series plots of wave parameters at the onshore station. Significant wave heights ranging from nearly nil to 2.0 m (6.56 ft) correspond to either a cold front passage or high wind conditions. Mean peak wave period was obtained as averaged 5.2s. Waves generally propagated from the southeast (150 deg). Significant wave heights correlate well with the meteorological data from the nearby station (Figure 3.8).

Figure 3.13 shows the wave spectrum based on pressure and velocity. Peak wave spectra due to both waves and currents were strongly associated with significant wave heights. High frequency waves were detected during the high wave heights that corresponded to the cold fronts and the high wind regime.
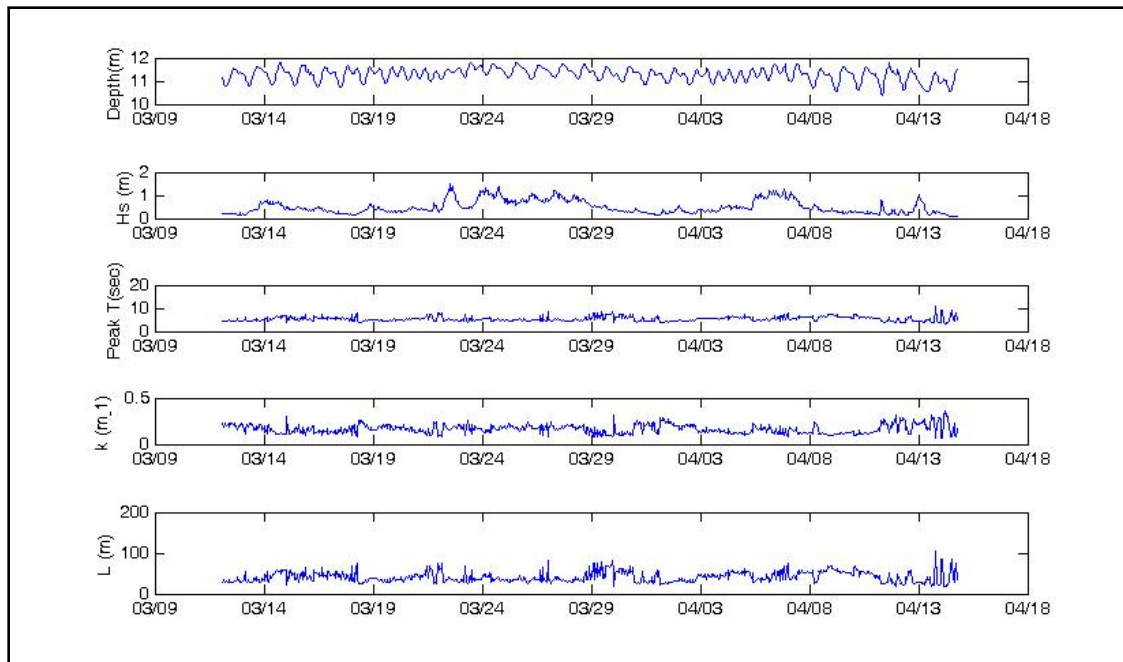
Figure 3.12   Time series plots of wave parameters at the onshore station.
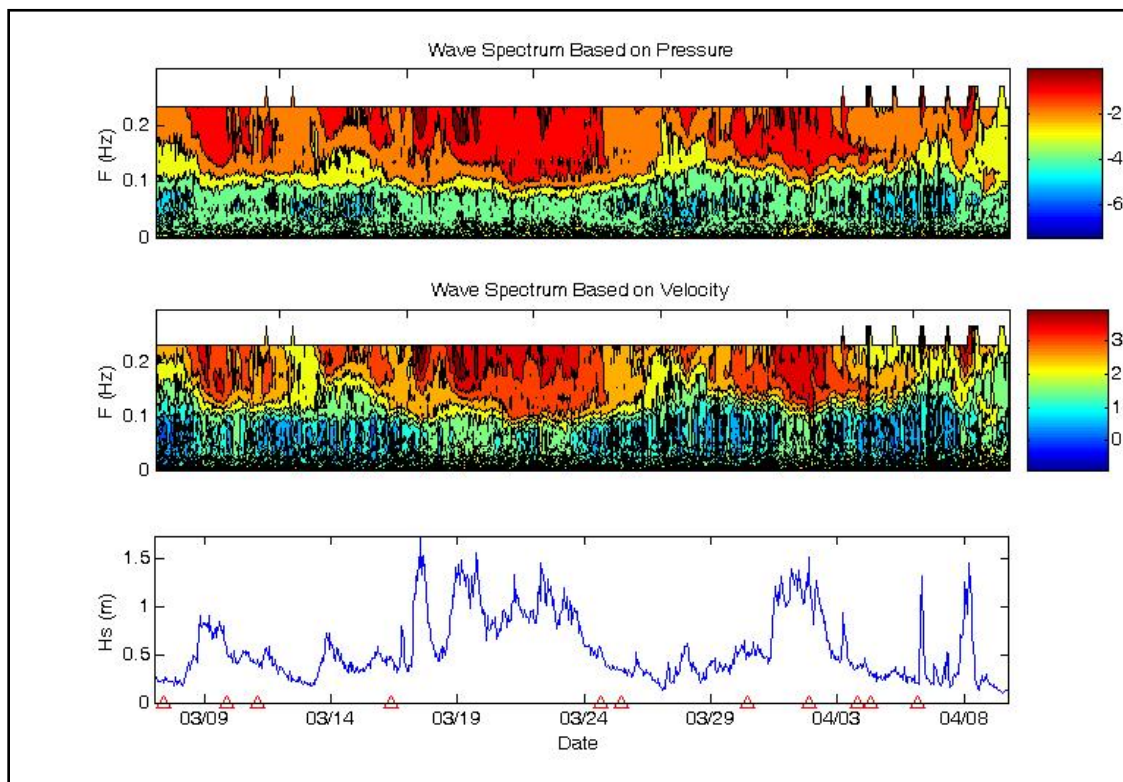
Figure 3.13   Time series plots of wave spectra on velocity, pressure and significant wave
               height.

Red-outlined triangles indicate the passage of the cold fronts.

Bottom Boundary Layer Parameters

Figure 3.14 shows the shear velocity and shear stress values computed using the log-linear method, from data containing the correlation coefficient (r^2) $\geqq$ 0.98. For r^2 $\geqq$ 0.98, the peaks of both parameters correspond to the wind directions and high wind period. The maximum shear velocity and shear stress due to currents was 3.5 cm/s (mean value = 1.9 cm/s) and 1.2 N/m^2 (mean value = 0.39 N/m^2) at the top of the bank.
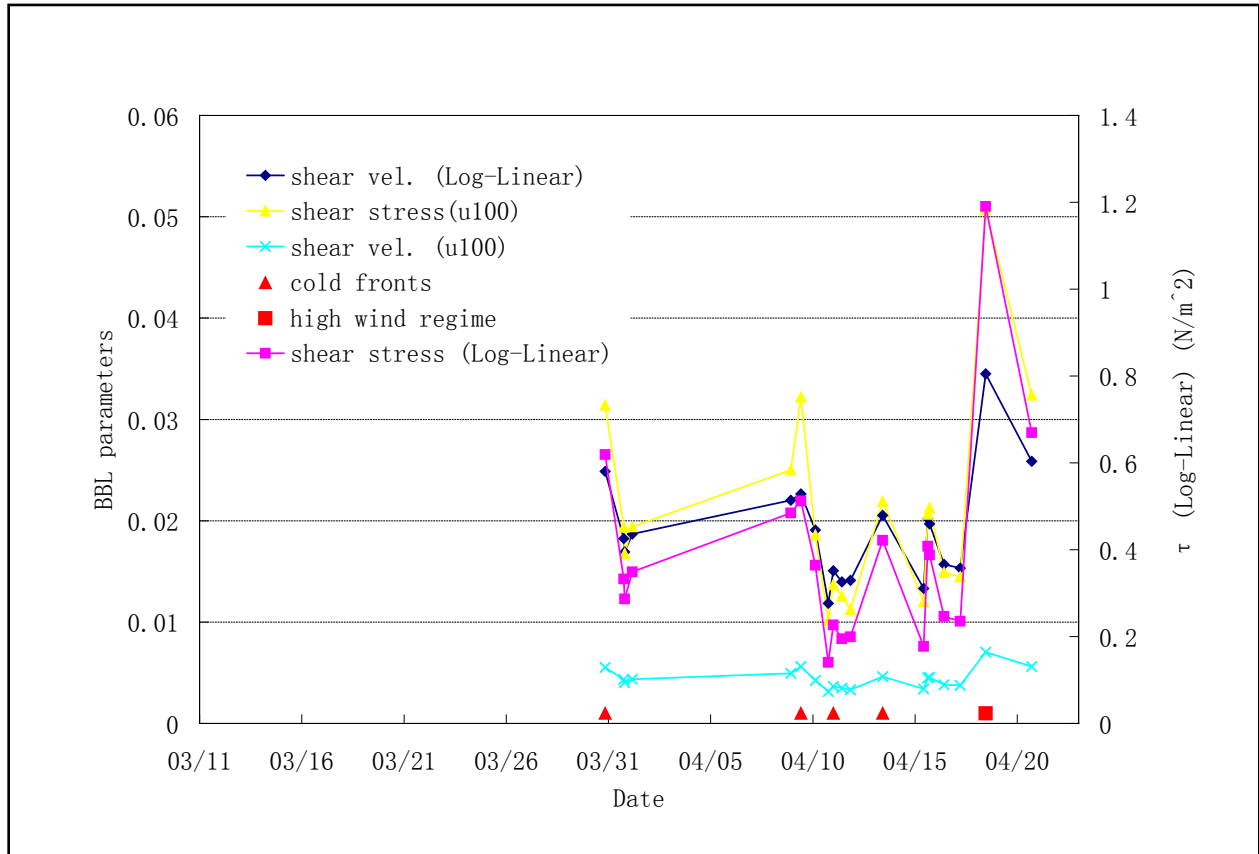
Figure 3.14   Time series plot of bottom boundary layer parameters over $r^2 \geqq 0.98$.

▲ indicates cold fronts passing and ■ indicates strong wind regime.

In Figure 3.15 the shear velocity and shear stresses are shown using the mean velocity 100 cm (39 in) above the bottom. No relationship was observed between the parameters and the meteorological data. Maximum shear velocity and shear stress due to currents were 5.5 cm/s (mean value = 1.3 cm/s) and 3.1 N/m^2 (mean value = 0.28 N/m^2), respectively.

30
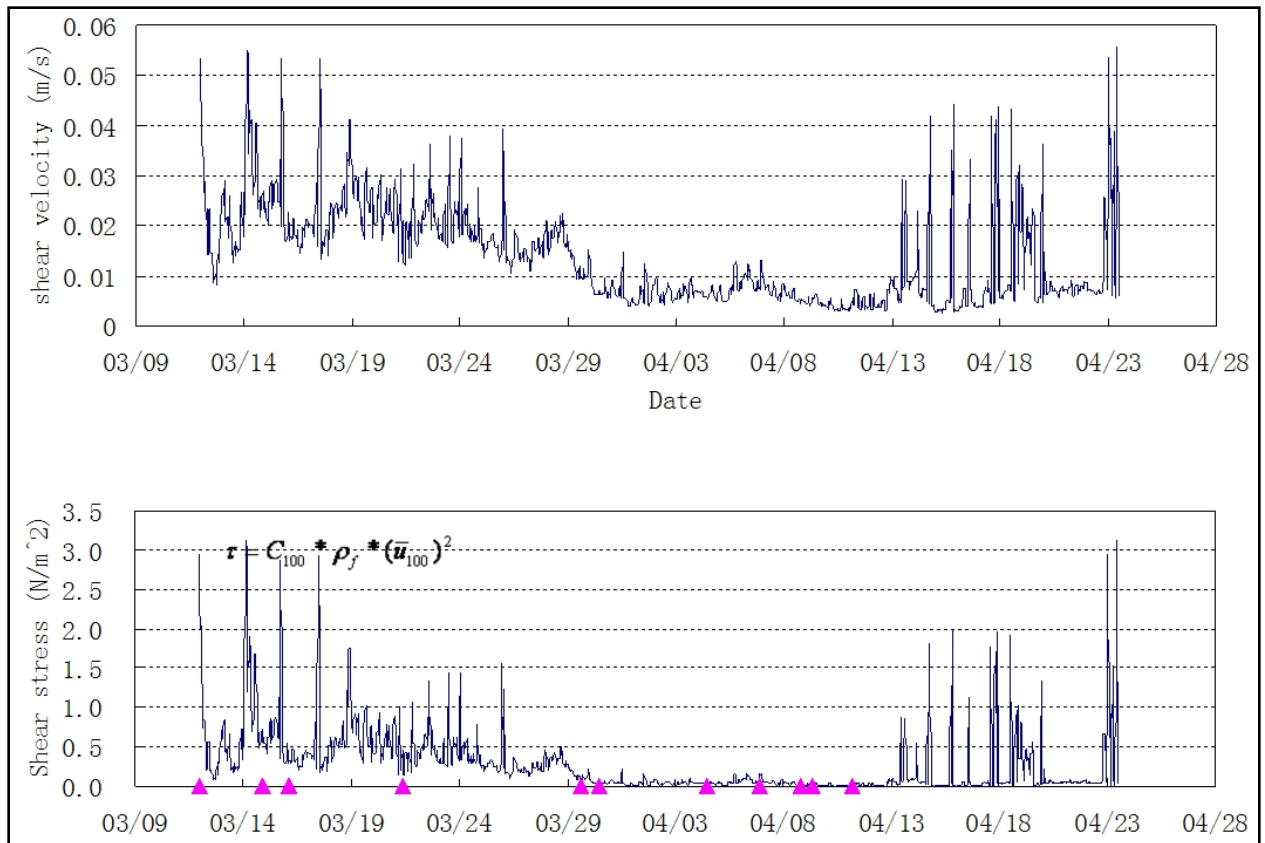
Figure 3.15   Time series plots of shear velocity and shear stress using mean velocity 100 cm above the bottom.

Magenta triangles indicate the passage of cold fronts.

Figure 3.16 shows the shear velocity and shear stress computed using the Reynolds stress method. The results indicate that many of the peaks correspond to the variation in wind direction and wind speed. The maximum shear velocity and shear stress were 7.0 cm/s (mean value = 1.2 cm/s) and 5.0 N/m^2 (mean value = 0.18 N/m^2), respectively.
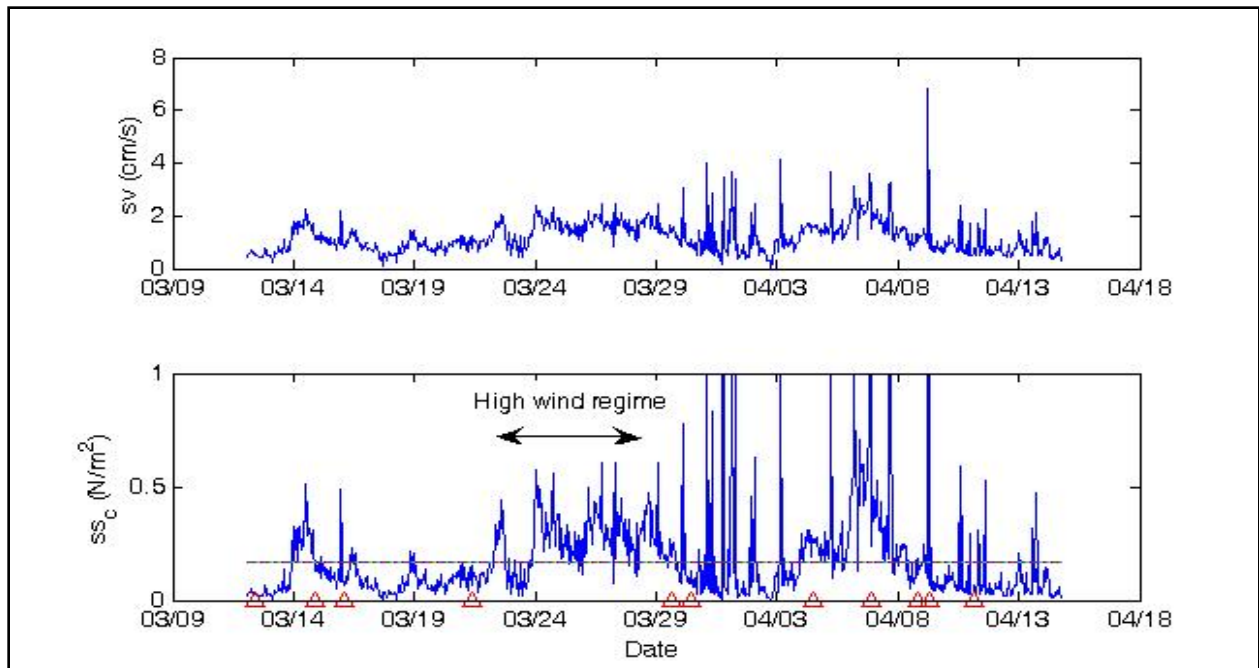
Figure 3.16   Shear velocity and shear stress using Reynolds stress.

Red triangles indicate the passage of cold fronts. The dashed line indicates the threshold stress for sediment re-suspension.

Figure 3.17 shows the shear velocity and shear stress due to waves computed from pressure gage data at the onshore station. The results indicate that many of the spikes of shear stress correspond to the wind direction and high wind speeds. Maximum shear velocity and shear stress due to waves were 2.0 cm/s (mean value = 1.1 cm/s) and 0.45 N/m^2 (mean value = 0.12 N/m^2), respectively, at the offshore station. Similar results were obtained from the other two stations.
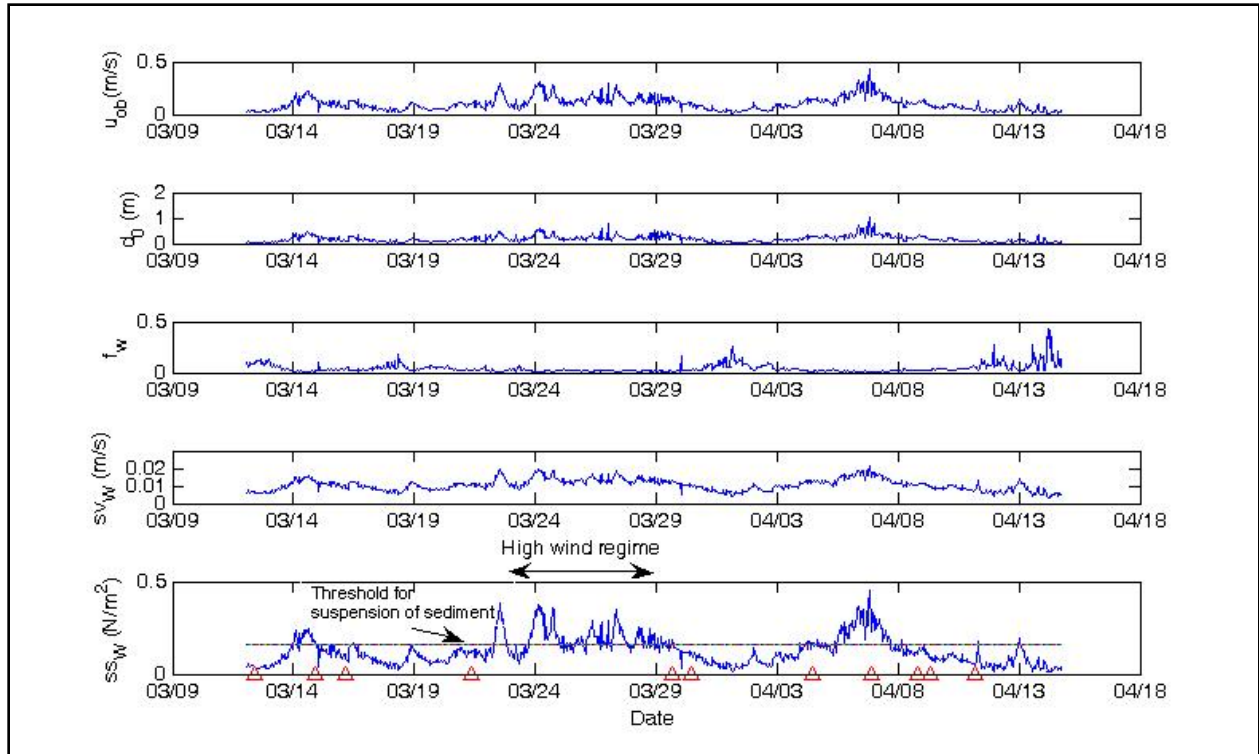
Figure 3.17   Time series plots of boundary layer parameters due to waves at the onshore station. Red triangles indicate the passage of cold fronts.

Sediment Transport Computation

The results from the sediment transport computations are given in Figure 3.18. The sediment transport rates were computed for the middle station. It is observed from Figure 3.18A & B that sediment re-suspension and transport processes are closely associated with the passage of cold fronts. Sand transport becomes conspicuous when the bottom bed forms are taken into consideration. Because the mean currents are towards offshore during the cold front events the net sediment transport also is directed towards offshore, which is well corroborated with the findings of Pepper and Stone (2002, 2004). Sediment transport occurs as discrete events with the highest value computed at 0.4423 $g.cm^{-1}s^{-1}$, when the bed form is also taken into consideration. The maximum transport computed for flat bed conditions is $1.38*10^{-4}$ $g.cm^{-1}s^{-1}$.

The combined wave and current bottom shear velocity is computed and presented in Figure 3.18C. The maximum value computed for the combined shear velocity is 4.29 cm/s and the minimum is 0.297 cm/s. The maximum wave orbital velocity is computed and presented in Figure 3.18D. The highest value obtained for this parameter is 39.1 cm/s and the minimum is 0.63 cm/s.

33
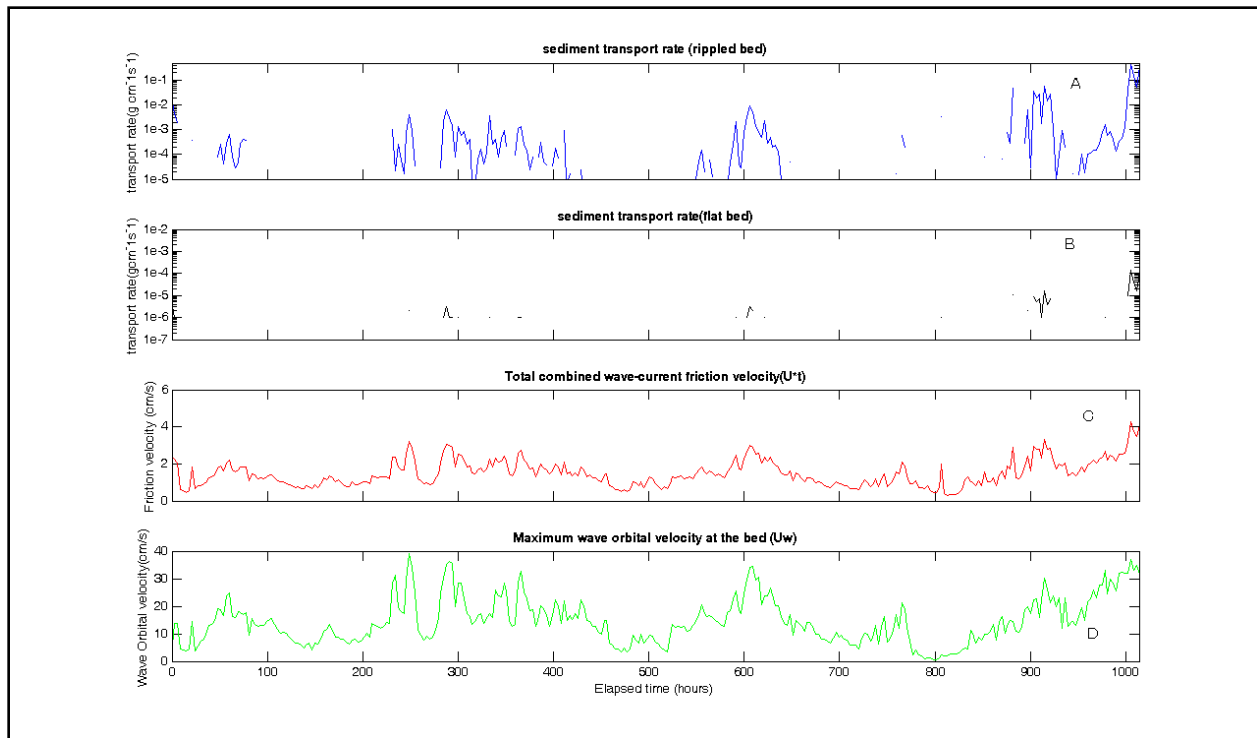
Figure 3.18   Results from the sediment transport computations.

Transport rate computed A) assuming a rippled bottom; B) for the flat bed; C) combined wave-current frictional velocity at the bottom; D) maximum wave orbital velocity at the bed.

3.3.2. 2006 Deployment

Meteorological Characteristics

In Figure 3.19, we present times series of meteorological data at NOAA SRST2 located along the west side of Sabine Pass 29.670°N 94.050°W (29°40'12"N 94°3'0"W). During the deployment, a total of six cold fronts passed over the study area. During fair weather, wind speeds were less than 10 m/s. Similar to 2004 deployments, high wind speeds, sudden wind shifts, and abrupt changes in air temperature and barometric pressure were evident during the passage of fronts. Maximal wind speed reached 15 m/s on December 31, 2006.

34
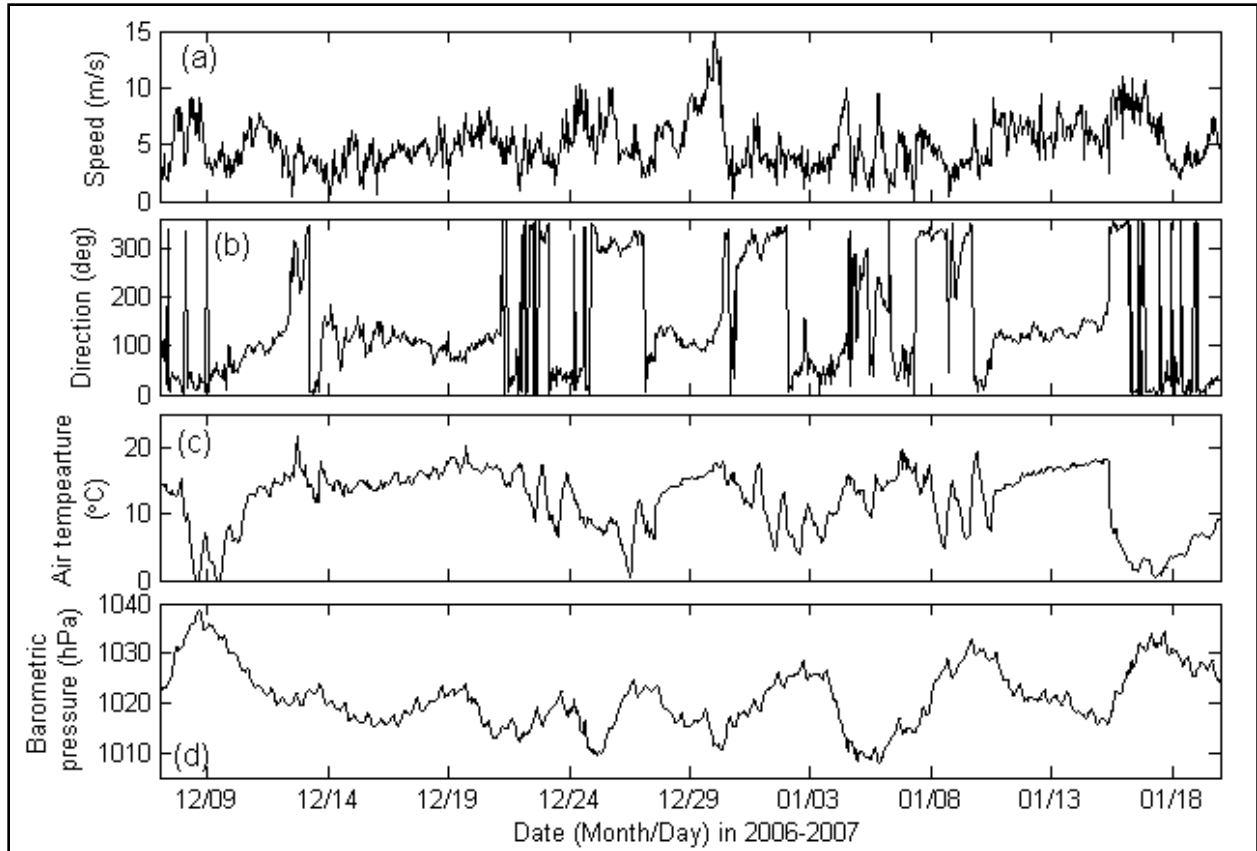
Figure 3.19   Time series of (a) wind speed, (b) wind direction, (c) air temperature, and (d) barometric pressure during the 2006 deployment.

Wave Characteristics

Figure 3.20 shows water level and bulk wave parameters at the north and south stations. High wave heights (Figure 3.20b) were associated with passages of winter storms. Wave height reached nearly 2 m (6.56 ft) on December 8 and December 25, and exceeded 2 m (6.56 ft) on December 31 when wind speed reached 15 m/s. Peak wave period shows that during the onset of storms, high frequency waves were generated. Southeasterly swells became dominant when cold fronts passed the study area. During the post-frontal phases, high frequency northerly waves became dominant following northerly/northwesterly post-frontal winds (Figure 3.20b and d). Wave height at the north station was lower than that at the south station. Maximal dissipation rates were 50.7 percent (ΔH_S=1.16 m) on December 30, 2006.
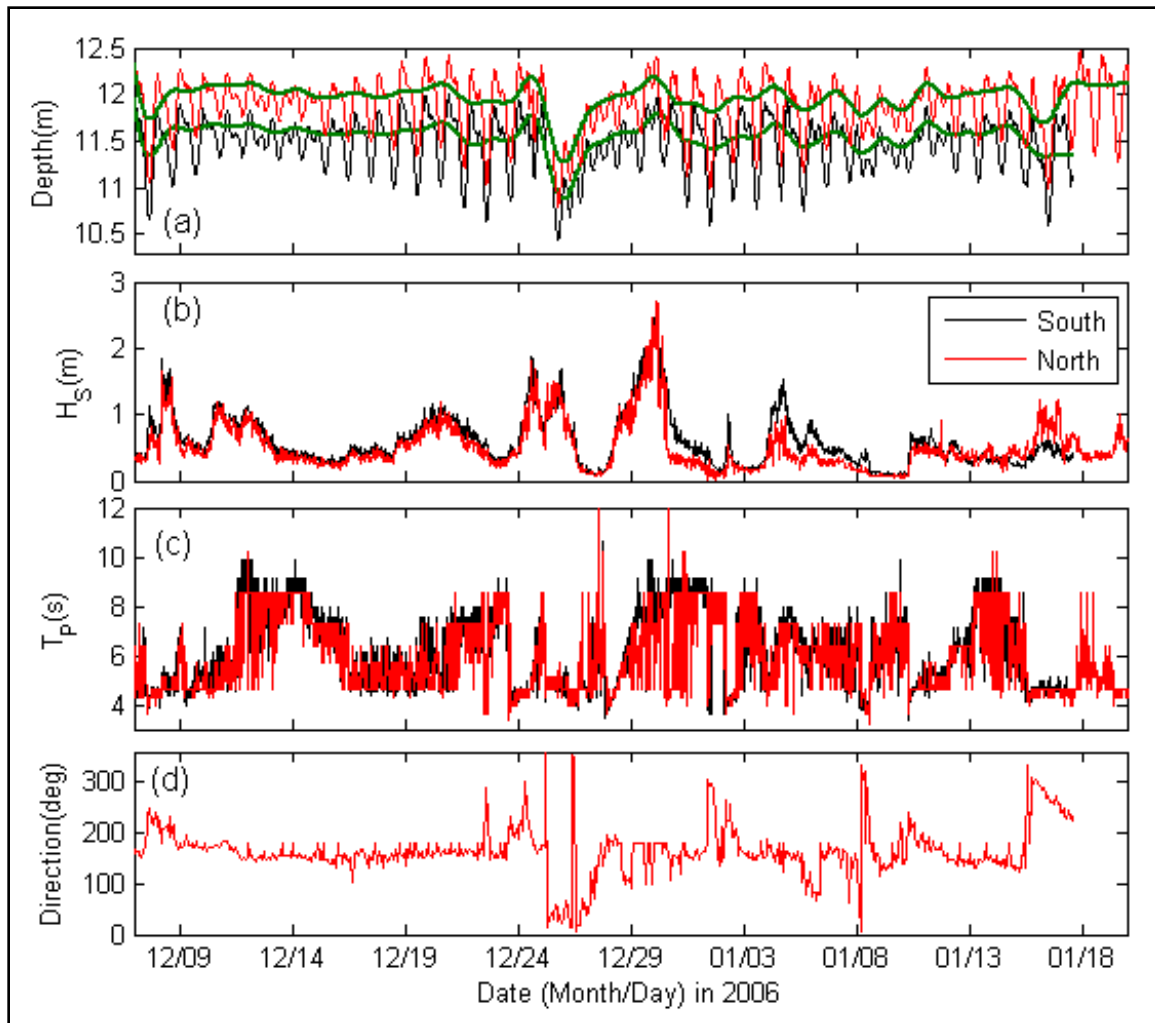
Figure 3.20   Time series of (a) water level, (b) wave height, (c) peak wave period, and
                (d) wave direction.

Black lines show the parameters at the south station and red lines indicate the parameters
at the north station. Green lines in (a) show 40-hr low-pass filtered water level.

Currents

Current variations at the north and south stations were conspicuously different, illustrated in
Figure 3.21. Currents at the north station varied strongly with passages of cold fronts: high
eastward and southward currents during winter storms following strong post-frontal winds.
Whereas, currents at the south station showed opposite variation, implying an importance of
bank complex bathymetry, as suggested by Pepper (2000) and Kobashi and Stone (2008a) for
Ship Shoal. Changes in water level fluctuations during storms were evident. Late December, a
pressure sensor recorded 0.92 m (3.02 ft) changes in low-frequency water level (> 40 hr period)
late December, which eventually generated northeasterly currents (Figure 3.21). East currents
were significantly higher than north currents, suggesting the importance of alongshore currents
over the bank.

36
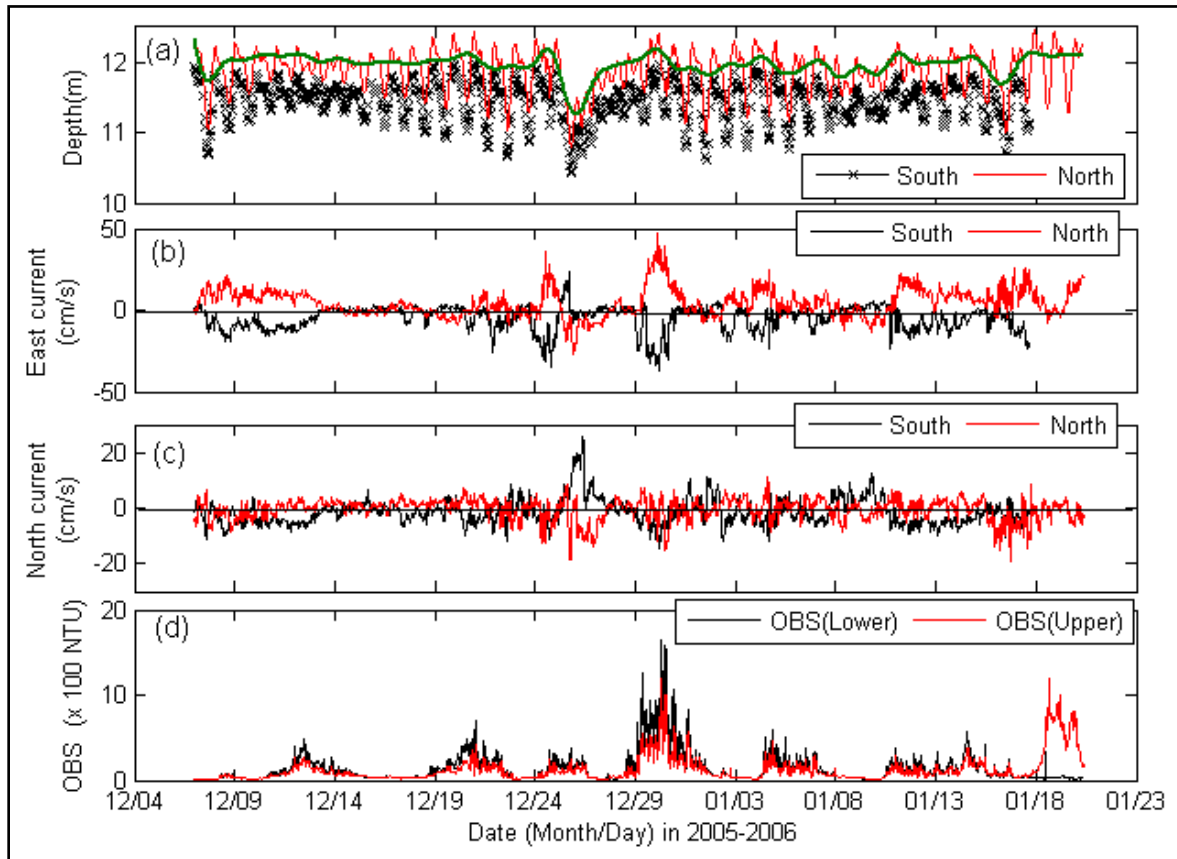
Figure 3.21   Time series of (a) water depth, (b) east currents, (c) north currents, and (d) turbidity.

Bottom Boundary Layer Characteristics

Bottom boundary layer parameters (i.e., shear velocity and stress) were strongly associated with passages of cold fronts (Figure 3.22), as with the 2004 deployment. High values of wave orbital velocity, shear velocity and shear stress were all associated with passages of cold fronts. Near bottom wave orbital velocity reached nearly 1 m/s and lower OBS's recorded a turbidity level of 400 NTU on December, 31, 2008. Changes in turbidity were associated with wave-induced shear stress rather than current-induced shear stress during late December, and both waves and currents had a profound influence on turbidity.

37
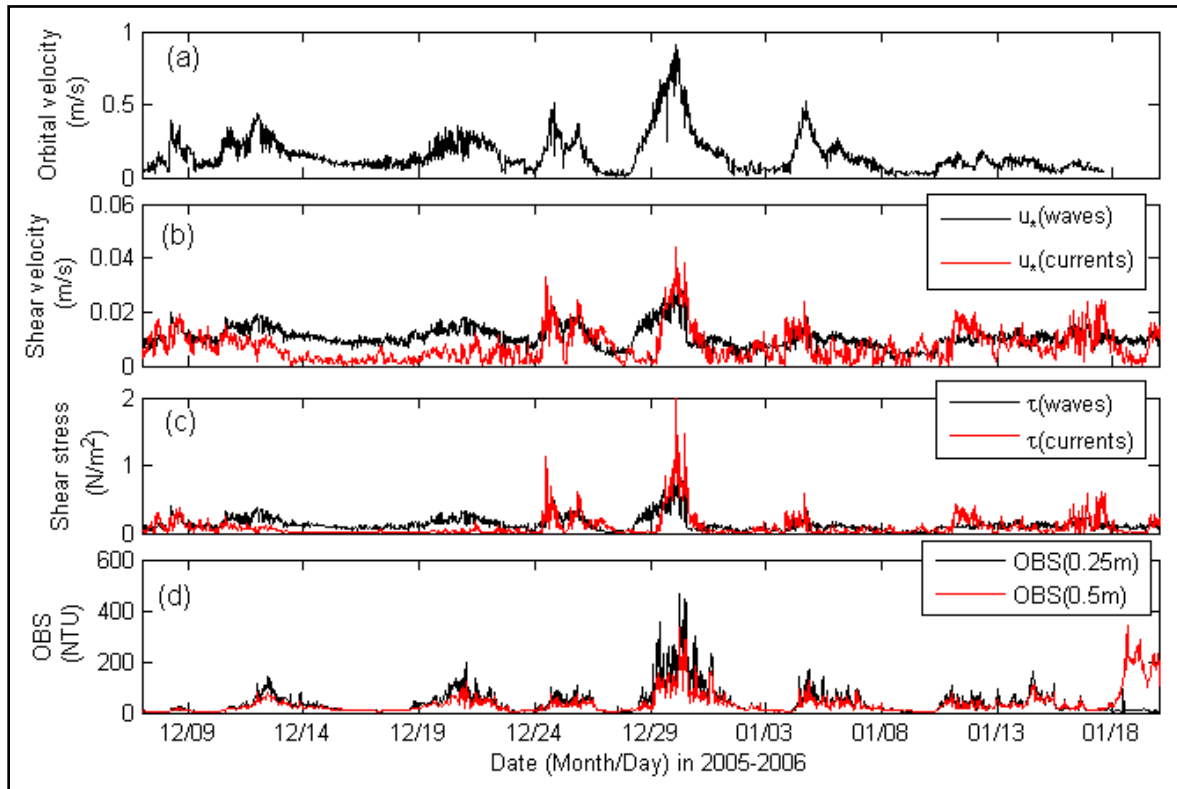
Figure 3.22   Time series of (a) near bottom wave orbital velocity, (b) shear velocity due to waves and currents, (c) shear velocity due to waves and currents, and (d) turbidity (OBS) at lower and upper layers.

3.3.3. 2008 Deployment

Meteorological Characteristics

Meteorological conditions during the 2008 deployment were characterized by the summer regime: infrequent winter storms and calm winds. During the deployment, a total of three fronts (two cold fronts and one stationary front) passed over or approached the study area. One of them eventually passed over the study area on June 18, 2008, when abrupt wind shifts were evident in Figure 3.23. Wind speeds were mostly less than 10 m/s except early June when strong winds blew from the southeast due to a high pressure system off the U.S. east coast.
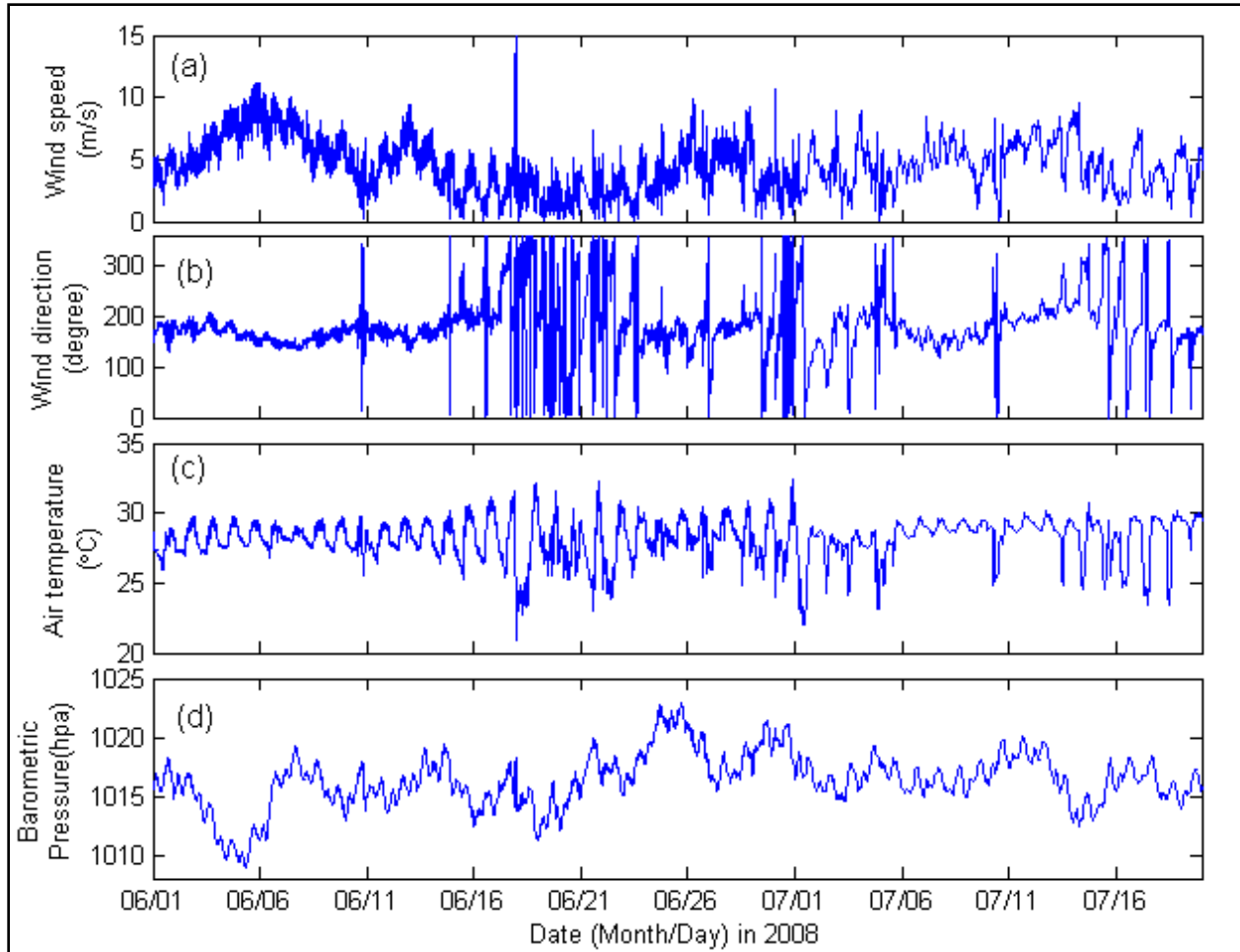
Figure 3.23   Time series of (a) wind speeds, (b) wind direction, (c) air temperature, and (d) barometric pressure during the 2008 deployment.

Wave Characteristics

In Figure 3.24, we present time series of water level and bulk wave parameters. The wave parameters were associated with meteorological forcing. During the 2008 deployment, no cold fronts passed over the study area; however, there were a few high wind conditions associated with high pressure cover of the northern Gulf of Mexico in early June, mid-June, and late June. During these periods, prevailing wind directions were from the southeast (Figure 3.24). In early June, wave height exceeded 2 m at the south and crest stations though this was not associated with winter storms. These high wind and wave conditions were also reported over the northern Gulf (e.g., Pepper 2000; Kobashi et al. 2005) and appear to be a dominant force during the summer and partial spring periods.

Waves over the north station were significantly dissipated compared to waves over the south station. Waves over the bank crest had little difference or higher wave height than those over the south. This can be attributed to wave shoaling effects. The results also suggest that wave dissipation was high on the lee side of the shoal. Similar results have also been reported for Ship Shoal (Kobashi et al. 2007a).

39

During most of the deployment period, low frequency swells characterized by wave periods higher than 5 seconds, were dominant. During some periods when wave height was low, seas in the higher frequency band were dominant (Figure 3.24 (c)).

Wave height over the north station was significantly dissipated compared to wave height over the south station. Differences in wave height between south and middle stations were minimal. Maximal dissipation rates between south and north stations were 73.2 percent in early June.
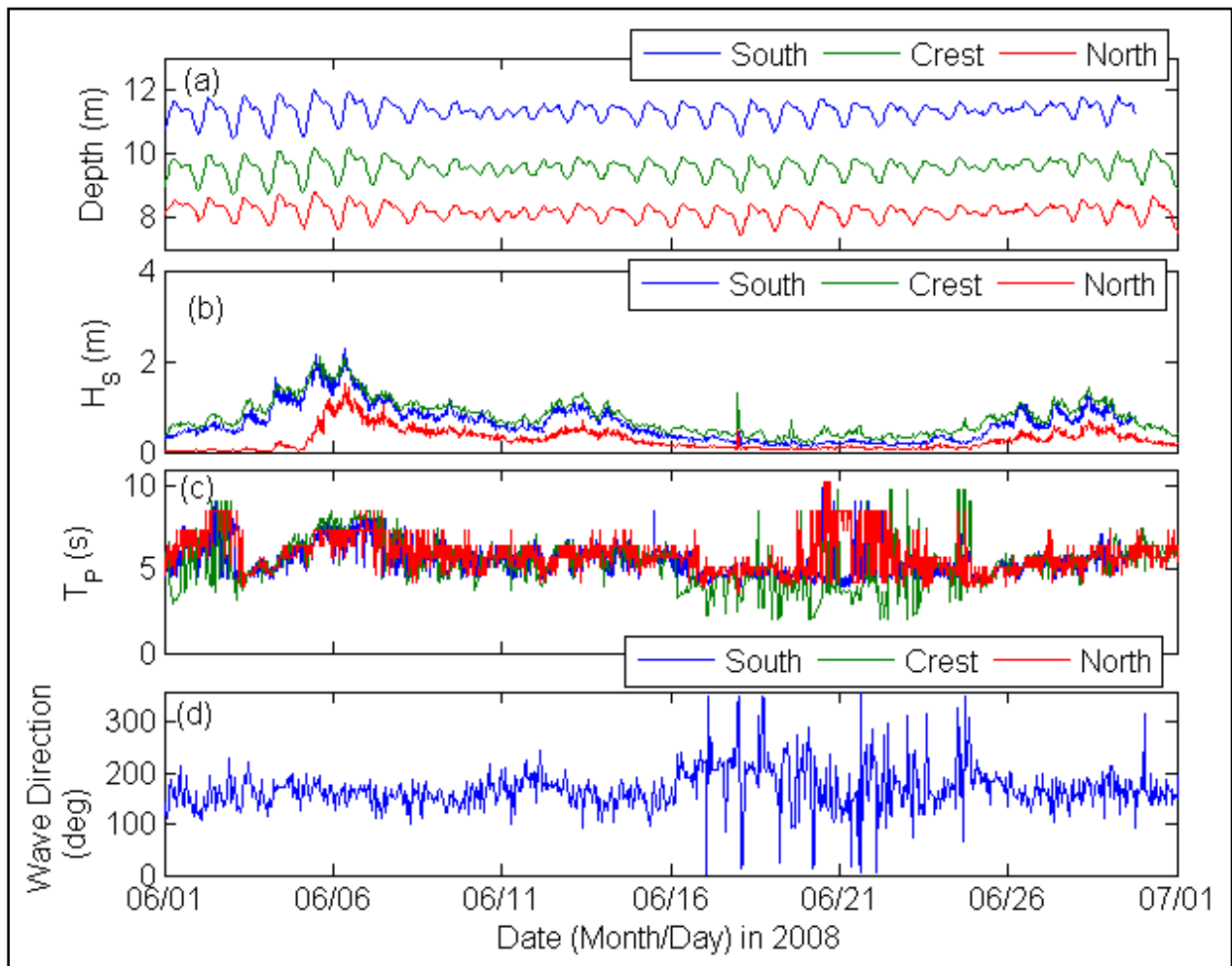
Figure 3.24   Time series of (a) water depth, (b) wave height, (c) peak wave period, and (d) wave direction for each station.

Currents

Currents varied with winds and changes in water level due to wind. East currents at the surface (approximately 9 m [29.53 ft] above the bottom) and middle layers (approximately 5 m [16.4 ft] above the bottom) had similar variations, but bottom currents were significantly smaller than those at surface and middle layers. West currents followed easterly wind; however, flow reversals were evident (Figure 3.25c). Surface currents moving north were also associated with north-south winds; however, currents at the middle and bottom layers varied differently from

those at the surface, suggesting slope currents and bathymetric modification, also reported by Pepper (2000) and Kobashi and Stone (2008b). Interestingly, the turbidities at the lower (0.25 m [.82 ft]) and upper (0.6 m [1.97 ft]) layers were high during calm weather and persisted over a period of several weeks.
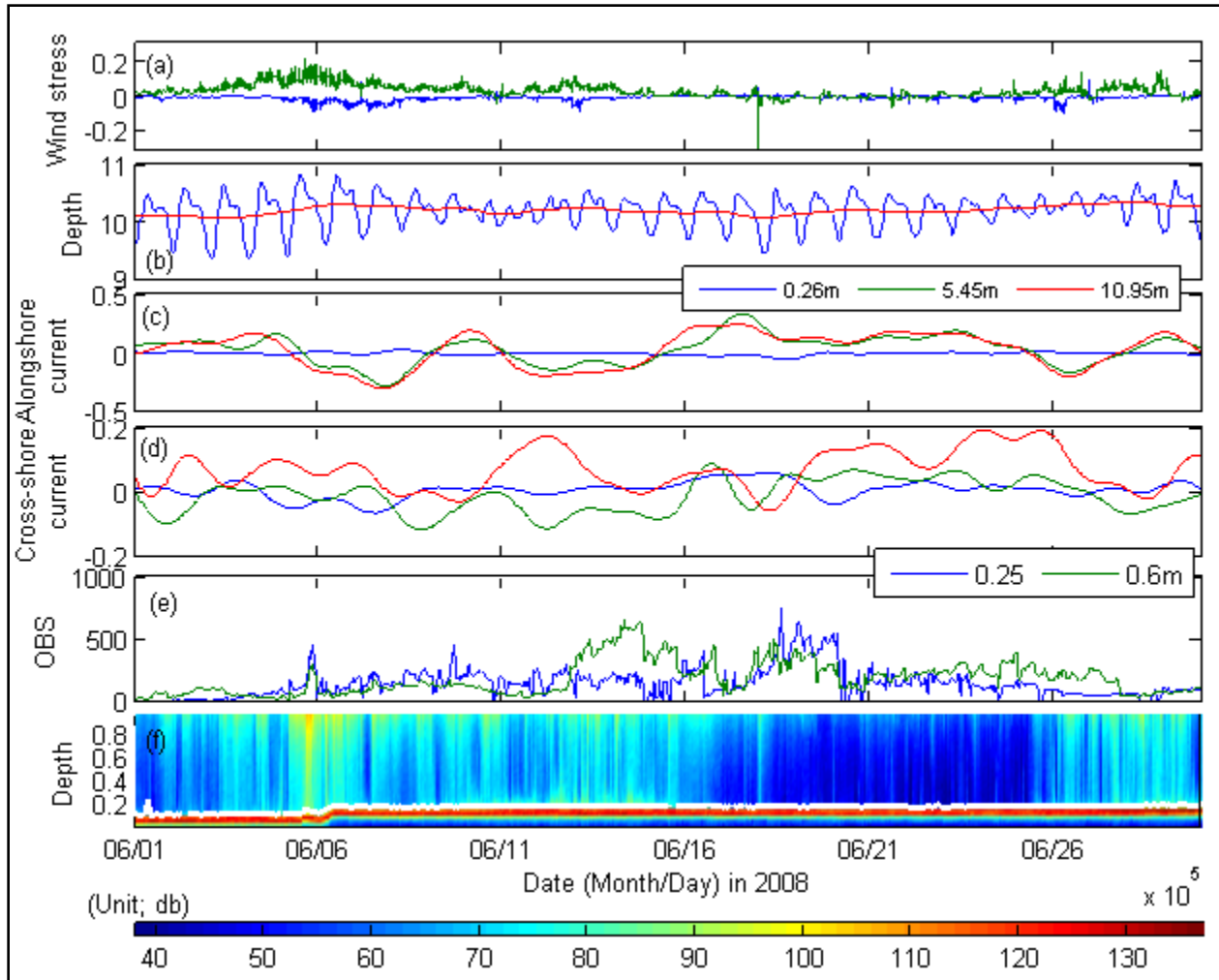
Figure 3.25   Time series of (a) wind stress (east in blue and north in green), (b) depth, (c) east current at surface (9 m above the bottom), middle (5 m above the bottom) and bottom (0.2 m above the bottom), (d) north current at surface (9 m above the bottom), middle (5 m above the bottom) and bottom (0.2 m above the bottom), and (e) turbidity, and (f) acoustic backscatter intensity.

Red line on the second figure from the top shows 40 hour low-pass filtered water level.

Bottom Boundary Layer Parameters

Figure 3.26 shows the bottom boundary layer parameters during the deployments. In early June, 0.7 m/s of near bottom orbital velocity was measured, which was associated with high wind speed and high wave height. During this time interval, shear stress due to waves was also high, which is consistent with a sharp increase in lower and upper turbidities (Figure 3.26(c)).

However, it is interesting that the wave and current shear stresses and turbidities were not correlative, particularly during mid-June, during which wave height and current speed were both low but turbidity at the upper and lower sensors were both high.
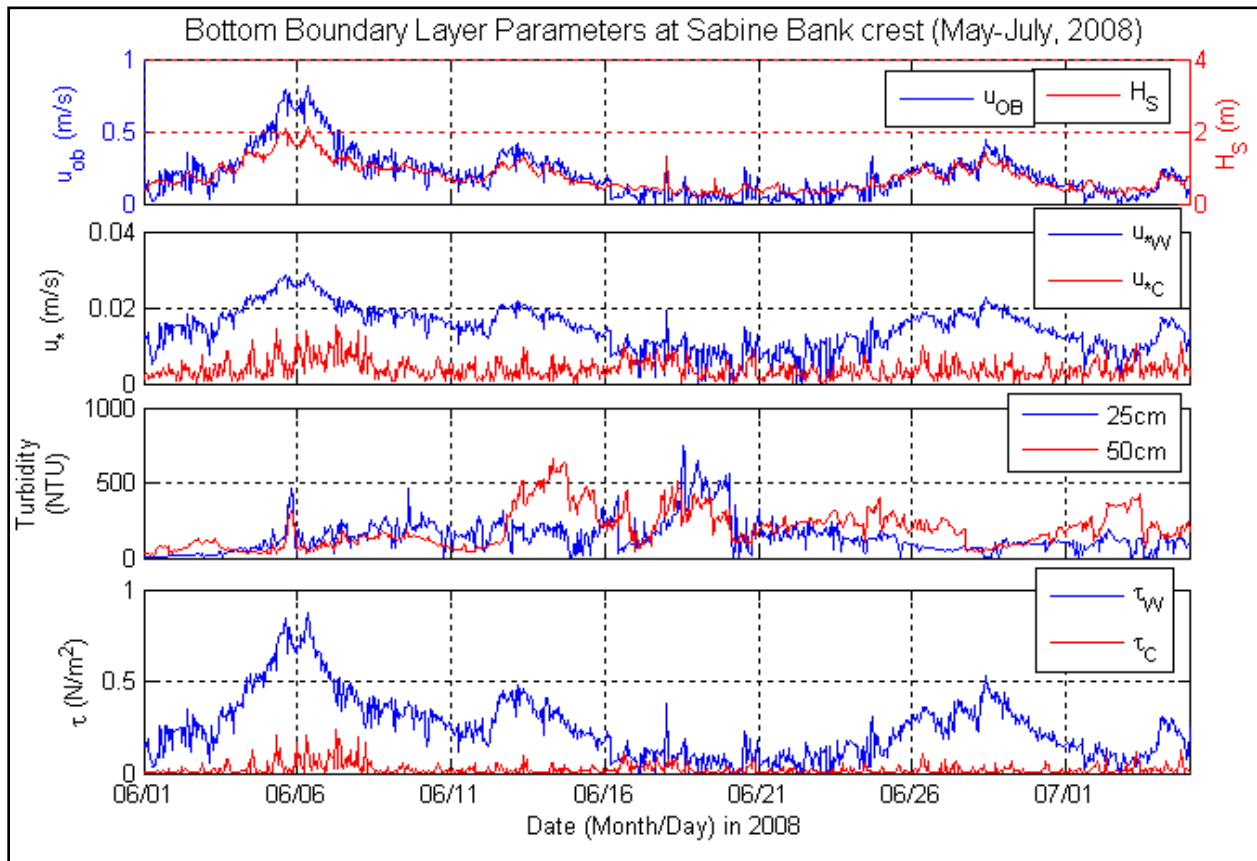
Figure 3.26   Time series of (a) wave orbital velocity (left) and wave height (right), (b) shear velocity, (c) turbidity, and (d) shear stress.

3.4. DISCUSSION

3.4.1. Atchafalaya Hydrology

It is well-documented that freshwater and fluvial sediments from the Atchafalaya River are transported toward the west, sometimes referred to as the mud stream (Wells and Kemp 1981; see also Figure 3.29). The river-borne sediments can be deposited along the western Louisiana coast and create mud flats. Some of these sediments can reach as far as Texas. This muddy river discharge appears to influence the hydrodynamics over the western Louisiana coast, including Sabine Bank, particularly during high river discharge in the spring. The Atchafalaya River discharge is characterized by high discharge in the winter and spring, and low discharge in the summer (Figure 3.27). High discharge during the spring is associated with ice melting from both the Rocky and Appalachian mountains. Such a characteristic can be deciphered from Figure 3.27. In 2008, maximum discharge exceeded 600,000 cubic feet per second (cfs), more than three times higher than 200,000 cfs which (Walker and Hammack 2000) characterized as the border between high and low discharges (Figure 3.28). During the high discharge of this period, a significant amount of fluvial sediments was likely debouched from the river, and significantly

42

influenced coastal current structure over western Louisiana as discussed in section 3.4.4. The river-borne sediments are further resuspended by high waves and strong currents, and are redistributed over the shelf (cf. Figures 3.29, 3.30).
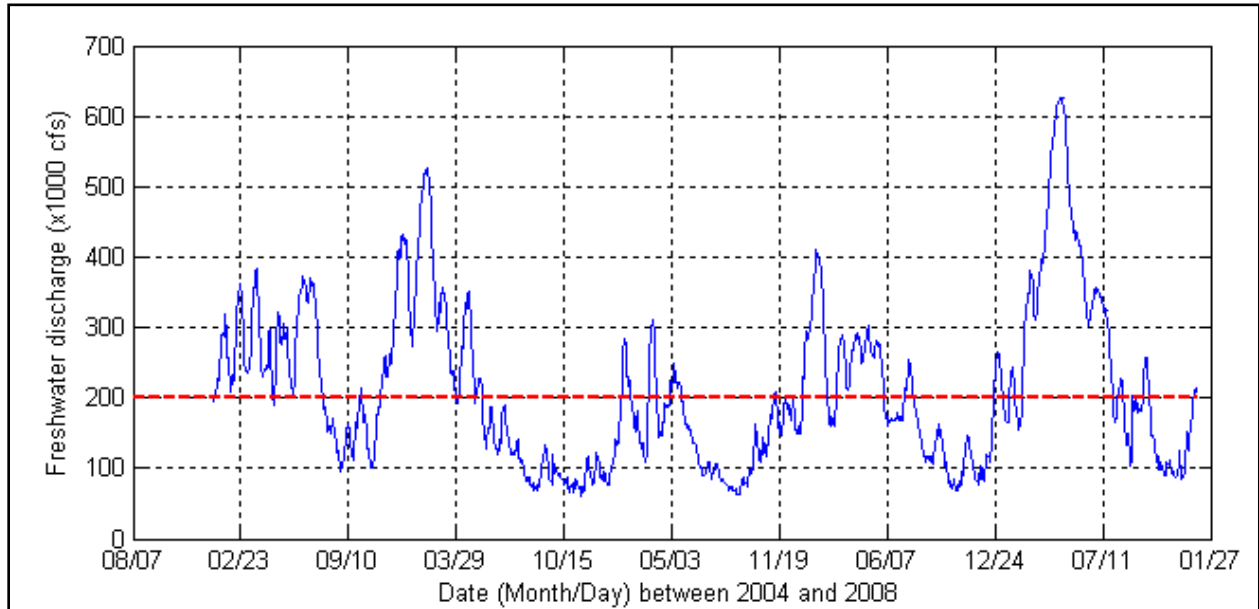
Figure 3.27   Time series of river discharge at Simmesport, LA between 2004 and 2008. Dashed line shows the border between high and low discharges by Walker and Hammock (2001). Source: U.S. Army Corps of Engineers, New Orleans District.
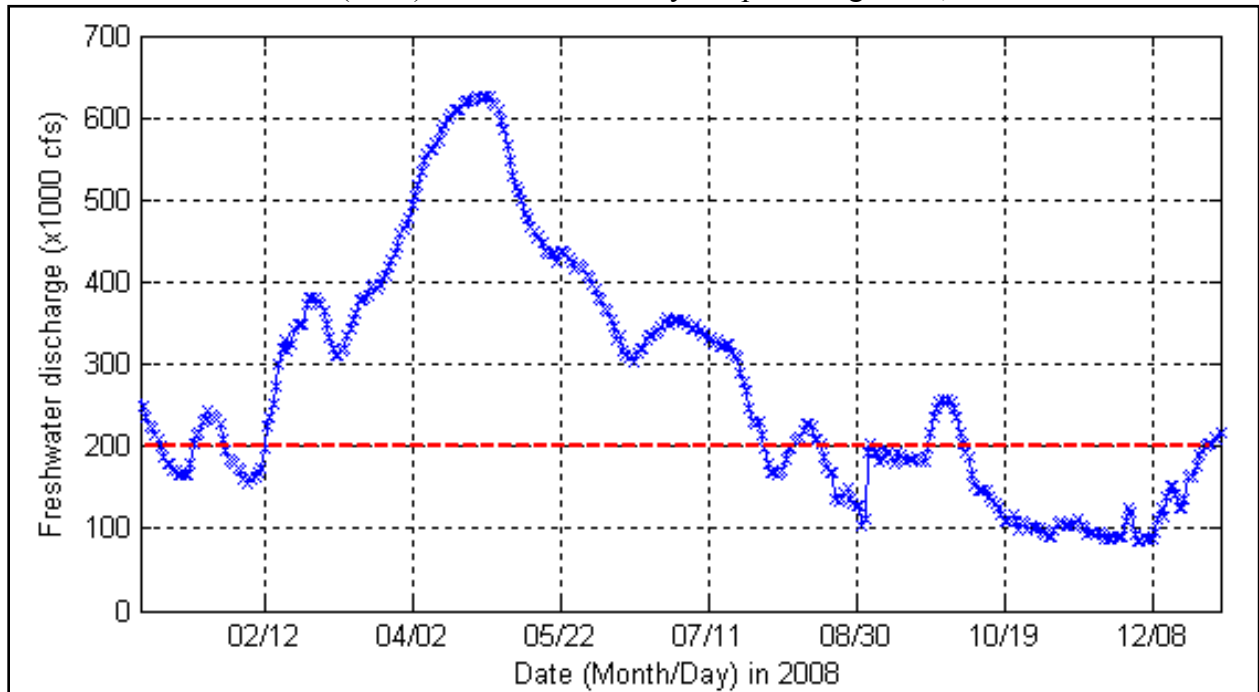
Figure 3.28   Time series of river discharge at Simmesport, LA in 2008. Dashed line shows the border between high and low discharges by Walker and Hammock (2001). Source: U.S. Army Corps of Engineers, New Orleans District.
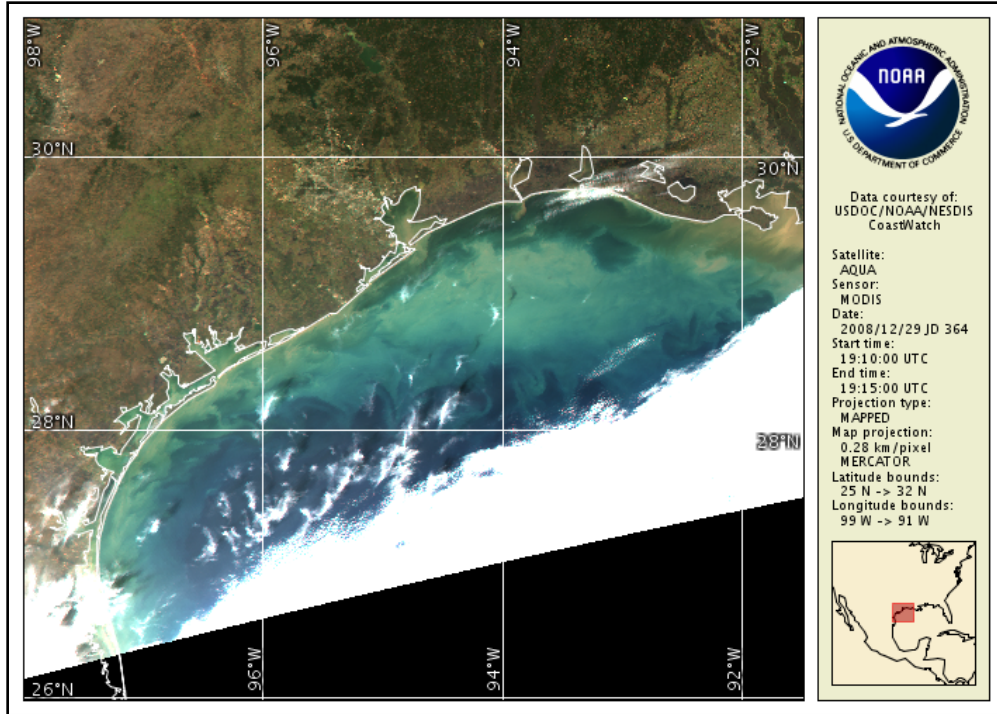
Figure 3.29 A MODIS satellite image taken on December 29, 2008.
Source: NOAA NESDIS.
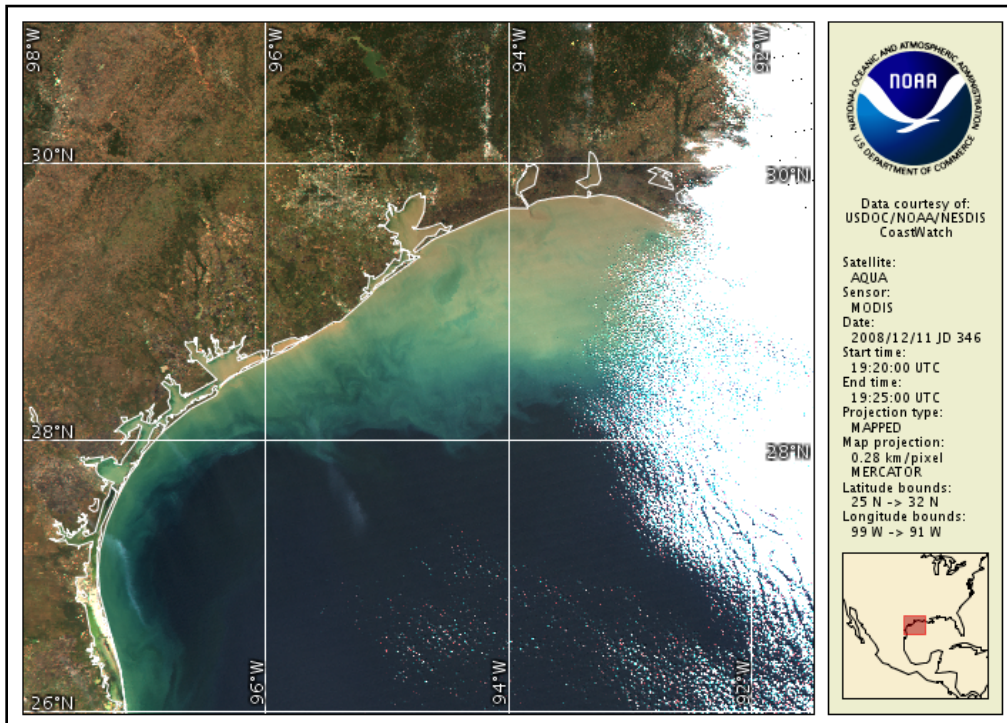
Figure 3.30   A MODIS satellite image taken on December 11, 2008.
Source: NOAA NESDIS.

3.4.2. Bed Characteristics

Anderson and Wellner (2002), after analyzing core samples for a location near the study area, reported that the surface sediments along the eastern Sabine Bank are silty sand with a mean size of 0.2576 mm (0.0101 in). They also addressed the existence of fine sediments (i.e., silt and clay) along the flank of eastern Sabine Bank based on their grain size analysis. However, seasonal changes in bed characteristics have received little attention. Based on the results of Anderson and Wellner (2002), results from our sampled sediments, and side-scan sonar bottom images from Brooks et al. (2004) and Dellapenna et al. (2006), suggest interesting spatial changes in bottom sediments, more specifically, sediment heterogeneity and patchiness, were unveiled.

Results from the grain size analysis of the bottom sediments sampled from our deployment sites in 2008 are shown in Figures 3.31–3.33. When the instrument arrays were deployed in the summer of 2008, sampled sediments were sand on the crest and south of the bank, and clay on the north bank. The sediments sampled on the bank crest were fine sand for both pre- and post-deployments with a median grain diameter of 150 and 154 microns, respectively (Table 3.5). For the results, silt percentage was substantially reduced for the samples taken during the post-deployment compared to those during pre-deployment. This implies the importance of sediment re-suspension during infrequent fluvial sediment supply from the river. The samples from the south station were fine sand during the pre-deployment and clay during post-deployment, suggesting fine sediment supply during the deployment. The samples from the north station were clay during both pre- and post-deployment. Sediments close to the shore are finer than those for offshore, likely associated with fluvial sediment from the Atchafalaya River. Since the north station is closer to the coast, which is likely on the pathway of the Atchafalaya mud stream, the station is more exposed to fine sediment supply, whereas, the south station located further offshore is outside of the stream and, therefore, is more exposed to marine processes. The bank crest can be exposed to both fluvial and marine processes and as a result, hydrodynamic and bottom boundary layer dynamics seem to be more complicated.

A side-scan image of western Sabine Bank from Brooks et al. (2004) is shown in Figure 3.35 (see location for the side-scan survey in Figure 3.36). Dark colors represent finer sediments and brighter colors represent coarser sediments (i.e., sand). The side-scan image suggests predominant fine sediment for the most of the area; however, spotted sand can be seen. Seismic data from Dellapenna et al. (2006) also shows patchiness of sediments along western Sabine Bank. This patchiness, as also suggested by Kobashi and Stone (2008b) for the Ship Shoal study, is likely associated with sediment supply from the river, and in part from outside the bank and sediment loss due to sediment re-suspension associated with storms (winter storms and tropical cyclones).
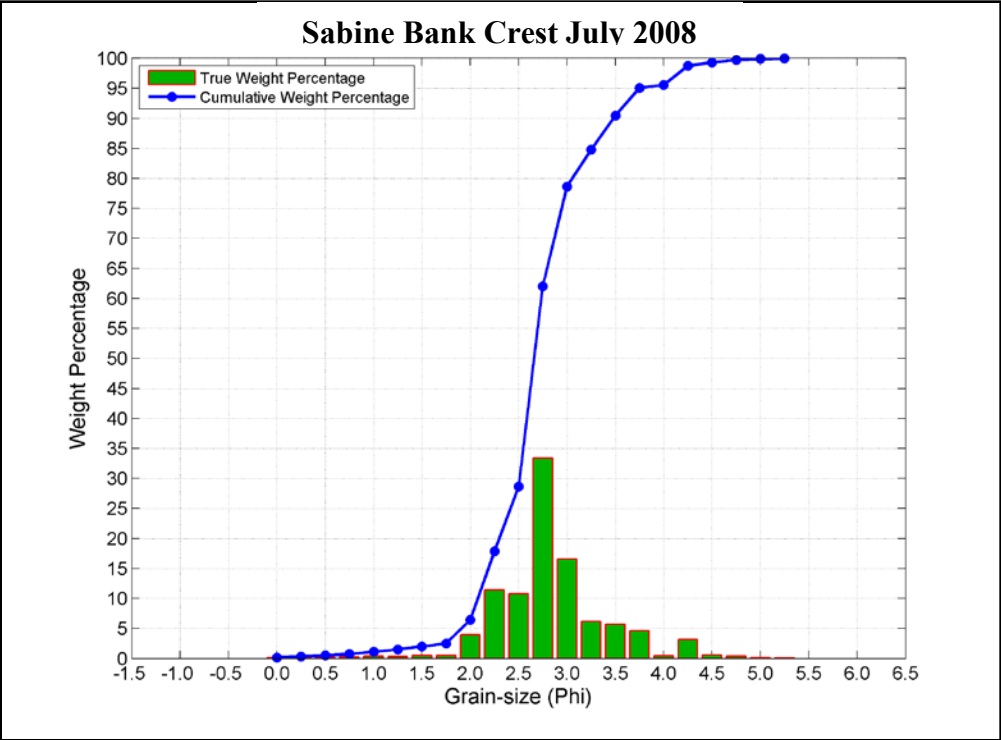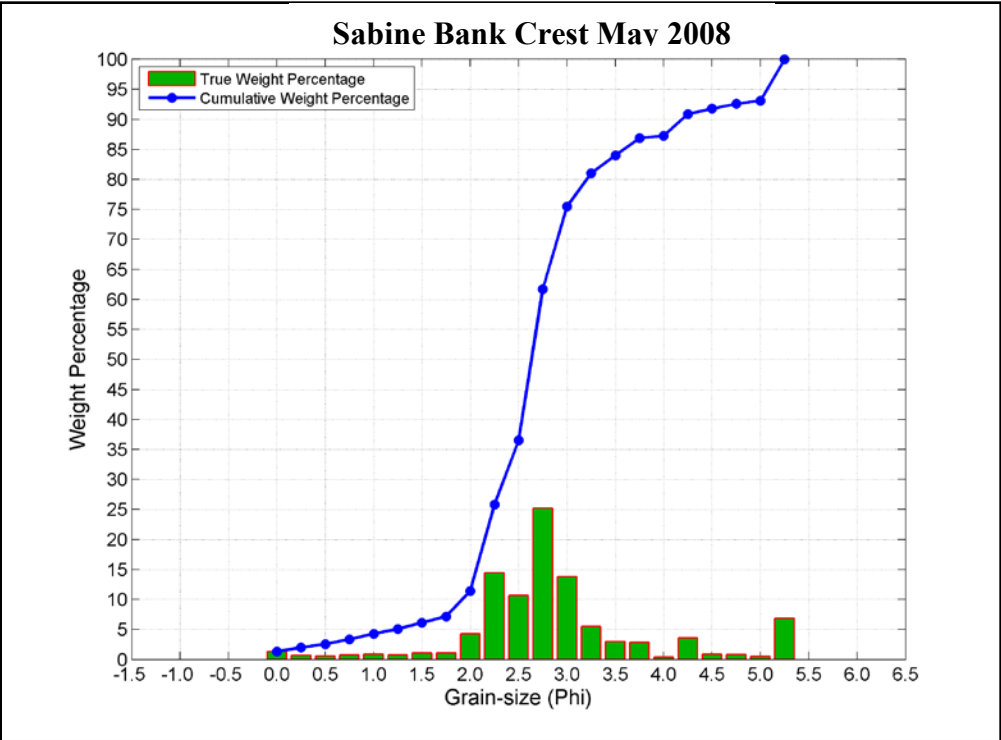
Figure 3.31 Grain size distribution for the Bank crest during the 2008 deployment.

(Top) pre-deployment and (bottom) post-deployment.
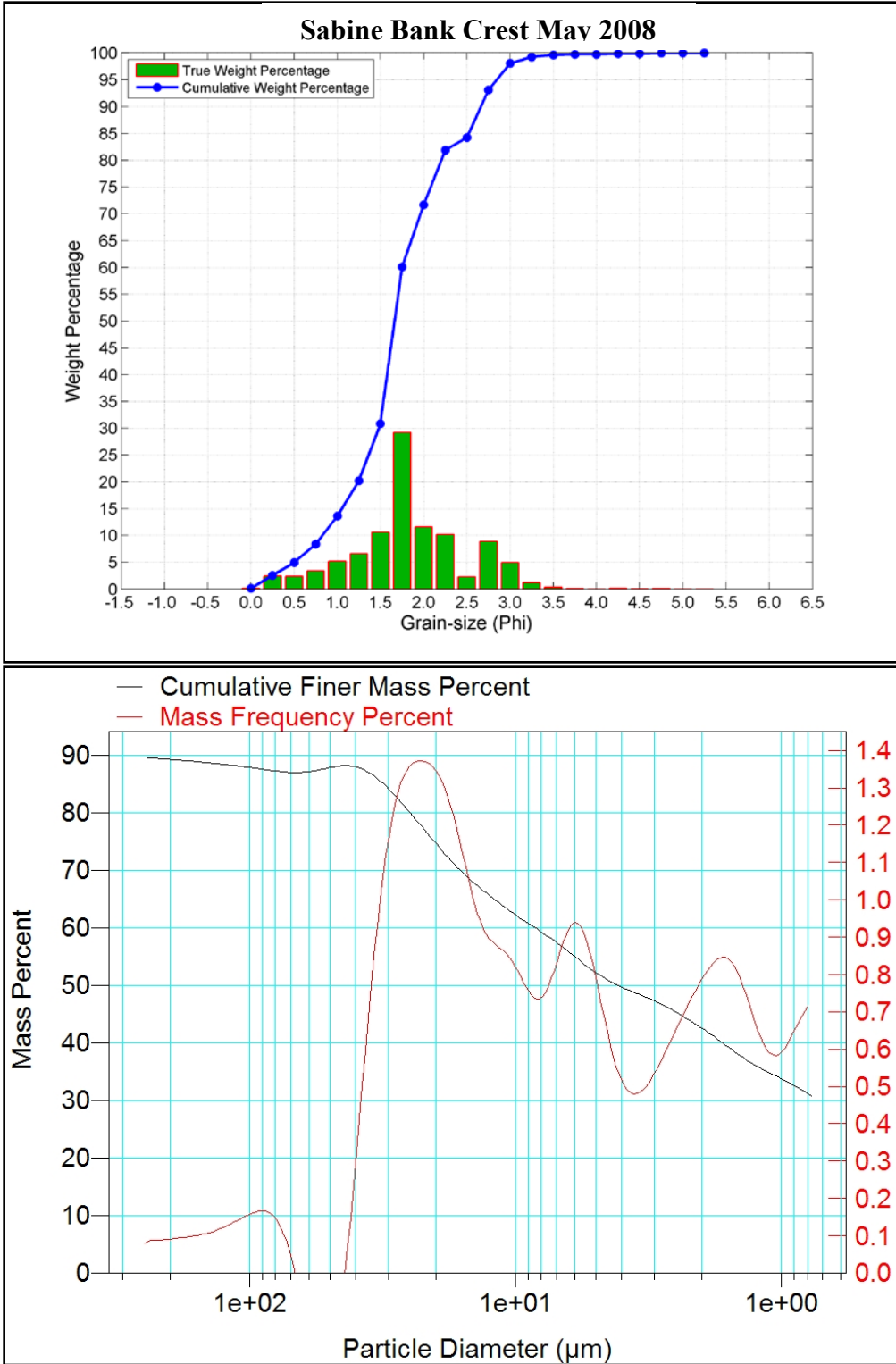
Figure 3.32   Grain size distribution for the south station (SB08_3) during
pre-deployment (top) and post-deployment (bottom).
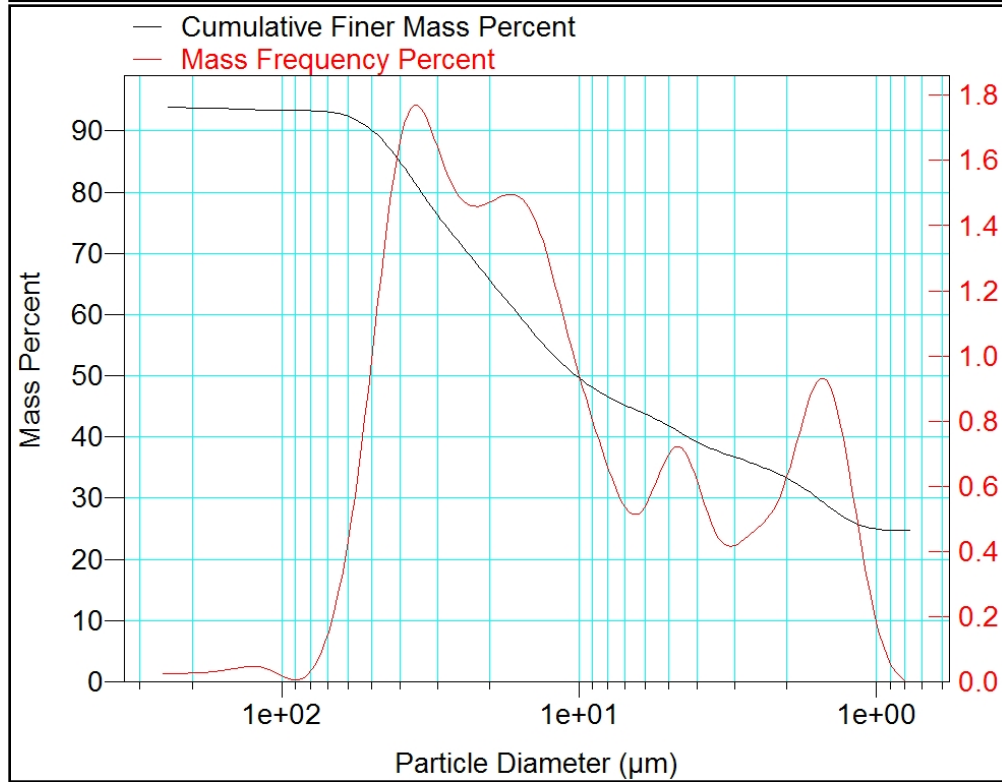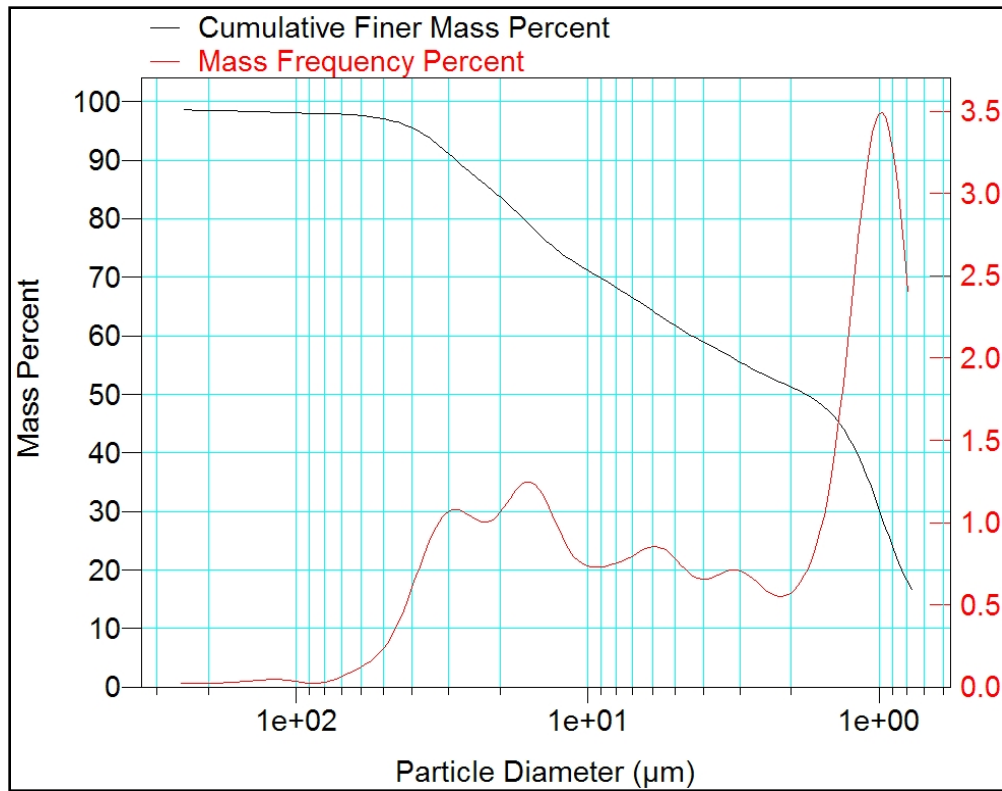
Figure 3.33   Grain size distribution for the north station (SB08_1) during
pre-deployment and post-deployment.

Figure 3.34   Sediments sampled from Crest (top), North (middle), and South (bottom).
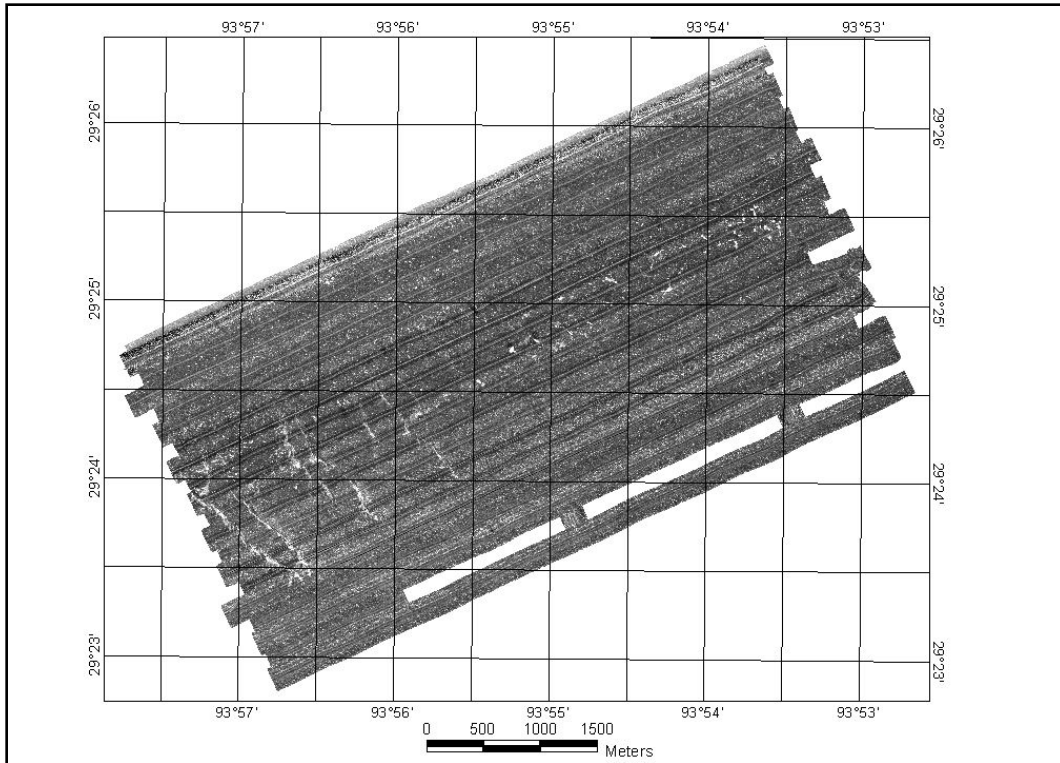
Figure 3.35   Side-scan image of a portion of Sabine Bank, Texas, performed by
                Dr. Dellapenna, Texas A&M University Galveston.
Source: Brooks et al. 2004.
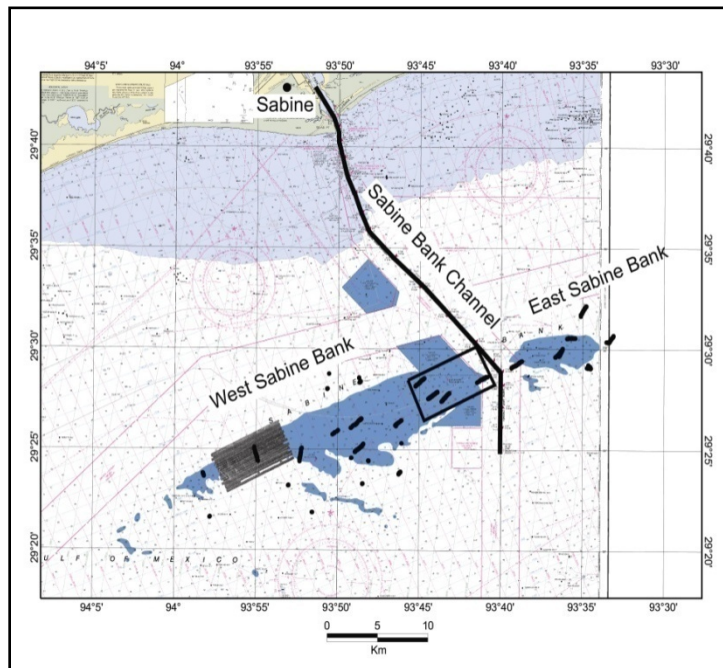
Figure 3.36   The location of the side-scan map
                overlaid on the Sabine Map.
Source: Brooks et al. 2004.

Table 3.5

Median Grain Size from Each Station

Time	Nearshore	Crest	Offshore
May 05/28/2008	10.72 microns	150 microns	299 microns
July 07/17/2008	20.26 microns	154 microns	15.68 microns

3.4.3. Meteorological System and Wave-Climate at Western Louisiana Coasts

The western Louisiana coast is characterized by three meteorological regimes: fair weather, winter storms, and tropical cyclones. During most of the year, the coast is characterized by a pre-dominantly low energy environment: low tide, low wave height, and weak currents (Kobashi et al. 2005; see also Figure 3.37). Between October and May, frequent passages of winter storms that accompany cold fronts occur every 3 to 10 days (30–45 times/year). As shown in the previous sections, the passages of the fronts are characterized by abrupt wind shifts, strong wind speed, and abrupt drops in air temperature and barometric pressure. Another storm, tropical cyclones, which strike the Louisiana coast every three years, accompany extremely high wind speed, wave height and storm surges. The Northern Gulf of Mexico has faced occasional storm and hurricane passages, both of which cause tremendous impacts on coastal areas. In southwest Louisiana, a total of 14 tropical storms and hurricanes hit the area from 1901 to 1996 (Stone et al. 1997). However, although they are weaker than tropical storms and hurricanes, cold fronts are more important than storms because they are generated more frequently and can persist even for a couple of days. Pepper (2000) and Georgiou et al. (2004) give a detailed explanation of the mechanism of cold front generation, sustenance and dissipation in the northern Gulf of Mexico. Cold fronts are generated at the boundary between cold continental air mass and warm ocean air mass. In the Louisiana coast, prevailing winds are from south-east during most of the year; however, once the cold fronts set up over the region, wind direction dramatically changes from the southeast to from the north, wind speed increases, and air temperature drops. According to Pepper (2000) and Georgiou et al. (2004), two types of cold fronts exist, parallel case and oblique case, subject to the initial position of air masses and how weather systems grow. After cold fronts passed to the east, high pressure covers the southern U.S. and occasionally causes high wind from east/southeast.
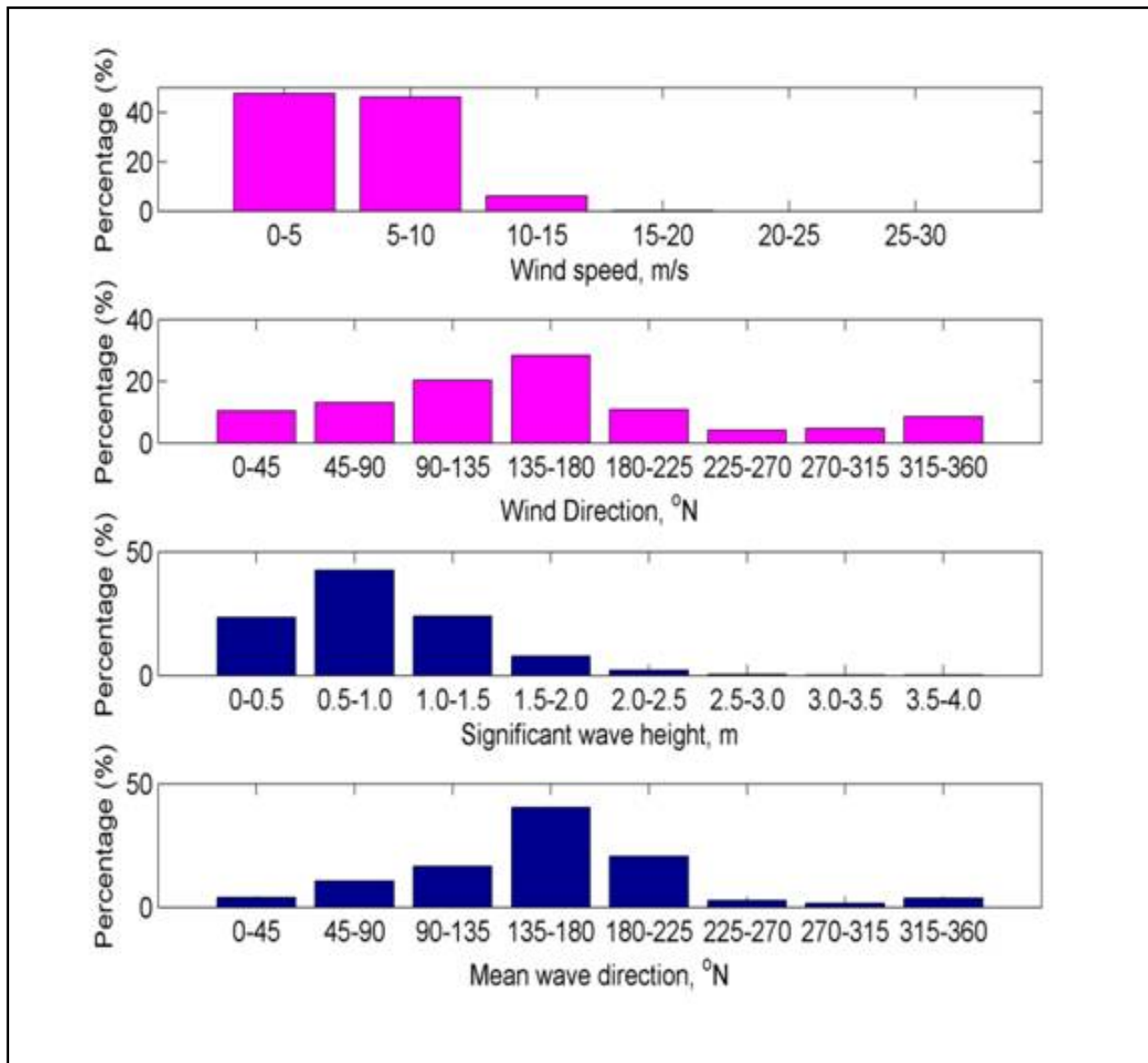
Figure 3.37   Wave climate at NDBC 42035 between 1/1/2006 and 12/31/2006.

3.4.4. Seasonal Coastal Currents

Seasonal changes in coastal currents have been discussed in greater detail by several papers and reports (e.g., Cochrane and Kelly 1986). The coastal current data from a station near the survey area were obtained from the Texas Automated Buoy System website (TABS-R) and are presented in Figure 3.38 as a supplement data for the 2008 deployment. For east-west currents, westward currents were dominant during most of the year, whereas, the current direction during the summer following wind reversal due to seasonal wind shifts. North- south surface currents were more variable following tidal currents and seasonal wind patterns: prevailing southeast winds and northwesterly winds during winter storms. The north-south currents were significantly weaker than the east-west currents, suggesting the importance of alongshore currents over cross-

shore currents. However, strong north-south currents can be seen as a result of post-frontal storm-induced currents and hurricane-induced currents. Strong westward currents during spring were correlated with high river discharge from the Atchafalaya River, suggesting influence of the river on hydrodynamics along the western Louisiana coast (Figures 3.28 and 3.39). Bottom currents are highly variable. Coastal currents during the observation period were predominantly to the west contrary to the north-easterly current prevalence along the bottom at the onshore study site. Also, the cold fronts and high wind regime influences the coastal currents in the same manner as it influences Sabine Bank circulation.
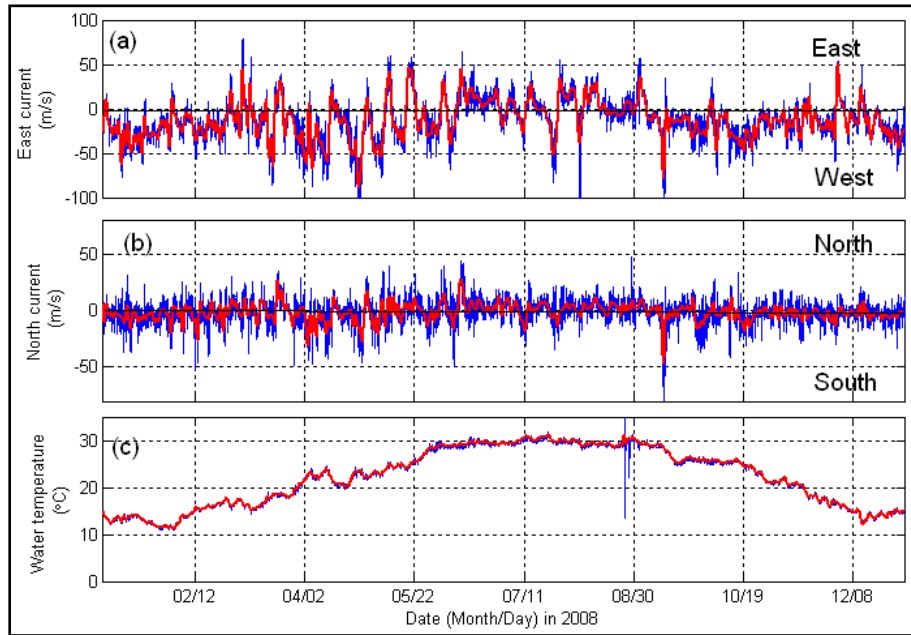
Figure 3.38   Time series of (a) surface east currents, (b) surface north currents, and (c) surface water temperature at TABS R in 2008 (see location in Figure 3.1).

Red lines show 40hr low-pass filtered values.
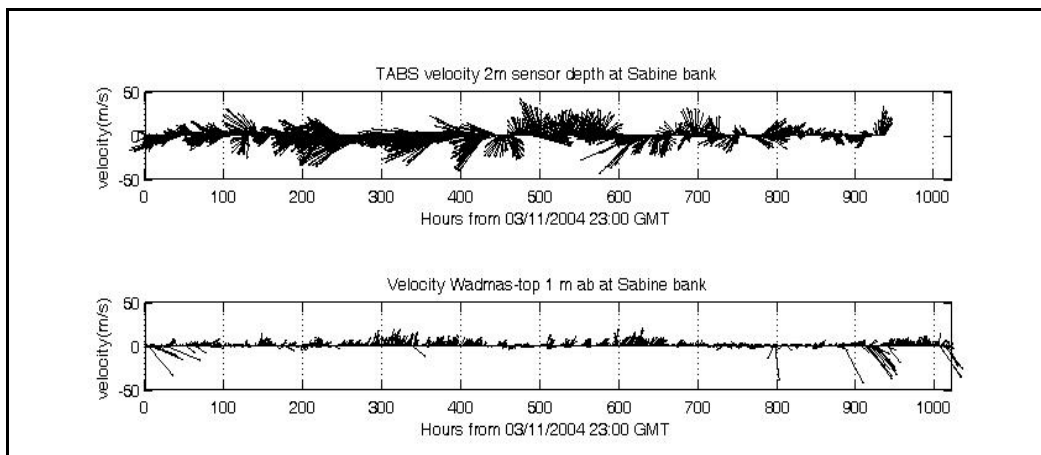
Figure 3.39   Surface current velocity data from TABS buoy No: R, further north of the study area (top).

53

Current velocity data for the corresponding period from the WADMS top ECM (1m asb) during the 2004 deployment (bottom).

3.4.5. Bottom Boundary Layer Dynamics and Sediment Transport Processes

Bottom boundary layer and surface waves are strongly associated with meteorological conditions. The results show that the bottom boundary layer characteristics in winter along the region can be classified into three groups depending upon the prevailing weather patterns; fair weather, cold front, and high wind regime. Bottom boundary layer characteristics in summer are associated with weak winds and occasional strong winds associated with the high pressure system. In summer, tidal currents and inertial currents become more important than winter due to weak wind-induced currents.

Winter Season

Fair weather

The northern Gulf of Mexico coast is a microtidal environment and generally exposed to low energy events; this means waves and tidal currents are very weak and the wave height range is less than 2 m (6.56 ft) (Wright et al. 1997). Therefore, waves and currents cannot usually re-suspend sediments during fair weather (Adams et al. 1987; Wright et al. 1997; Friedrichs et al. 2000).
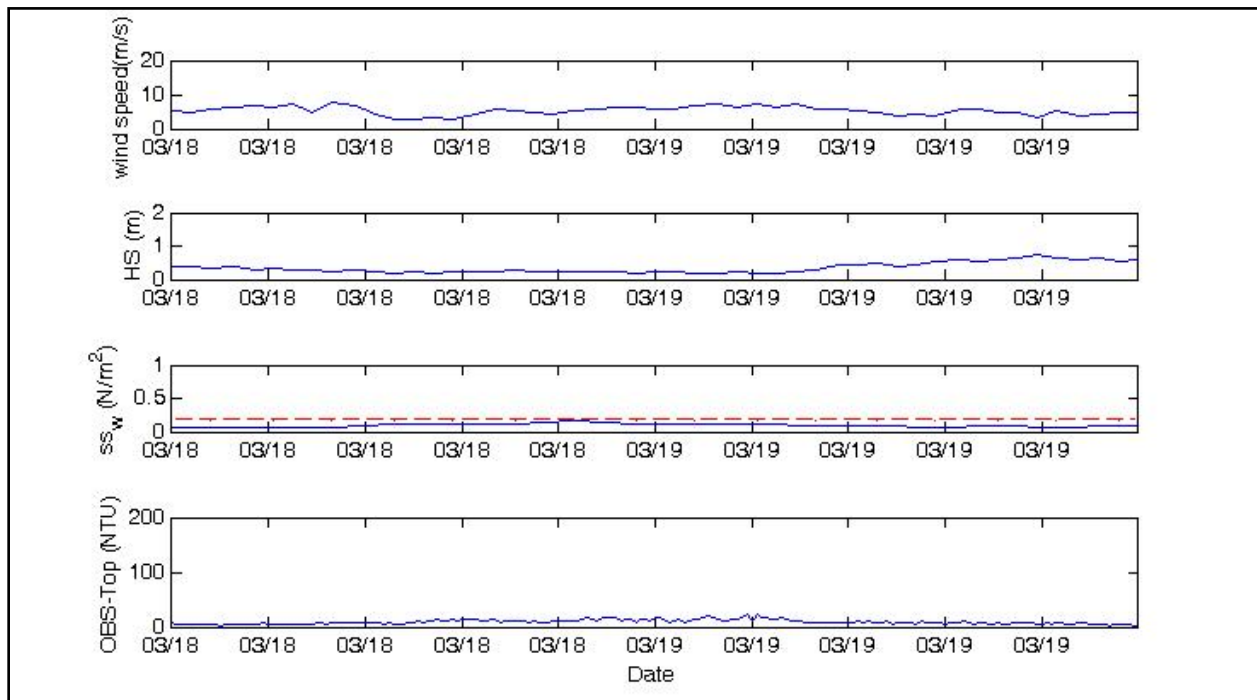
Figure 3.40   Boundary layer parameters during fair weather.

The dashed line in red corresponds to threshold for re-suspension of the sediment.

Figure 3.40 shows time series plots of bottom boundary parameters during fair weather conditions. In our survey area, significant wave height was actually less than 1 m (3.28 ft) during fair weather. Maximum shear stress due to waves during was less than 0.16 N/m^2, which is less than the computed threshold for the re-suspension of bottom sediments. Shear stress due to currents is usually greater than the threshold value. It is clear that waves are too small to re-suspend sediment during fair weather conditions. Currents can re-suspend the sediment efficiently even during this weather.

Cold Fronts

On the Louisiana coast, waves and bottom boundary layer dynamics are strongly affected by cold fronts as well as tropical storms (Pepper 2000; Stone 2000). Although they are not as strong as the storms the cold fronts are more important than the storms because they affect the Louisiana coast more frequently than the storms. During our survey period, at least 10 cold fronts impacted the area within a period of 44 days. When we compared the meteorological data with wave and bottom boundary parameters most of the peak values of wave spectra, Hs, the shear velocity, the shear stress and OBS were associated with the cold front passages. Shear stresses due to both waves and due to currents were greater than the threshold of the sediment re-suspension during the cold fronts (Figure 3.41). Hence, it is suggested that waves and currents can effectively re-suspend the sediment during the cold fronts.
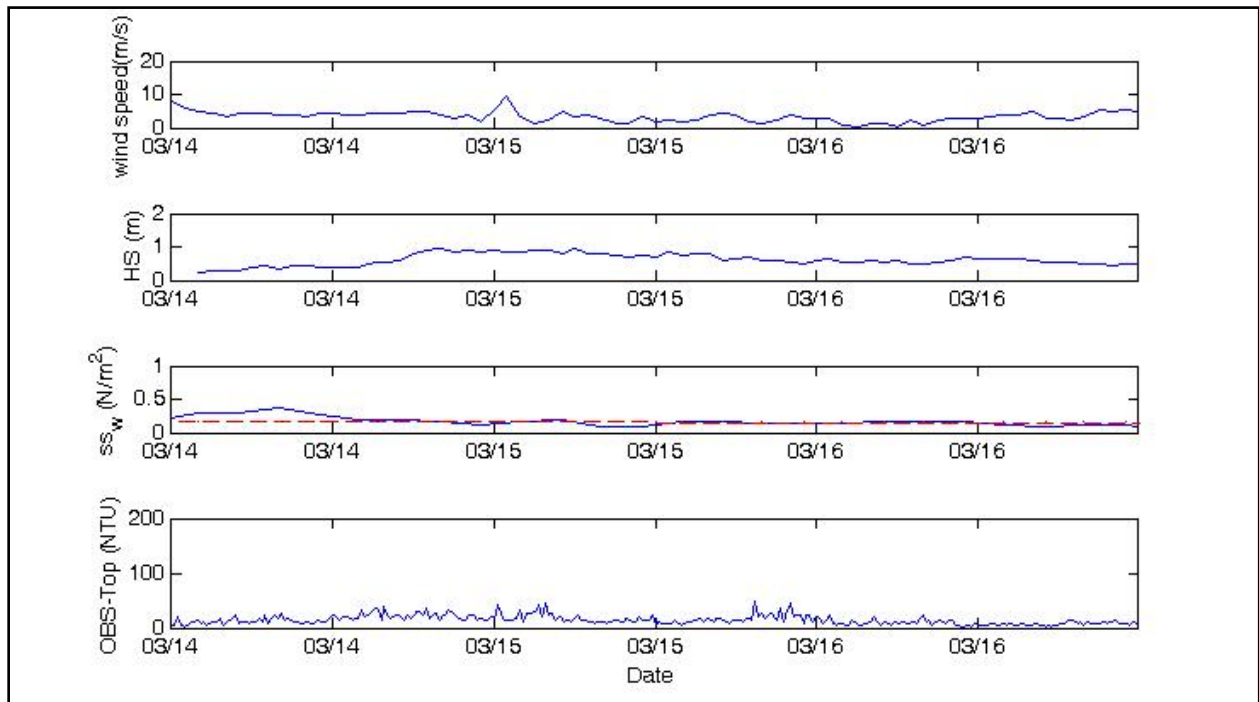
Figure 3.41   Bottom boundary layer parameters during the cold fronts.

The dashed line in red corresponds to the threshold for re-suspension of the bottom sediments.

High Wind Regime

As shown in the results, some of the wave and bottom boundary parameters did not correspond to the cold front passages but did correspond to the high wind regime (e.g., from March 22 to 30 and from April 15 to 23). Figure 3.42 shows time series plots of wind speed, Hs, the shear stress, and OBS data from March 22 to 29, corresponding to a high wind event in the study area. According to the weather maps, during the above period high wind from south or south east persisted. These wind regimes were associated with the high shear velocity, shear stress and OBS values. OBS had the maximum value on March 24 (Figure 3.42).
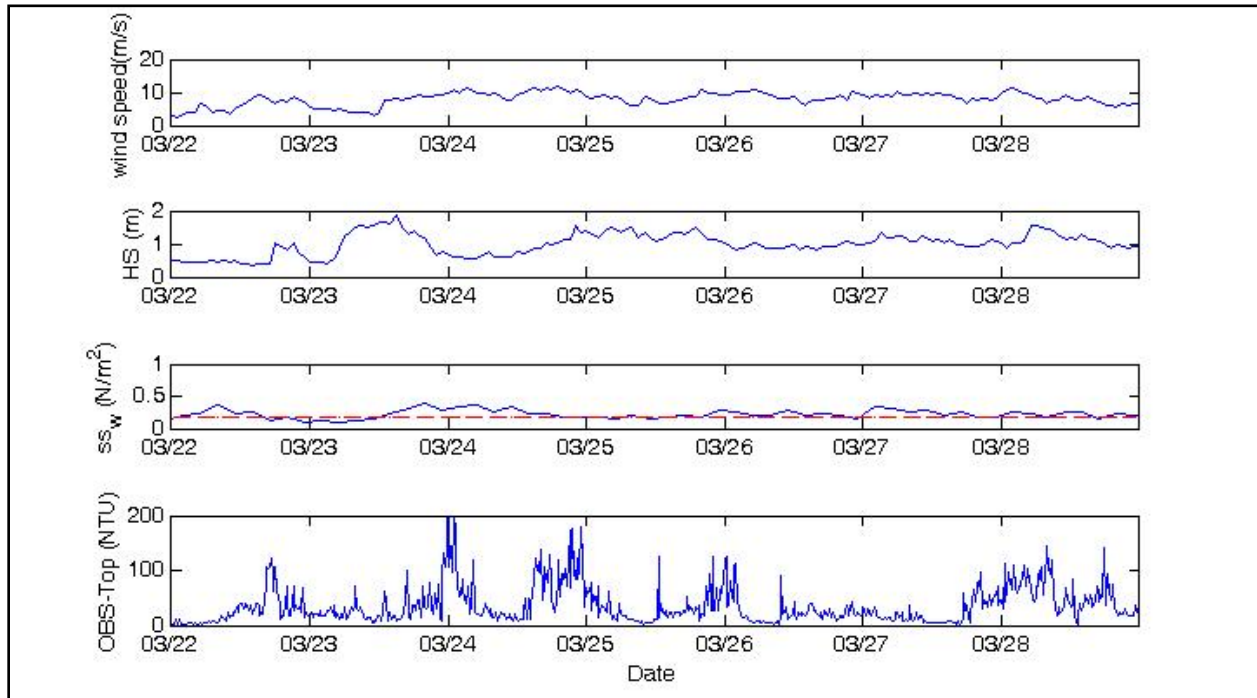
Figure 3.42   Bottom boundary layer parameters during high wind regime.

The dashed red line corresponds to the threshold for re-suspension of the sediments.

This study shows that during the high wind period, waves had high shear velocity and shear stress which were higher than the threshold for the sediment re-suspension and as strong as that during cold front events. Hence, both waves and currents can strongly re-suspend the sediment during this period as well as during the cold front events. We checked the meteorological data, wave data, and OBS at the CSI3 station, corresponding to our survey period (Stone et al. 2001; Stone et al. 2003). OBS data had high values from March 22 through 30 at CSI3, which corroborates with our survey results. Therefore, it is inferred that this situation is not only confined to the western Louisiana coast but a common characteristic all along coastal Louisiana. Crout and Hamiter (1981) showed the relationship between seasonal wind variations and sediment transport based on the field measurements along the western Louisiana inner shelf; however, no detailed discussion is available from that study. We are also not attempting detailed discussion at this point due to the shortage of data from our pilot study. Additional data should be collected; especially on sediment characteristics, bed form characteristics (ripple height and

wavelength), as well as supplemental wave and current data, so that we can correlate the high wind events with the sediment transport processes.

Considering these three conditions, waves during fair weather usually cannot re-suspend the sediment, and waves during the cold fronts and high wind regime can sufficiently re-suspend the sediments. Therefore, it is suggested that cold fronts and high wind regime considerably affect bottom boundary layer dynamics on Sabine Bank.

Summer Season

For the summer season bottom boundary layer dynamics and sediment transport are not significant because cold fronts passages are infrequent and do not enter the Gulf of Mexico. However, our results indicate that occasional high wind, due to high pressure systems following summer cold fronts, significantly influence hydrodynamic and bottom boundary layer dynamics in summer. Meteorology is more complicated during summer than during winter, including the seasonal wind reversal from the southeast to southwest (cf. Cochrane and Kelly 1986). The dynamics are also affected by the bank topography; the currents are deflected due to the shallow complex bathymetry (Pepper 2000) and are accelerated over the bank crest due to shallow bathymetry to satisfy continuity (Snedden and Dalrymple 1999). Results during the 2008 deployments and from Kobashi et al. (2005) suggest that a dominant force that may affect bottom sediment suspension is occasional high wind associated with high pressure following cold fronts. The frequency of this high wind regime is not as frequent as cold fronts, approximately once every two to three weeks; however, hydrodynamic forcing can be as high as winter storms and, as a result, the influence of this high wind regime on bottom boundary layer is likely significant.

Current structure is complicated and affected by wind, tide, water level and shallow bathymetry, although the primary forcing is likely wind. Kobashi and Stone (2008b) discussed a strong response of water level and wind variation to currents for their Ship Shoal study. They also discuss the influence of Ekman currents associated with the Coriolis force on currents, particularly when winds blow alongshore. Such a characteristic was not captured during all Sabine Bank deployments.

Hydrodynamics and bottom boundary layer dynamics vary considerably with bed characteristics; for example, sediment type (sand or mud), existence of wave or mega ripples. Limited available data did not allow us to further examine such heterogeneous sediment dynamics which are in greater detail discussed by Kobashi and Stone (Kobashi and Stone 2008a, b).

CHAPTER 4: WAVE AND HYDRODYNAMIC MODELING

4.1. INTRODUCTION

The potential for exploiting offshore sand resources from the outer continental shelf as a source of sediment for beach and barrier island restoration has grown rapidly as similar sources in state waters are depleted or are in a position not to be borrowed from for the sake of adjacent beaches (Byrnes et al. 1999; Michel et al. 2001; Kelley et al. 2004; Maa et al. 2004; Pepper and Stone 2004; Khalil et al. 2007). This situation becomes even more relevant along the northern Gulf Coast as these areas have been eroding at an alarming rate (National Research Council 2006). However, beach nourishment programs can potentially cause adverse environmental impacts at beach fill locations and borrow sites when an offshore sediment source is mined. The physical effects of offshore sand mining on the incident wave field and associated sediment transport regime may alter local shoreline change. Moreover, irregular bottom topography, associated with offshore shoals and banks, has been known to influence coastal hydrodynamics and bottom boundary layer dynamics (Stone and Xu 1996; Pepper and Stone 2004). Inner shelf shoal bathymetry generates unique hydrodynamics which may have a profound influence on the endemic biological and sedimentary environments (Swift 1985; Snedden and Dalrymple 1999; Condrey and Gelpi 2008). Bathymetric highs act as submerged breakwaters to mitigate deep water waves and, therefore, changes wave refraction, flow patterns, and consequent sediment transport patterns (cf. Stone and Xu 1996; Pepper and Stone 2004; Stone et al. 2004; Jose et al. 2007; Kobashi and Stone 2008a, b).

Wave transformation studies in shallow water have been limited primarily to numerical model analysis and laboratory experiments, given the complex nature of dynamics (e.g., Horikawa et al. 1977; Kraus et al. 1988; Stone and Xu 1996; Byrnes et al. 2003; Maa et al. 2004; Johnson et al. 2005). Stone and Xu (1996) investigated wave transformation over a shore-parallel sand body, Ship Shoal, located roughly 25 km (15.53 mi) off the coast of south-central Louisiana and surrounded by the 10 m isobath. They implemented a spectral wave model, STWAVE (Smith et al. 2001), with constant input parameters (i.e., deepwater wave height/direction and wind speed/direction), based on wave-climate analyses and hypothetical post-dredging bathymetric configuration in which the entire shoal was removed. They concluded that prevailing southeast waves impacted the most in terms of wave refraction and dissipation, particularly along the western flank of the shoal; the ultimate impact of sand removal on the shoreface of barrier islands were negligible for all model runs. STWAVE is, however, a "half-plane" wave model and this study was limited to waves (both swells and seas) from the southern quadrant, and, therefore, detailed mechanisms of waves, particularly associated with post-frontal winds, current variability and sediment transport associated with sand removal, are not well understood. Jose et al. (2007) implemented a "full-plane" third generation spectral wave model, MIKE21 SW, to investigate wave transformation over a shallow shoal and qualitatively addressed the importance of wave dissipation and wave-wave interaction associated with winter cold fronts. There is a growing number of publications that examine hydrodynamics associated with sand mining, particularly waves and their impacts on longshore transport along beaches and barriers (Stone and Xu 1996; Byrnes et al. 2003); however, little has been discussed regarding the alteration in hydrodynamics and sediment transport over the sand bodies as a consequence of targeted mining.

Kobashi et al. (2009b) implemented a coastal ocean model package, MIKE, developed by DHI^{TM} Water and Environment, to investigate wave transformation and current variations on Ship Shoal, further east of the study area. The study examined wave and current variability and sediment transport over the shoal with respect to the bathymetry modification that was based on the proposed barrier island restoration scenarios to be implemented for the region. This study has also taken into consideration two representative energetic events viz., winter storms and tropical cyclones.

Little work has been conducted to investigate Sabine Bank (see Figure 2.2 in Chapter 2), particularly in considering the wave and hydrodynamic characteristics associated with the bank. Sand mining from the bank for restoring the adjacent beaches may cause profound impacts on the local physical and biological environments; therefore, understanding the prevailing hydrodynamics has a key role in assessing these impacts. Using a third-generation, state-of-the-art numerical model, the hydrodynamics of the region corresponding to three contrasting bathymetric configurations have been compared: one with shoal and the others with the shoal partially excavated for (a) a series of coastal restoration projects proposed for the Louisiana-Texas coast and (b) for the Holly Beach, Louisiana, restoration. The mining area and the estimated volume to be borrowed have been provided by the MMS (now BOEM).

Two mining locations were proposed for Sabine Bank (Figure 4.1). The areas demarcated with yellow polygons over the west and the east shoal corresponds to a number of beach nourishment projects along the Louisiana and Texas coasts (hereafter referred to as a "cumulative scenario"). Post-mining bathymetry for this cumulative scenario is given in Figure 4.2. The area designated with a light blue polygon within the yellow polygon is assigned for Holly Beach restoration; the post-mining bathymetry is given in Figure 4.3. The details of the volume of sand to be extracted from these sites are provided in Table 4.1. Unlike Ship Shoal, Sabine Bank is comparatively devoid of pipelines connecting the offshore oil and gas infrastructure.
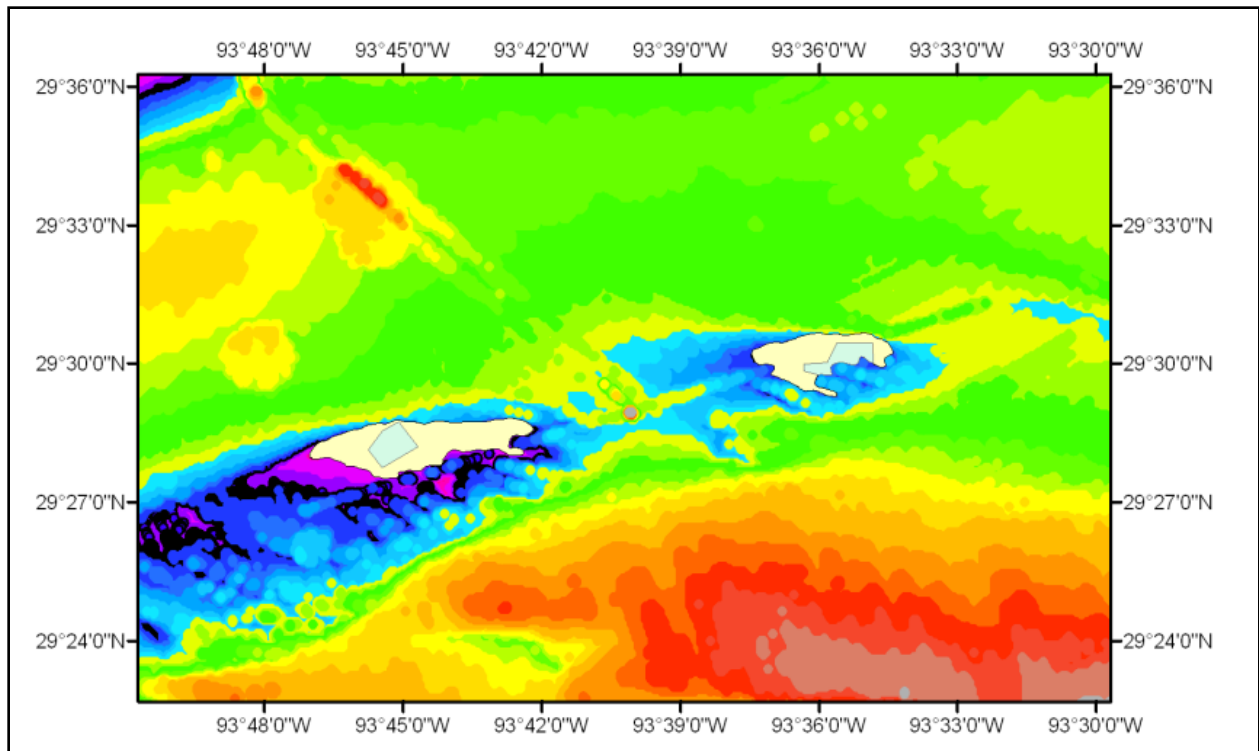
Figure 4.1   Proposed mining areas designated for Sabine Bank.

Yellow polygons over the west and east shoals are designated for a number of beach nourishment projects. The smaller light blue polygons are designated for Holly Beach restoration. The volume and area are provided by MMS (now BOEM).
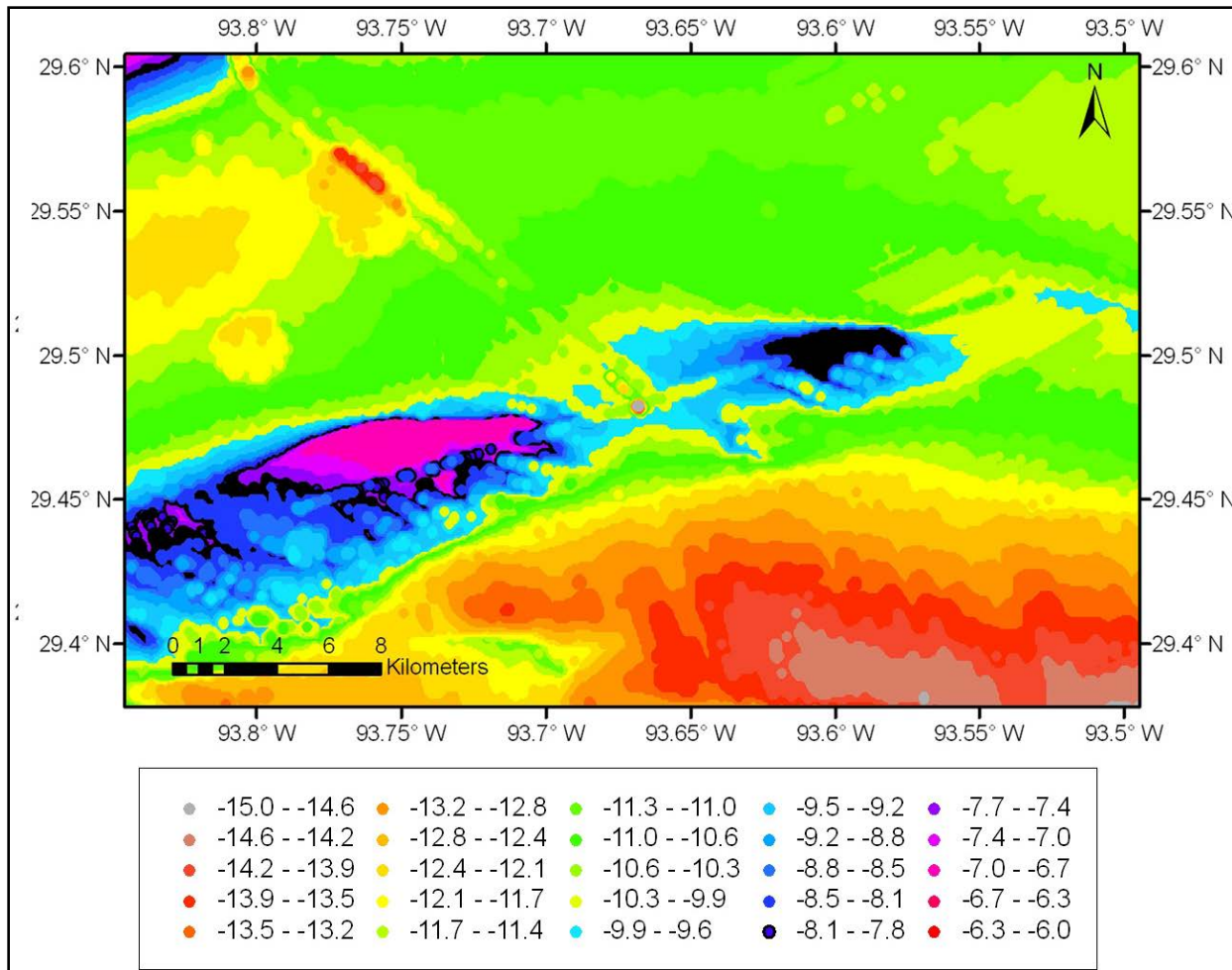
Figure 4.2   Post-dredging bathymetry for the cumulative scenario.

The western shoal would be dredged down to the 7 m isobath, while the eastern shoal would be dredged down to the 8 m isobath. Volume and area were provided by MMS (now BOEM).
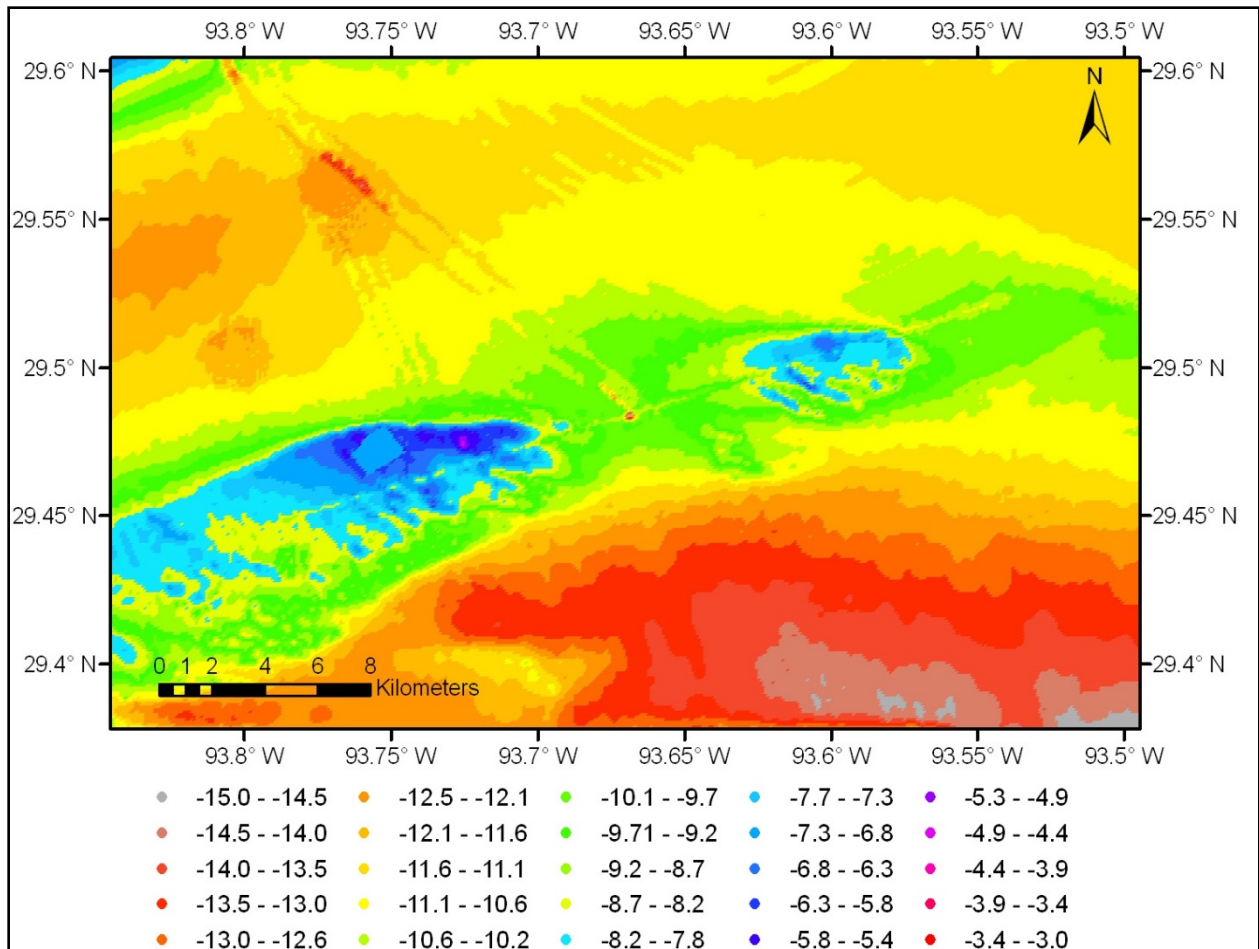
Figure 4.3   Post dredging bathymetry for the Holly Beach restoration project.

The western shoal would be dredged down to the 7 m isobath while the eastern shoal would be dredged down to the 8 m isobath. Volume and area are provided by MMS (now BOEM).

As a complement to our comprehensive research for Ship Shoal, covering the physical, biological and fisheries aspect of the largest shoal in Louisiana coast, the inferences from the present physical study for Sabine Bank can be extended to such similar shallow banks elsewhere.

Table 4.1

Sabine Bank Sand Resources

Area	Restoration area	Volume (m^3)	Post mining bathymetry	
			West	East
West and East Shoals	TX/LA coast	17 million	7m	8 m
West and East Shoals	Holly Beach	3.2 million	7 m	8m

Source: Geoffrey Wikel, MMS (now BOEM)

4.2. MET-OCEAN CONDITIONS OF THE REGION

Wind and wave data from the region were analyzed using *in-situ* data from the National Data Buoy Centre (NDBC) buoy 42035. Surface current data from the TABS database were analyzed for the current variability. In addition, wave data from deployments conducted along the eastern shoal were also analyzed for the regional variability of wave fields in the region. Annual met-ocean conditions of the region, based on NDBC 42035 are provided in Figure 4.4. Wave-climate for the study area is characterized by low-energy regime that has been well documented (Georgiou et al. 2005). The *in-situ* data from the offshore buoy (2006/01/01-2006/12/31) indicated that approximately 86 percent of the duration of this study, wind speed was less than 10 m s^{-1} and 14 percent between 10 and 15 m s^{-1}. Because no major hurricanes or tropical storm made landfall on the coast in 2006, no wind speeds greater than 15 m/s were recorded. Wind predominantly blew from the north to southwest, but its direction was variable (Figure 4.4). Significant wave height (hereafter "wave height") was usually less than 1.0 m and only 2.0 percent of the wave heights exceeded 2.0 m (6.56 ft). Wave direction varied between the east and southwest.
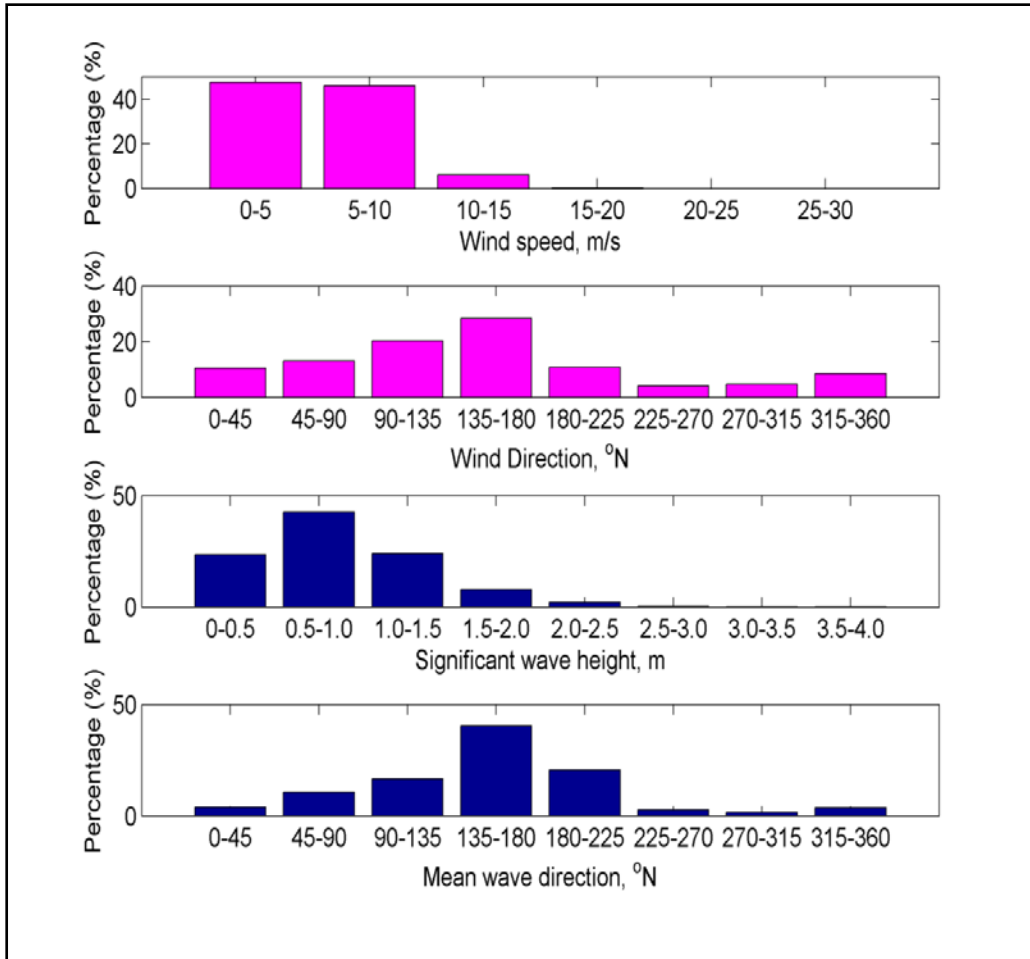
Figure 4.4   Annual met-ocean statistics compiled from NDBC 42035 buoy data.

The buoy is located off the Galveston Bay, Texas.

The wave direction from the northern quadrant was associated with winter storms and to some extent with the sea and land breezes (Hsu 1988; Kobashi et al. 2005; Stone et al. 2005; Kobashi et al. 2009a).

4.3. MODEL EXPERIMENT

A third-generation spectral wave model, MIKE21 SW (SW) and three-dimensional hydrodynamic model, MIKE3 HD (HD) were implemented in this study. Both models have been developed by DHI[TM] Water and Environment. The SW model has been successfully implemented for the Gulf of Mexico and the Louisiana shelf (Jose and Stone 2006; Jose et al. 2007) as part of a wave forecasting study. Kobash et al. (2009b) implemented the model for Ship Shoal and Spaziani et al. (2009) implemented the model for the Florida Panhandle. The HD model has been implemented for the south central Louisiana coast (Kobashi et al. 2009b), to study the flow characteristics of the Ship Shoal. Detailed model descriptions including the

models, domain, and input parameters, as well as initial conditions are briefly described in the following sections.

4.3.1. SW module

SW is a third-generation spectral wind wave model based on unstructured meshes. The unstructured mesh approach gives the model a high degree of flexibility. The model solves the wave action balance equation, the spatial discretization of which is performed using an unstructured finite volume method. The integration in time is based on a fractional step approach, where the propagation steps are solved using an explicit method (Sorensen et al. 2004). The wind input, the main source function in the equation, is based on Janssen's quasi-linear theory of wind-wave generation (Janssen 1989; Janssen 1991) and implemented as WAM Cycle 4. The non-linear energy transfer through the four-wave interaction is represented by the discrete interaction approximation (DIA) proposed by Hasselmann and Hasselmann (1985) (see also Komen et al. 1994). The dissipation due to white capping is implemented according to Hasselmann (1974) and further adjusted according to Janssen (1989). Detailed descriptions of all the source functions and the numerical methods used in the model are elaborated in Sorensen et al. (2004).

4.3.2. HD module

HD simulates water level variations and flows in response to a wide variety of forcing in lakes, estuaries, bay and coastal areas (DHI 2005). The module solves a three-dimensional incompressible Reynolds-averaged Navier Stokes equation. The model consists of momentum and continuity equations; temperature and salinity equations are closed by a turbulent closure scheme. The model solves horizontal terms explicitly and the vertical term implicitly (DHI 2005). Horizontal and vertical eddy viscosities were based on Smagorinsky formulation and the k-ε equation, respectively (DHI 2005). Bed resistance is computed based on the quadratic stress law. Vertical discretization can be selected from either equidistant, layer thickness, or variable grids, which consist of uniform distribution, user specified distribution, stretched distribution, and top/bottom specified distribution, respectively (DHI 2005). In the study, the equidistant discretization was used. More detailed model information is elaborated on in DHI (2005).

4.3.3. Model domains

The model domain (origin: 95.0ºW, 29.0ºN) covered Sabine Bank, the entire coastline sheltered by the bank, the NDBC station 42035, and TABS stations F and R (see Figure 2.2 in chapter 2). Three bathymetries were used: one with Sabine Bank and the others with two mining scenarios (Figures 4.2 and 4.3). The computational grids were unstructured triangular mesh grids with an embedded high resolution mesh grid encompassing the shoal boundary (Figures 4.5 and 4.6). The mesh size was based on the volume of each grid each with a maximum size of 1.0×10^{-5} degree^2 over the shoal and 2.5×10^{-4} degree^2 over the surrounding areas. An intermediate mesh with resolution 5.0×10^{-5} is used to connect the two regions. For the HD model, offshore mesh size was selected as 2.0×10^{-3} degree^2. For the case study A (Table 4.3), deep water boundary conditions were applied along the southern boundary and the east and west boundaries were

selected as radiative boundaries for the SW model. In the HD model, all three boundaries (North is land) were treated as closed boundaries (Table 4.3). The coastal wave model was nested with the Gulf of Mexico (GOM) regional model for the additional case studies. A detailed description of the regional wave model is addressed in Jose and Stone (2006). For the HD model, in order to avoid vortex effects near the closed boundaries, the computational domain was selected much larger than that of the wave model and the southern boundary extended up to 28°N.
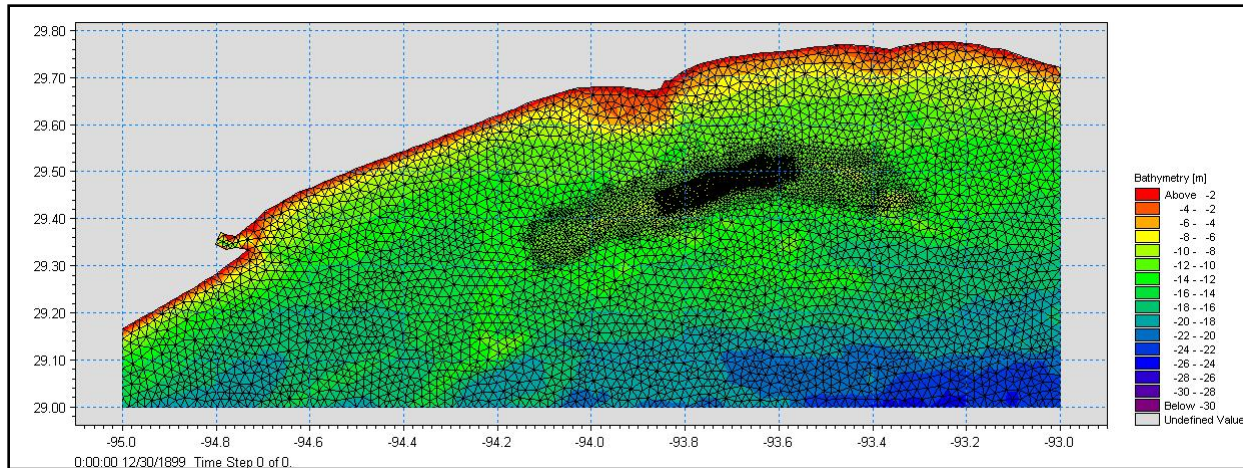
Figure 4.5   Computational mesh used for wave modeling.

High resolution grid for the bank is nested with the coastal model.
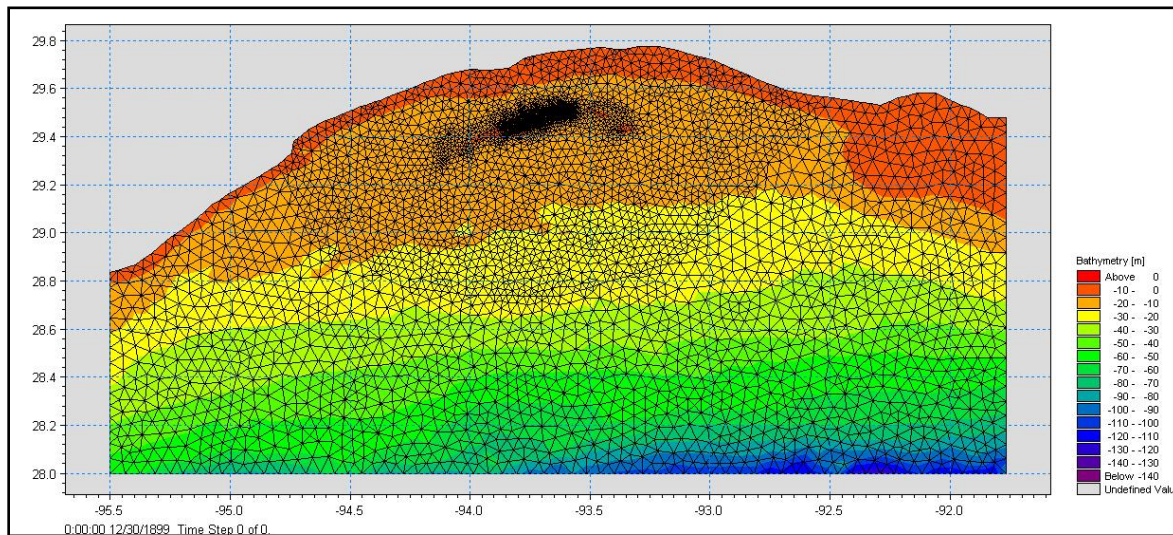
Figure 4.6   Computation mesh used for hydrodynamic modeling.

The domain has been extended to 28° south.

4.3.4. Input parameters and initial conditions

Input parameters were carefully selected from various data sources. For both GOM regional and high resolution coastal models, wind data from a re-analyzed hindcast model by NOAA NCEP

66

(North America Regional Reanalysis: NARR) were used (Mesinger et al. 2006). A wind friction coefficient was selected as the constant value of 0.003 rather than linearly varying coefficients.

Bathymetry data from the NGDC (National Geophysical Data Center) coastal relief model (Divins and Metzger 2008) were used. For the GOM model, ETOPO2 bathymetry was also used. In order to keep initial conditions of all model cases consistent, bottom friction for the SW model was estimated from a constant, Nikraudse roughness height as 0.04 m (0.13 ft), rather than that from grain diameters based on Nielsen (1979); results of this preliminary model implementation showed little difference between the two friction factors. For the HD model, the bottom friction was estimated from the quadratic stress law using bottom drag coefficient. Water level was obtained from a global tide prediction model (Andersen 1995) for each boundary (east west and south). The HD model was implemented as barotropic, and mode and density changes (e.g. stratification) were not considered. Also, for simplicity, effects of waves on currents were not included.

Time step was selected as 150 seconds for the SW model and 10 seconds for the HD model. It should be noted that the MIKE 21 SW wave model is not capable of simulating waves over the muddy seabed, which is the case for the Louisiana shelf (Sheremet and Stone 2003). Therefore, wave dissipation over a muddy bottom is not discussed in this report.

The HD model implementation for the shoal is incomplete as the model calibration and validation need even higher resolution bathymetry. The results from the hydrodynamic study will be included in the final report submission.

4.3.5. Case studies

Based on the annual met-ocean statistics from the study area and the data used by Stone and Xu (1996), various wave climate conditions were selected to implement the wave and hydrodynamic models for Bank, with three different bathymetric configurations: one with the shoal and the other two with realistic mining scenarios, viz., cumulative scenario and Holly Beach restoration. For both models, four wind conditions were selected, namely, severe storms (case A1), strong storms (case A2), moderate storms (case A3) and weak storms (case A4) (see Table 4.2). Stone and Xu (1996) concluded from their case study, which consists of offshore waves propagating from three different directions along the southern boundary, that the waves from the southeast along with predominant southeast winds yielded maximal changes in wave refraction and the highest dissipation rates. In this study, based on the annual wave statistics compiled from NDBC 42035, deepwater wave boundary conditions were selected as the south-southeast waves (i.e., 160 degrees) along the southern boundary (Figure 4.5 and Table 4.3). Constant winds in the domain were incorporated for varying wind speeds and directions listed in Table 4.2. In this study, four wind directions were selected based on our wave climate result as shown in Figure 4.4. Wave model results were further analyzed to estimate sediment re-suspension intensity (RI).

In addition, another case study based on winter storm conditions (2004/03/11- 2004/03/22) was also conducted. Three scenarios based on different bathymetries were carried out in order to examine impacts of potential sand mining on wave transformation over the shoal.

Table 4.2

Case Study A: Wind Condition (Constant in Domain)

Case	Speed (m/s)	Direction (degree)
A1	15	NE(45), SE(135), SW(225), NW(315)
A2	12	NE(45), SE(135), SW(225), NW(315)
A3	10	NE(45), SE(135), SW(225), NW(315)
A4	5	NE(45), SE(135), SW(225), NW(315)

Table 4.3

Case Study A: Offshore Wave Boundary Condition (South Boundary)

Case	H_S (m)	T_P (sec)	Direction (degree)
A1	6	11	160
A2	4	9	160
A3	3	7	160
A4	2	6	160

4.4. SKILL ASSESSMENT OF THE MODELS

Model validation was conducted using various *in situ* data sets, ranging from tripod deployments (March 2004 deployments, see Figure 2.2 in Chapter 2 for the locations), and archived data NDBC 42035 station. Figures 4.7 and 4.8 show comparisons between the measured and the simulated values of various parameters including wind speed, wind direction, wave height, peak period and mean wave direction at NDBC 42035. *In situ* wind data is in good agreement with the NARR wind data except during storm peaks when the NARR wind speed was often lower than the *in-situ* data, as also reported by Jose et al. (2007) (Figure 4.7). Figure 4.9 shows the comparison between the *in situ* observations from 2004 winter deployments and the simulated wave parameters. The wave data measured from the crest of the shoal and an offshore location (see Figure 2.2 in Chapter 2 for the locations) was used for this purpose.

For the spectral wave model, all measured and simulated wave parameters agreed reasonably well. The discrepancy between the model results and measured data can be attributed to the resolution and accuracy of the input wind data. It is clear that wave models are extremely sensitive to wind inputs. For a fully developed sea, sensitivity experiments revealed that small errors in the input wind can result in considerable differences in the computation of wave parameters (Sarkar et al. 2000). However, for the offshore locations, the model winds are generally in good agreement with the measured data. Jose and Stone (2006) reported very strong correlation between the NARR model wind data and measured data from the National Data Buoy Centre (NDBC) buoys off the Louisiana coast.
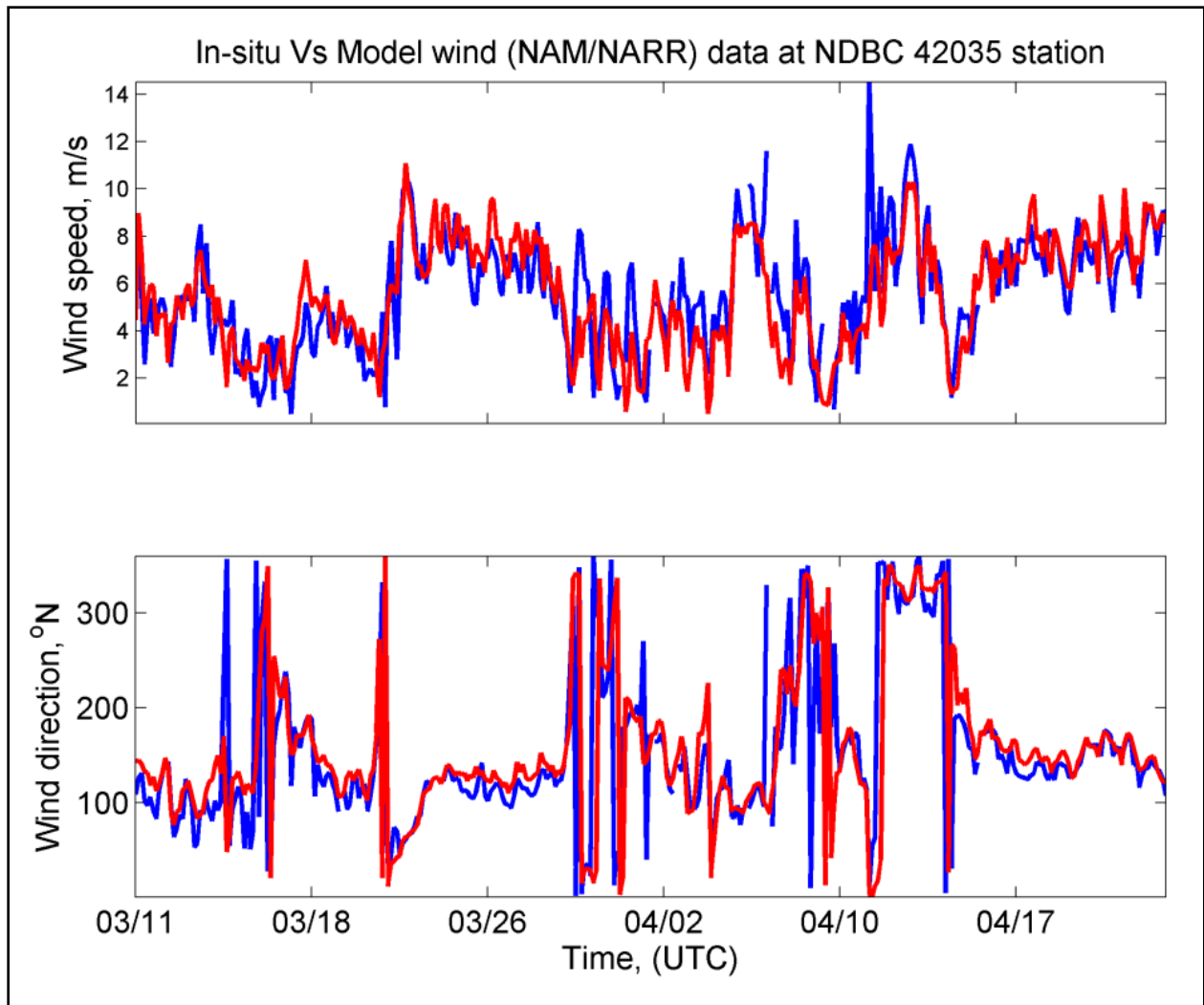
Figure 4.7   NCEP/NARR (North American Regional Re-analyzed) model wind data used for driving the wave and hydrodynamic models.

The model winds are in good agreement with the *in situ* observations from NDBC Buoy 42035.
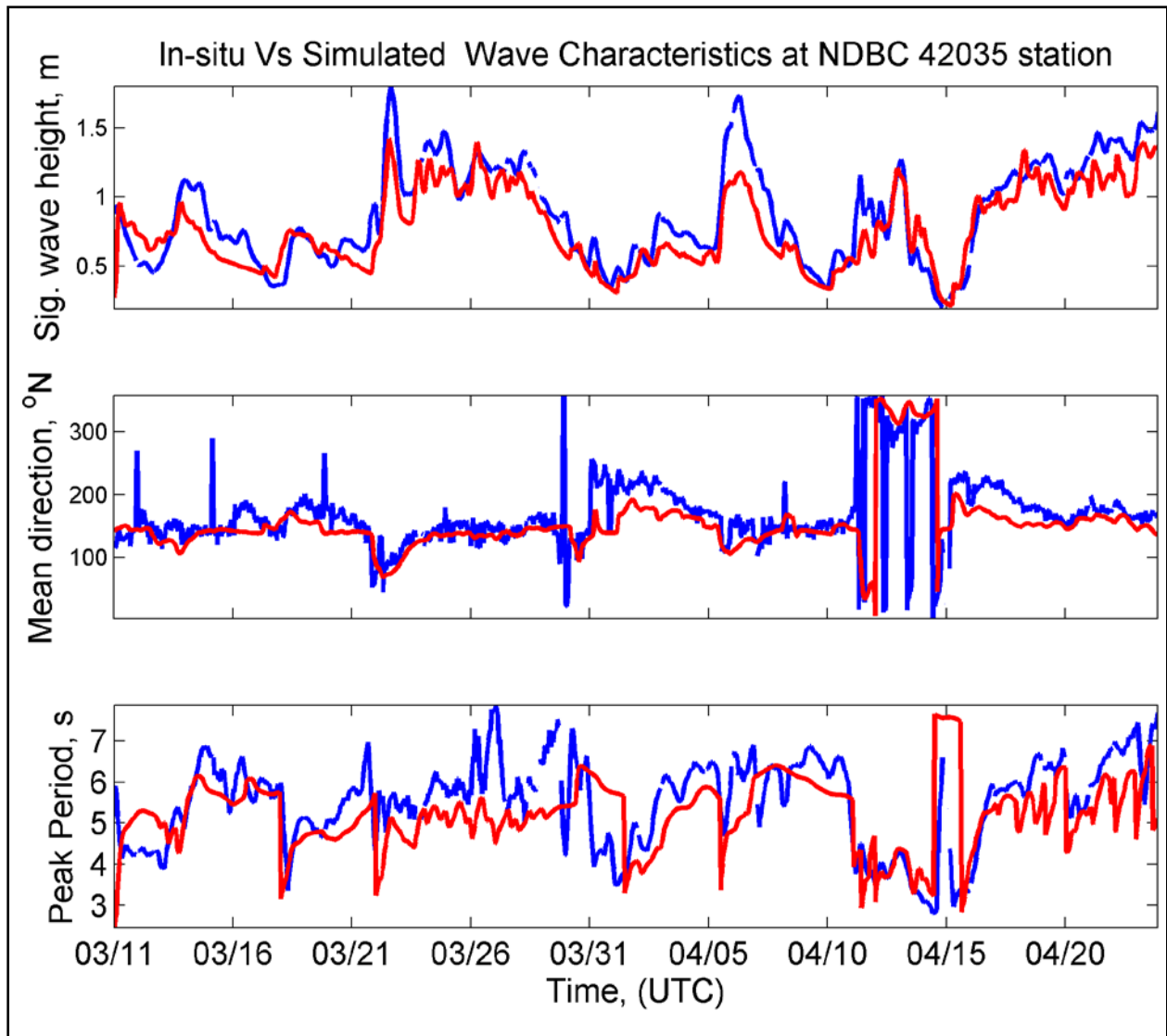
Figure 4.8   Simulated bulk wave parameters plotted against the in situ wave observation from
             NDBC buoy 40235.

Note that during the peak of the winter storms the model generally under-predicts the wave
parameters.
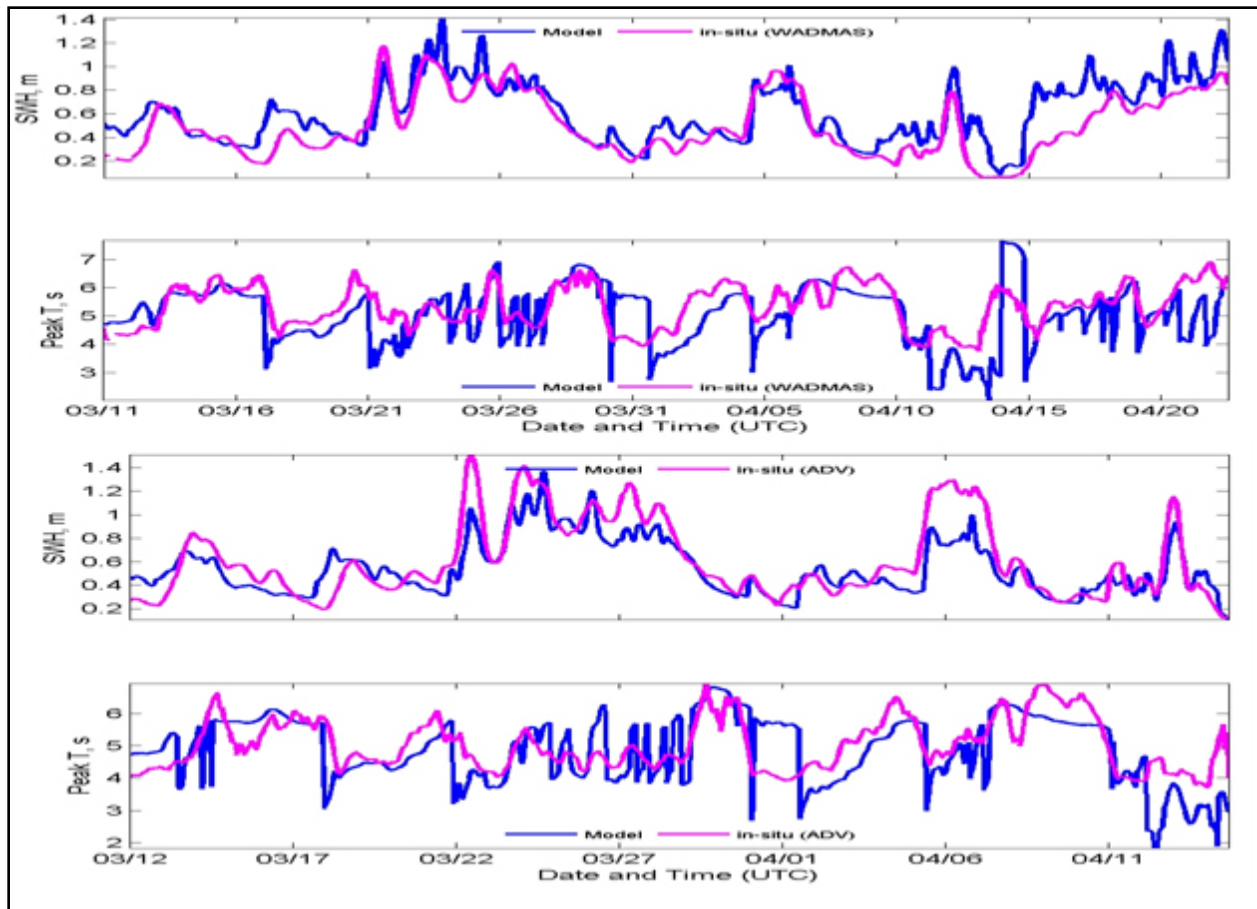
Figure 4.9   Simulated wave parameters for Sabine Bank plotted against measured data from the March 2004 deployments.

Top figures correspond to wave observations from the crest of the shoal and the bottom figures correspond to observations from an offshore location. The measurement locations are given in Figure 2 (Chapter 2).

4.5. RESULTS AND DISCUSSION

4.5.1. Wave transformation over the shoal

Incoming deep water waves significantly transformed as they propagated over complex shoal bathymetry. Six locations, with contrasting bathymetry, were selected from the study area where wave and re-suspension characteristics were computed for comparison (see Figure 4.10). Station A was located at the extreme western boundary of the shoal and B and D were located at the crests of the western and eastern shoals. Station C was in the Channel, separating the two shoals. Stations E and F were taken as controls for monitoring the offshore and nearshore conditions. Data from these latter two stations were not presented nor discussed here as the hydrodynamic variability associated with mining scenarios was confined to the vicinity of the shoal. Spatial difference in the wave transformation was similar for all cases although differences in magnitude occurred (Table 4.4). Particular attention was given to wave dissipation and refraction for

71

different bathymetries. Figure 4.11 provides the wave transformation over the shoal for different model waves and atmospheric conditions (Cases A1- A4). It has been observed that the presence of the shoal substantially dissipates the incoming waves even for moderate storm conditions (Case A4). In Figures 4.12–4.15, wave height and wave vector distributions for different mining scenarios are presented. When the wave height was high (Case A1 in Figure 4.12), substantial wave refraction on the western shoal was clearly evident compared to that with partial removal of the shoal (Cumulative scenario, Figure 4.12 middle). As the deep water wave height was low, the difference became less evident. On the eastern shoal the difference in the refraction with partial removal of the shoal was minimal (Figure. 4.12). The alteration in wave conditions associated with the Holly Beach mining scenario was un-noticeable for both the western and eastern shoals (Figure 4.12 bottom). The wave height on the western shoal was lower than that on the eastern shoal (up to 15 percent difference between the east and west). When the shoal existed, the difference was up to 3 percent higher than the difference with partial removal of the shoal (cumulative scenario). The spatial difference in wave height decreased as the deepwater wave height decreased (less energetic conditions as given in Table 4.4). Wave height between the two shoals, as a general trend, increased from the west toward the east with the percentage of difference decreasing with decreasing offshore wave conditions. The dissipation in the wave height on the western shoal was approximately 12 percent higher than that on the eastern shoal; for the model result with partial mining (cumulative scenario), the difference in the height was just 2 percent lower. The dissipation rate progressively decreases for lesser met-ocean conditions (see Figures 4.13–4.15). The variability in the peak wave period for different met-ocean boundary conditions are provided in Figures 4.16–4.19. Peak wave period simulated for the two shoals, with Case A1 met-ocean conditions, showing insignificant changes for the cumulative mining scenario (Figure 4.16). The above results indicate that the shoal has significant influence on wave energy dissipation; however, the impacts of restricted mining on the wave refraction, were minimal. The above results further influence sediment re-suspension on the shoal, which is discussed in section 5.2.

Table 4.4

M21 SW Model Result with Shoal (left) and with Cumulative Mining (right) and
Holly Beach Restoration Case (in red)

Parameter	Case	Outer west	West	Channel	East
H_S (m)	1	3.75 (3.75) 3.75	2.72 (2.89) 2.79	3.57 (3.57) 3.57	3.18 (3.27) 3.20
	2	3.28 (3.29)3.28	2.65 (2.80)2.70	3.11 (3.12) 3.12	2.99 (3.04) 3.02
	3	2.29 (2.29) 2.29	2.29 (2.32) 2.30	2.22 (2.22) 2.22	2.31(2.25) 2.31
	4	0.87 (0.87) 0.87	0.98 (0.97) 0.97	0.95 (0.95) 0.95	0.78 (0.78) 0.78
PeakT (seconds)	1	11.18 (11.18)11.18	11.15 (11.17)11.16	11.22 (11.22)11.22	11.17 (11.19)11.17
	2	9.23(9.23) 9.23	9.20 (9.22) 9.21	9.25 (9.25) 9.25	9.20 (9.20) 9.20
	3	7.3 (7.3) 7.3	7.47 (7.47) 7.47	7.43 (7.43) 7.43	7.50 (7.48) 7.50
	4	6.05 (6.05) 6.05	6.14 (6.13) 6.13	6.12 (6.12) 6.12	6.16 (6.15) 6.16
RI ($N\ m^{-2}$)	1	1.38(1.38)1.38	1.25 (1.22) 1.76	1.23 (1.23) 1.23	1.37 (1.28) 1.38
	2	1.25 (1.25) 1.25	1.30 (1.25) 1.21	1.10 (1.10) 1.10	1.36 (1.25) 1.37
	3	0.83 (0.83) 0.83	1.17 (1.06)1.05	0.74 (0.74) 0.74	1.05 (0.90) 1.05
	4	0.19 (0.19) 0.19	0.40 (0.34) 0.34	0.19 (0.19) 0.19	0.24 (0.19) 0.24
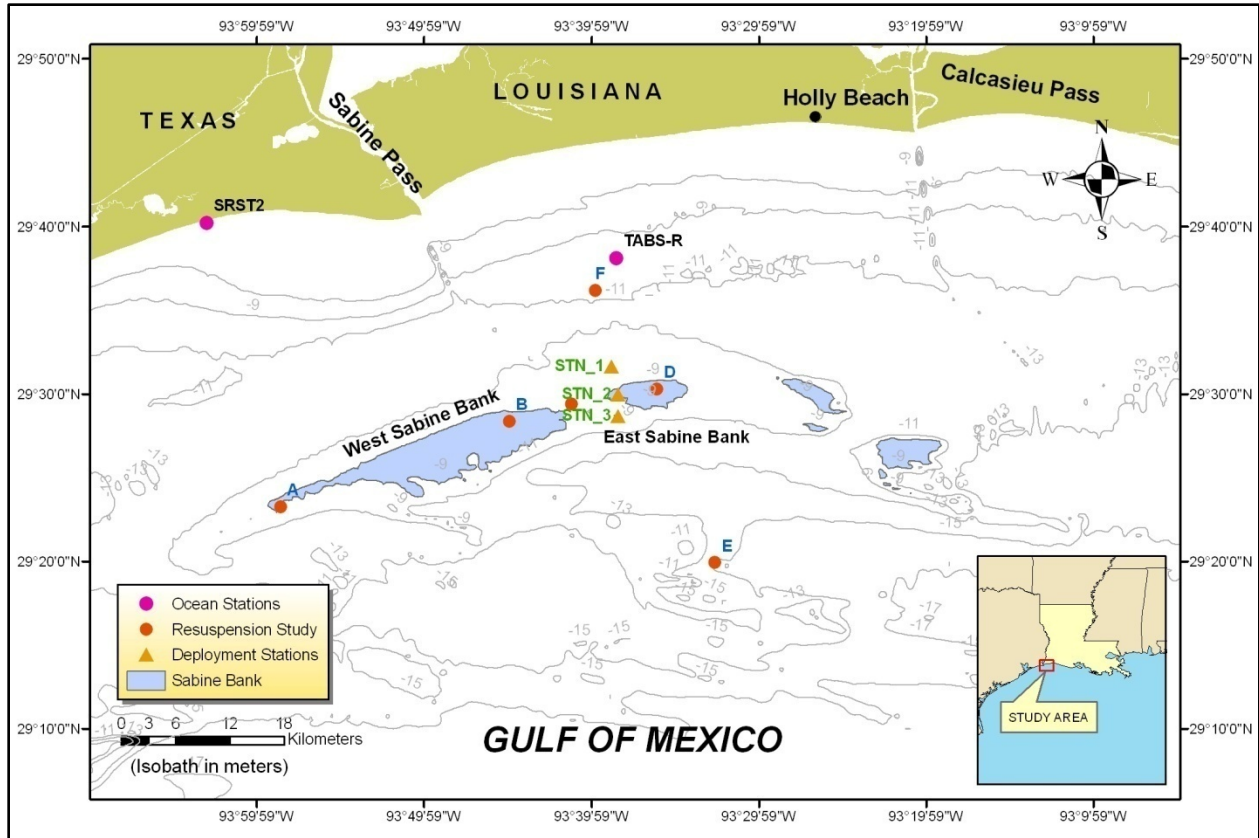
Figure 4.10   Location map for the study area with the locations where wave and re-suspension characteristics were computed for comparison.

Station A is located at the extreme western boundary of the shoal. Stations B and D are located at the crests of the western and eastern shoals, respectively. Station C is in the channel separating the two shoals. Stations E and F were taken as control points.
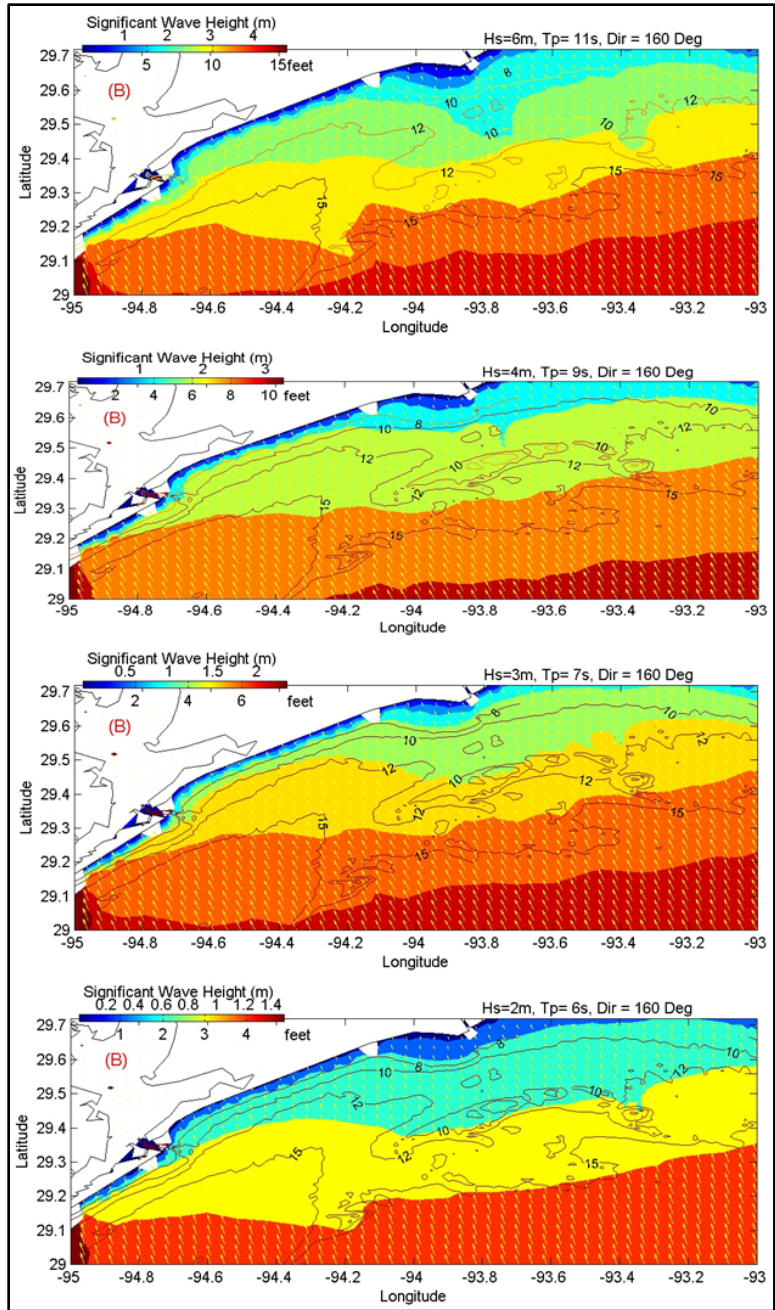
Figure 4.11   Wave transformation over the shoal for different model waves and atmospheric conditions.

From top to bottom the wind direction is from 135°N (SE wind) with speed ranging from 15 m/s, 12 m/s, 10 m/s and 5 m/s. This represents different storm conditions for the Louisiana-Texas coast. Note the model wind characteristics for each case.
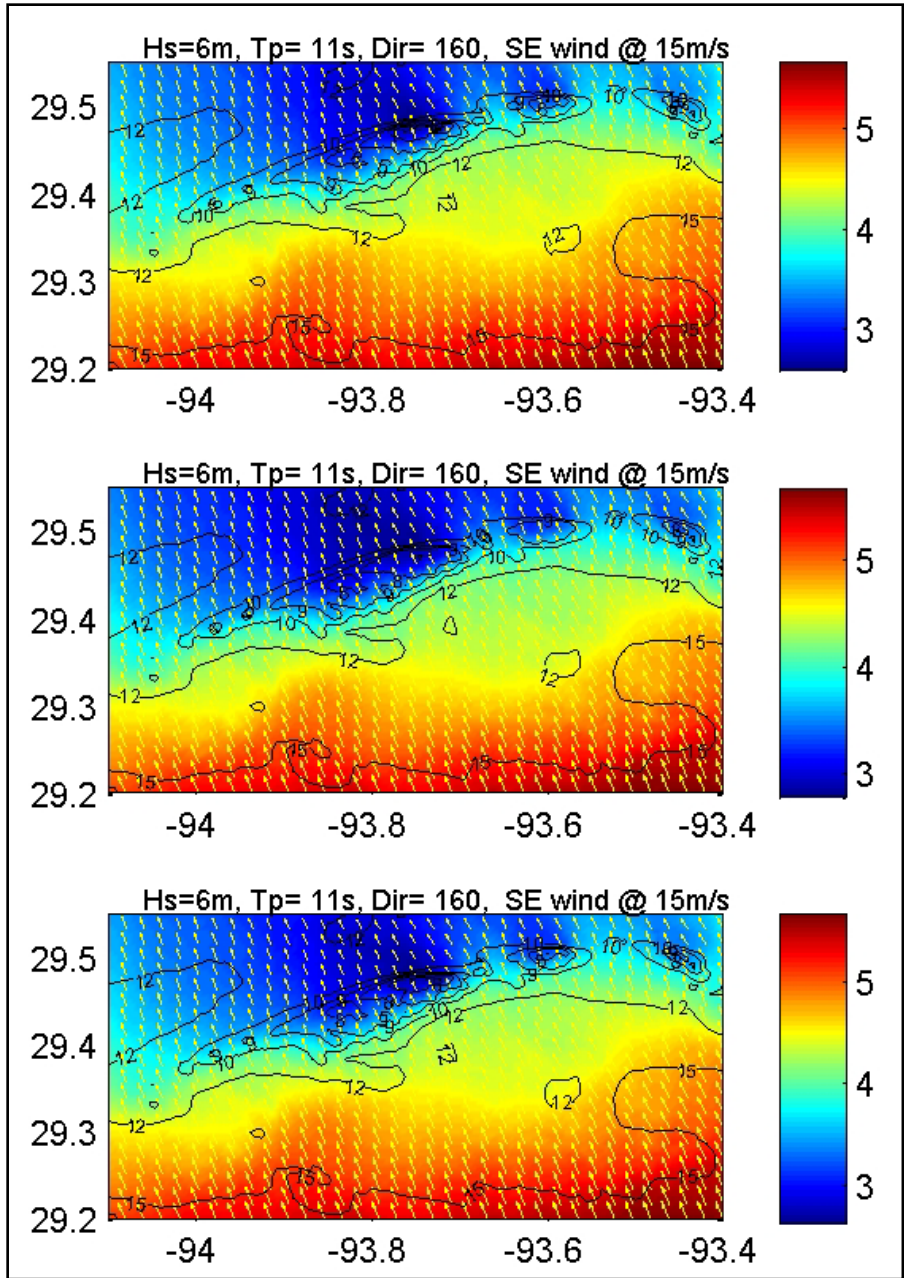
Figure 4.12 Significant wave height transformation over the shoal
            for Case A(1) met-ocean conditions.

(Top) without mining, (middle) cumulative scenario, and (bottom)
Holly Beach restoration.
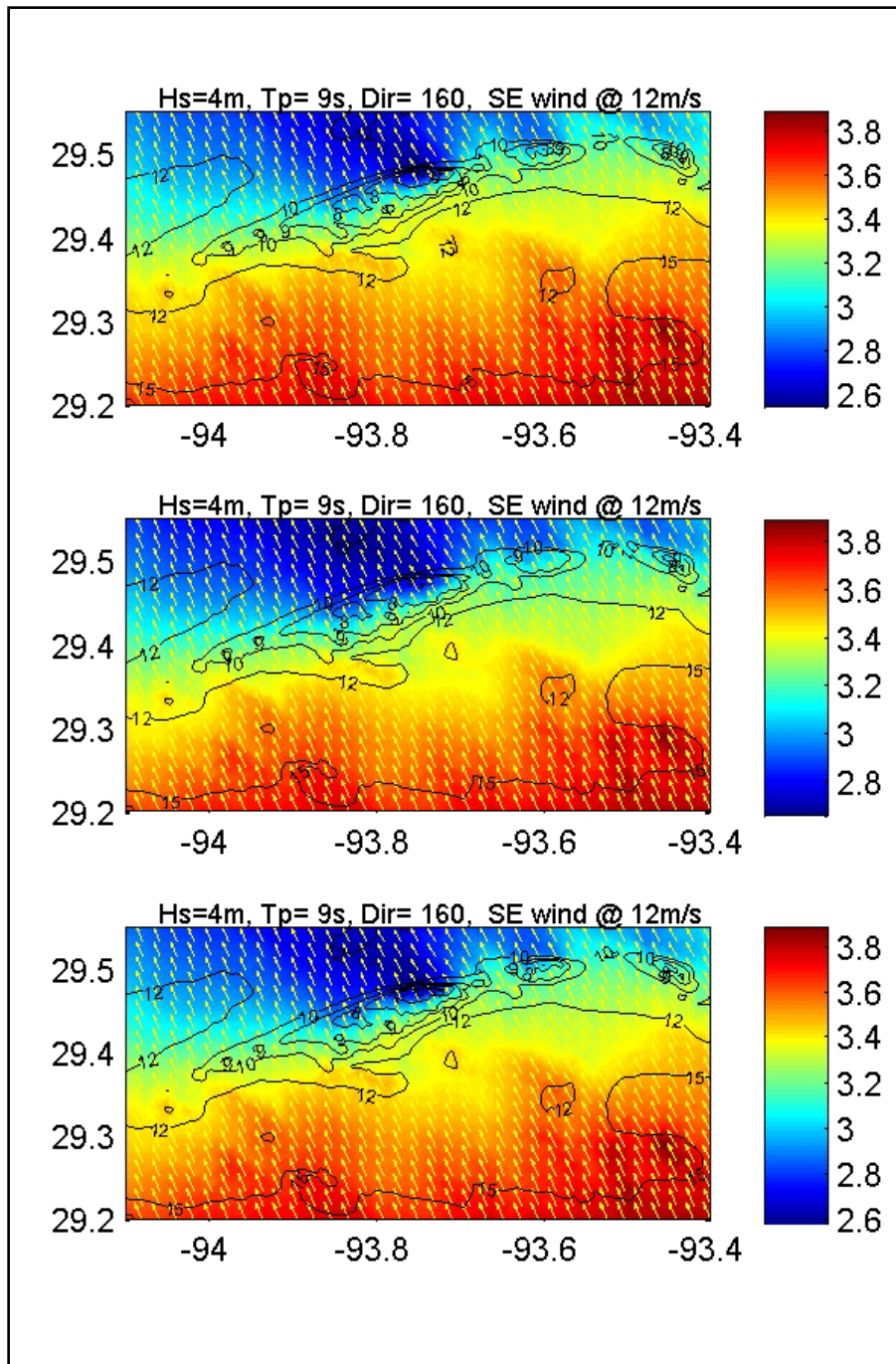
Figure 4.13   Significant wave height transformation over the shoal
                for Case A(2) met-ocean conditions.

(Top) without mining, (middle) cumulative scenario, and (bottom)
Holly Beach restoration.
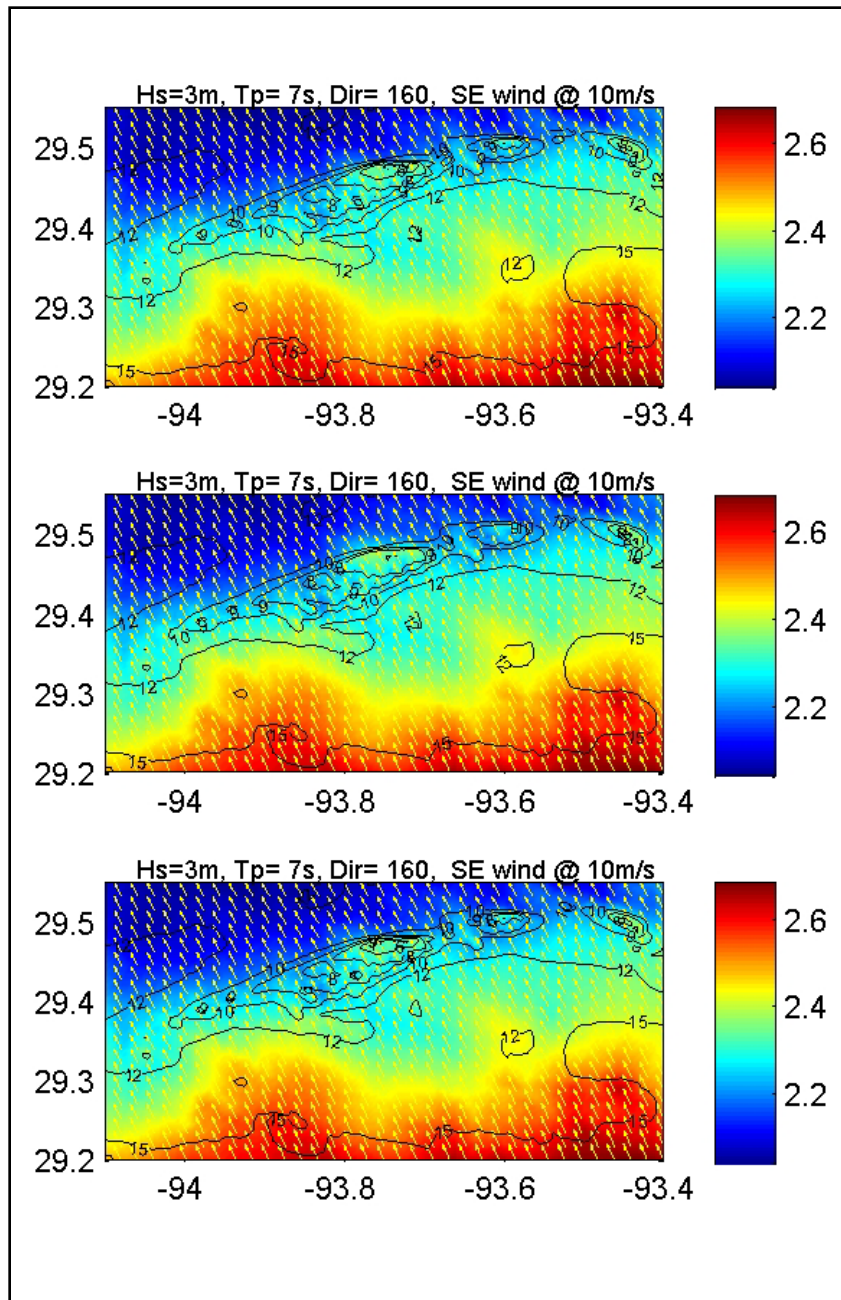
Figure 4.14   Significant wave height transformation over the shoal for Case A(3) met-ocean conditions.

(Top) without mining, (middle) cumulative scenario, and (bottom) Holly Beach restoration.
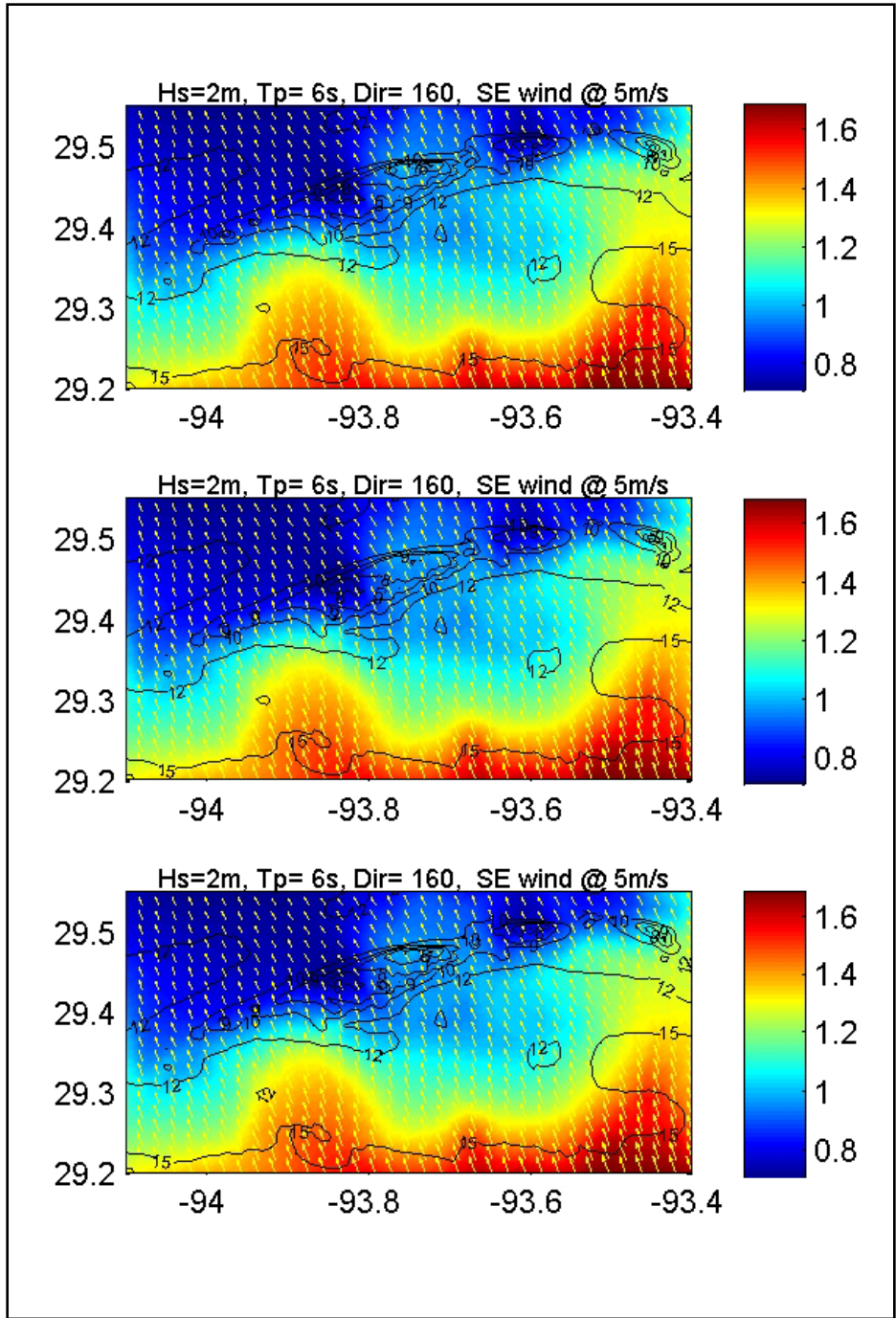
Figure 4.15 Significant wave height transformation over the shoal for Case A(4) met-ocean conditions.

(Top) without mining, (middle) cumulative scenario, and (bottom) Holly Beach restoration.
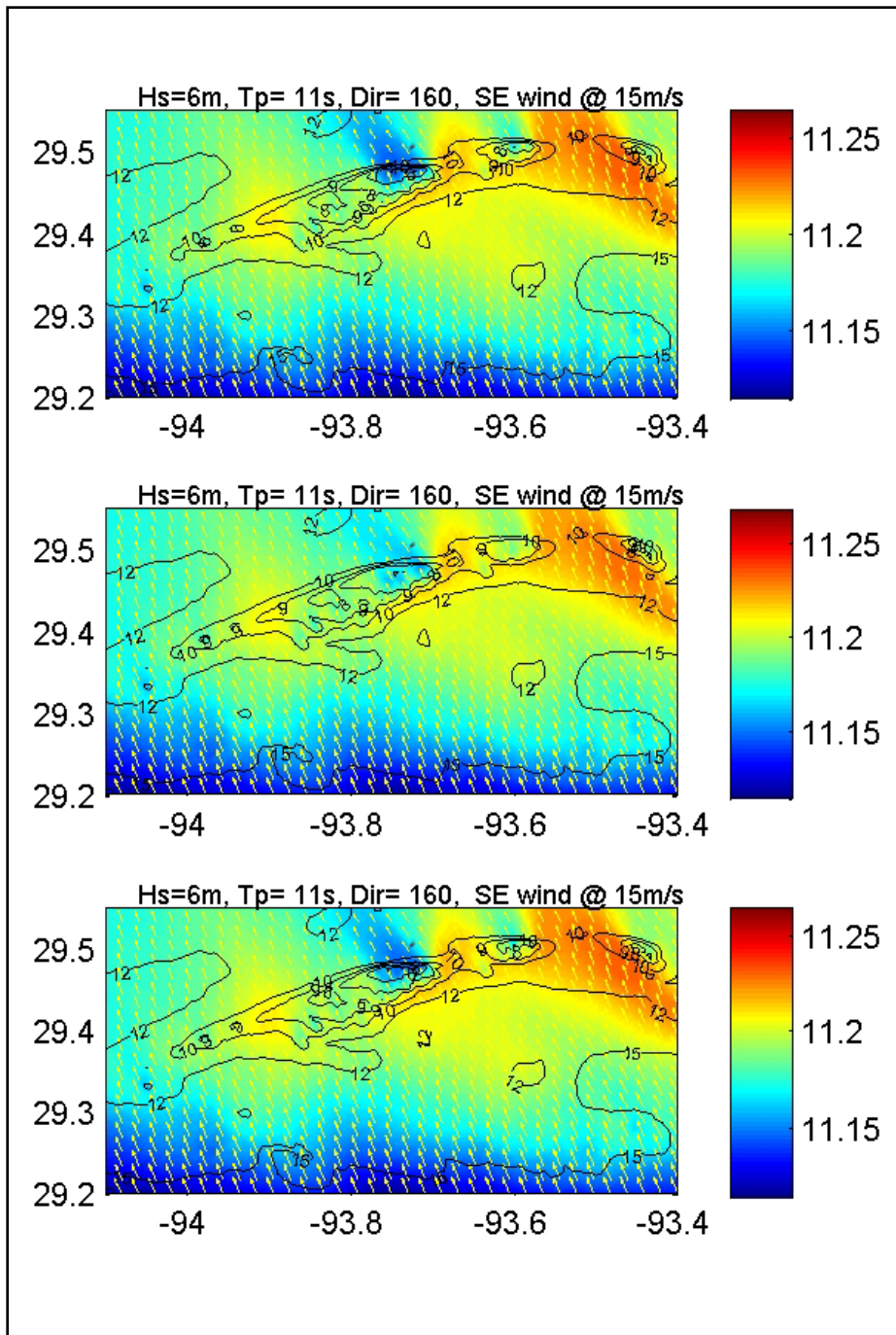
Figure 4.16   Peak wave period transformation over the shoal for Case
            A(1) met-ocean conditions.

 (Top) without mining, (middle) cumulative scenario, and (bottom)
 Holly Beach restoration.
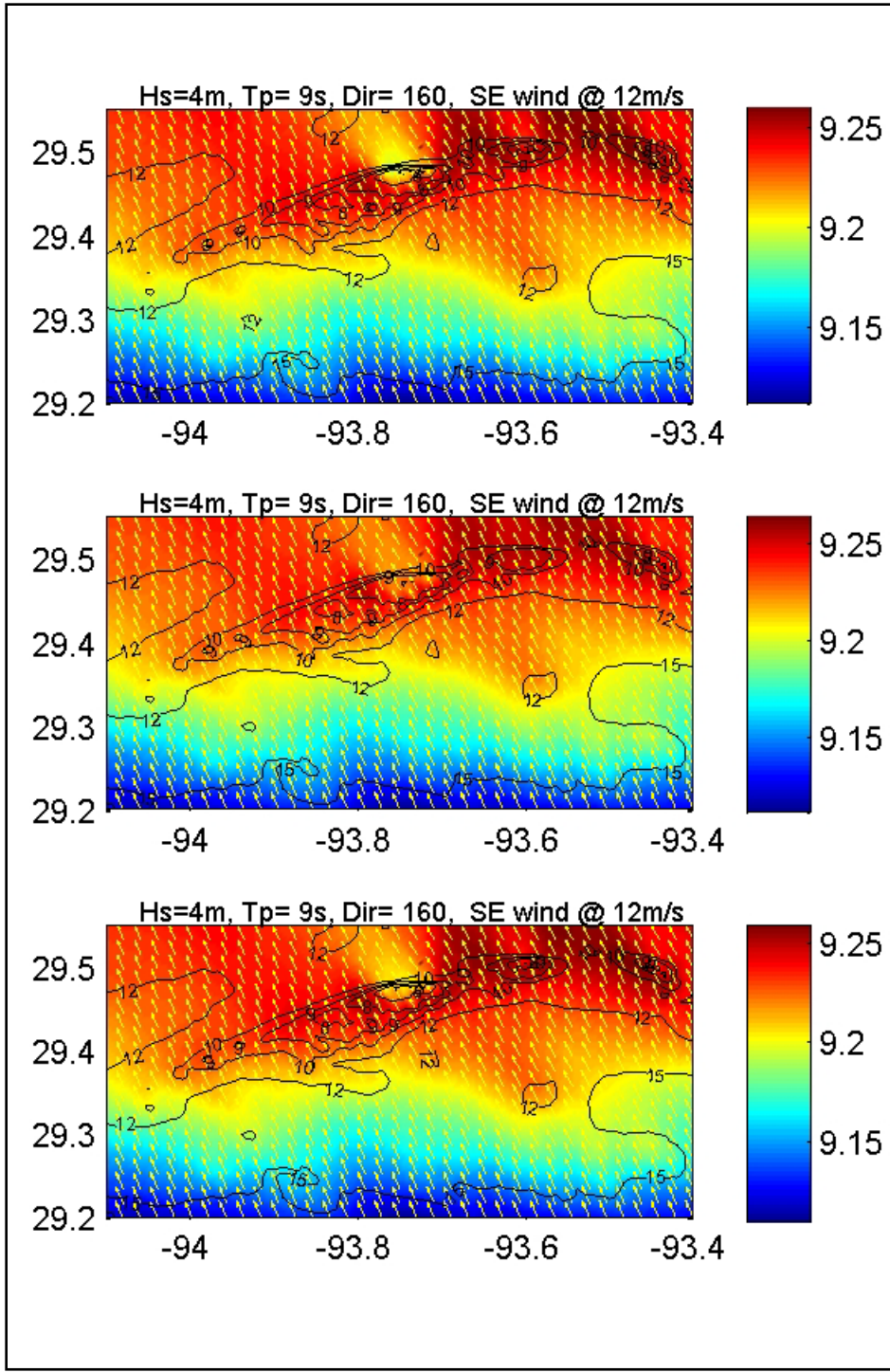
Figure 4.17   Peak wave period transformation over the shoal for Case
A(2) met-ocean conditions.

(Top) without mining, (middle) cumulative scenario, and (bottom)
Holly Beach restoration.
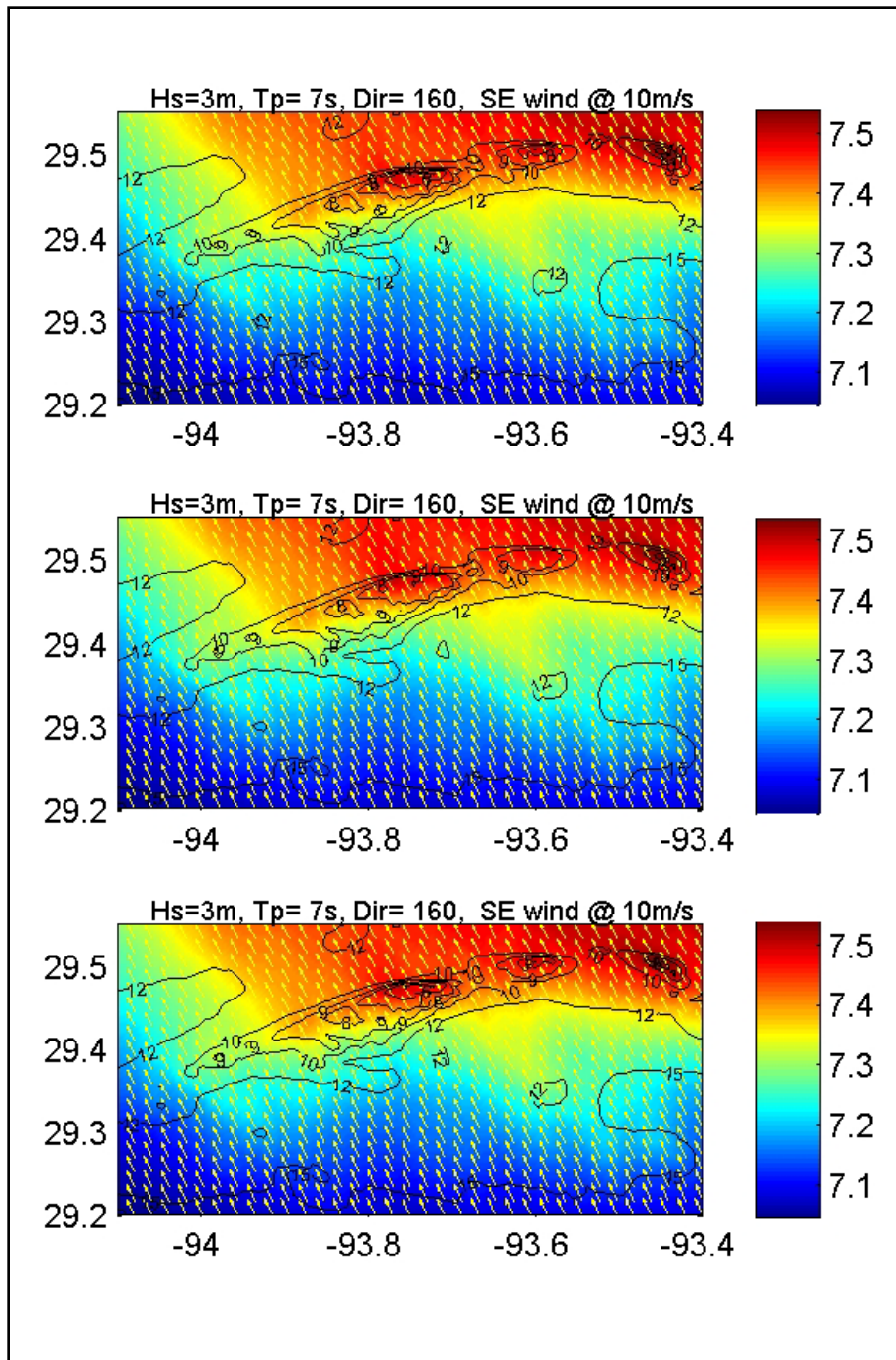
Figure 4.18   Peak wave period transformation over the shoal for Case
A(3) met-ocean conditions.

(Top) without mining, (middle) cumulative scenario, and (bottom)
Holly Beach restoration.
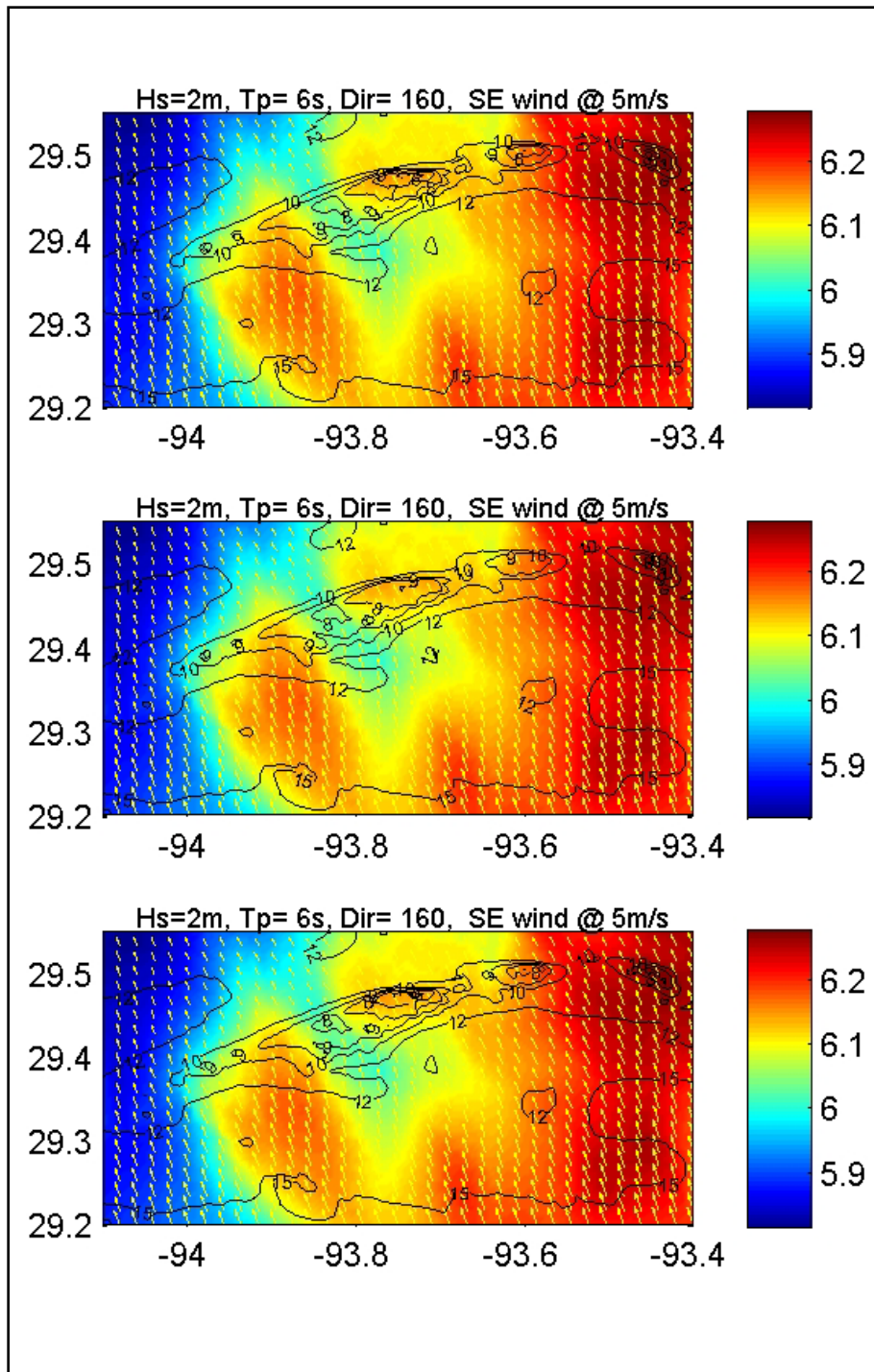
Figure 4.19   Peak wave period transformation over the shoal for Case A(3) met-ocean conditions.

(Top) without mining, (middle) cumulative scenario, and (bottom) Holly Beach restoration.

4.5.2. Re-suspension of bottom sediments

Changes in sediment re-suspension have strong implications for sediment transport and bed characteristics. Sediment re-suspension from the computed bulk wave parameters was estimated as follows: the re-suspension intensity (RI) is defined as wave-induced shear stress minus the critical shear stress. Wave shear stress was estimated from Madsen (1976) and the critical shear stress for sand bottoms was estimated based on Li et al. (1997); critical stress for sediments finer than 63 micro-meters was chosen as a constant value of 0.15 (N m^{-2}) (Kobashi and Stone 2008b). Due to the scarcity of sediment data from the shoal, a mean size of 0.2 mm was used for computing the threshold shear stress for the entire shoal. Results are summarized in Table 4.4 and illustrated in Figure 4.20 and 4.21. The RI corresponds to wave height and water depth; the higher the wave height and the shallower the depth, the higher the RI is. When storms were strong (i.e., case A1 and A2), the RI was high across the domain, but was higher at Station A (Figure 4.10 for location) and Station D than on the western shoal, due to wave dissipation on the western shoal. As wave energy decreased, as a general trend, the RI on the shoal decreased from the west to east following the change in the shoal bathymetry. For A4 (moderate storms), the RI on the western shoal was twice as high as that on the eastern shoal and approximately 2.5 times as high as that for the western most boundary of Sabine Bank (Station A). For the fair weather conditions, the RI was positive on the western shoal (Station B) and was negative at Stations A, C, and D. The negative values are characterized by sediment deposition, suggesting, except for the crest of the western shoal, no sediment re-suspension occurs during fair weather conditions. The results were corroborated by *in-situ* measurements during the summer 2008 deployments which were discussed in Chapter 3.

Results from the RI with partial mining (Cumulative scenario as well as Holly Beach restoration case) indicated that the variability is insignificant. The reduction in RI value at the western shoal is significant for moderate storm conditions (A4) (Figure 4.21). For the eastern shoal, the Holly Beach restoration scenario did not alter the RI values at all. It can be summarized that the alteration in RI is insignificant for the two mining scenarios.
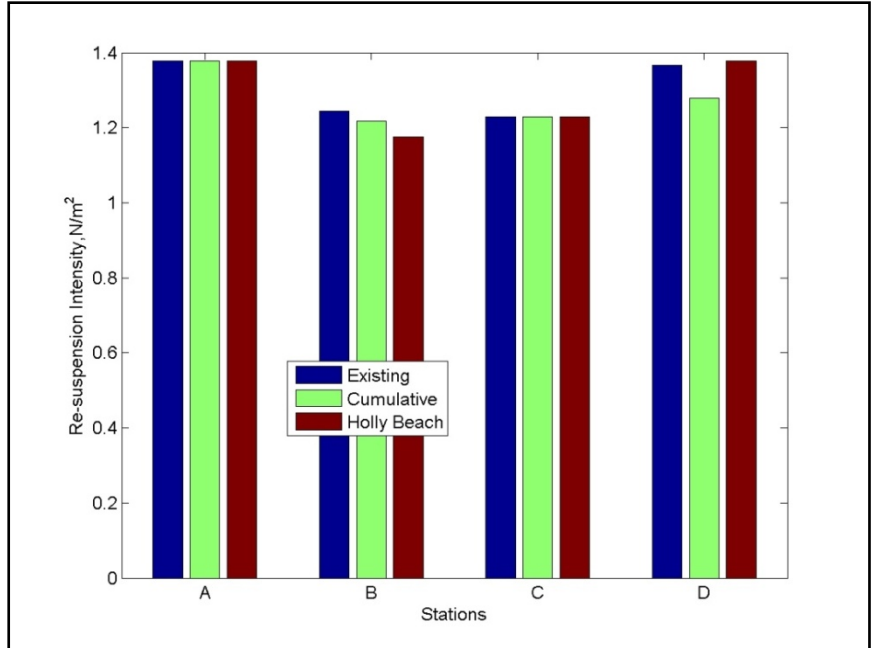
Figure 4.20   Resuspension   Intensity   computed   for   the   four
stations (see Figure 4.10 for the station reference).

The met-ocean boundary conditions corresponds to Case A(1).
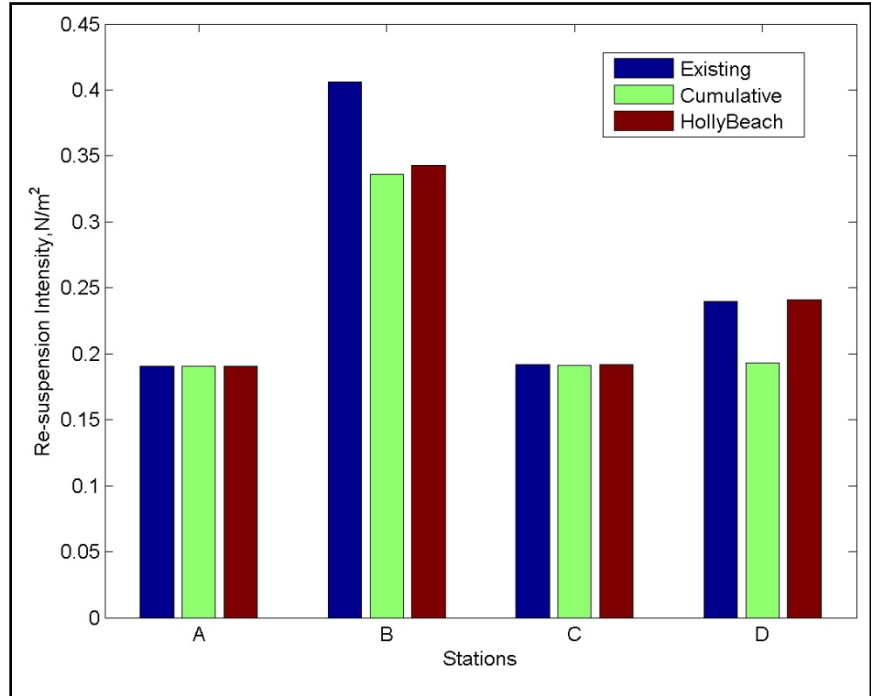
Figure 4.21   Resuspension   Intensity   computed   for   the   four
stations (see Figure 4.10 for the station reference).

The met-ocean boundary conditions corresponds to Case A(4).

CHAPTER 5: IMPACT OF HURRICANES GUSTAV AND IKE ALONG SABINE BANK, LOUISIANA-TEXAS COAST

5.1. INTRODUCTION

Waves generated by hurricanes can exceed 20 m (65.62 ft) in deep open ocean waters. Wang et al. (2005) reported that the maximum significant wave height reached 27.7 m (90.88 ft) during the passage of Hurricane Ivan. Even though hurricane-generated waves lose much of their energy before reaching the coast, it is well documented that hurricane-induced waves cause extensive destruction along the coast (Liu et al. 2007). The hurricane-generated waves generate runup in addition to storm surge in the coastal zone to cause even more damage along the coast as well as into low-lying areas behind the barrier islands and beaches. Therefore, the ability to predict hurricane-induced waves accurately is an important challenge and is of great value to many coastal communities, as well as for those engaged in offshore activities. In this study we have attempted to quantify the effect of Sabine Bank in mitigating high-energy waves that were generated by Hurricanes Gustav and Ike. This study becomes increasingly more relevant given the proposal of the federal and state agencies to use offshore sand resources for replenishing the barrier islands and beaches along the Louisiana-Texas coast. The coast under investigation has already been ravaged by a series of hurricanes since 2000, viz., Lili in 2002, Rita in 2005, and Gustav and Ike in 2008.

5.2. HURRICANES GUSTAV AND IKE

Hurricane Gustav was the seventh tropical cyclone and the second major hurricane of the 2008 Atlantic hurricane season. It formed on August 25, 2008, approximately 420 km (260.98 mi) southeast of Port-au-Prince, Haiti. It rapidly strengthened to tropical storm status that afternoon and into a hurricane early on August 26. It made the first landfall near the Haitian town of Jacmel on the same day, and, after inundating Jamaica and ravaging western Cuba, Gustav entered the Gulf of Mexico. The hurricane made final landfall along the Louisiana coast, near Cocodrie, Louisiana, as a strong category 2 hurricane.

Hurricane Ike was the third major hurricane of the 2008 season. It developed as a tropical disturbance near Cape Verde, Africa and on September 1, 2008, it became a tropical storm. By the early morning of September 5, Ike was a category 4 hurricane, with maximum sustained winds of 230 km/h and a pressure of 935 mbar. Ike made its final landfall in Baytown, Texas, as a category 2 hurricane.

5.3. MODELS USED IN THIS STUDY

5.3.1. WAVEWATCH-III

WAVEWATCH-III is a free open-source model developed at Marine Modeling and Analysis Branch of National Centers for Environmental Modeling Prediction. It is designed for deep water and runs on Unix/Linux platforms where it can be compiled for parallel mode. The source code is well-documented and the user can add new wave physics to the model.

Quadruple wind-wave interactions and wave dissipation can be calculated from WAM cycle 1-3 which is based on the empirical formula of Snyder et al. (1981) and the white capping (S_{wc}) formula based on Komen et al. (1984). There is an also newer formula in WAVEWATCH-III proposed by Tolman and Chalikov (1996). In this version, the temperature difference between water and sea can be included and different coefficients in stable and unstable sea states are used. Moreover two different mechanisms of dissipation are proposed for high and low frequency waves.

$$S_{in}(k,\theta) = \sigma\beta N(k,\theta) \qquad (1)$$

In which σ is frequency, k is wave number and β is the nondimensional wind-wind interaction parameter and can be determined from a set of a series of dependant equations (see WAVEWATCH-III manual for more details). Wave dissipation consists of two terms: The dominant term describes the low-frequency constituent and is based on an analogy of energy dissipation due to turbulence, and the empirical formula is used for high frequency dissipation (see WAVEWATCH-III manual for more details).

Quadruplet wave-wave interaction can be included as an approximation method (DIA) or an exact method referred to as the Webb-Resio-Tracy (WRT). The bed friction is the only shallow water effect in this model. Different time steps can be considered for spectral, special, and source term calculations to optimize the time needed to complete the calculations.

A simple first order upwind or third order ULTIMATE QUICKEST method can be selected by the user. The numerical scheme is explicit Finite Difference while the implicit scheme is used for source terms. WAVEWATCH-III is a very efficient and accurate model for ocean scale domains.

5.3.2. SWAN

SWAN (Simulating WAve Nearshore) continues to be developed in the Delft Hydraulics Institute for shallow water wave transformation and it includes all deep water processes. SWAN is free open-source software with well-documented code. The user can select an implicit first, second, or third order Finite Difference scheme. The user can also select rectangular or curvilinear computational grids. The latest version provides an opportunity to use unstructured triangular meshes for domains that can help the user incorporate a finer mesh in points of interest with almost no change in total computational cost. Moreover, the implicit scheme provides the opportunity to avoid small time steps for small mesh girds in shallow water.

Both WAM cycles (1-3) and WAM cycle 4 formulae are available for input energy and white capping dissipation. Transfer of energy from wind to wave is considered in the WAM cycle 4 by Janssen's formulation (Janssen 1989; Janssen 1991) which is based on a quasi-linear wind-wave theory. Moreover, despite cycles (1-3), white capping is no longer dependent linearly on wave number. A quadratic dissipation (suggested by Janssen 1989) is also added to adjust proper balance at high frequencies. Some modification for shallow water zones are applied for both formulations. For example, cut off frequency is 1 hertz regardless of wave spectrum.

The following equations briefly describe the wave input and wave dissipation formulae from WAM cycle 4:

$$S_{in} = A + BE(\sigma, \theta)$$

$$A = 1.5 \times \frac{10^{-3}}{2\pi g^2} (U_* \max[0, \cos(\theta - \theta_w)])^4 e^{-\left(\frac{0.13g\pi}{14\sigma U_*}\right)^4}$$

$$B = \beta\sigma \frac{\rho_a}{\rho_w} \left(\frac{U_*}{c}\right)^2 \max[0, \cos(\theta - \theta_w)]^2$$

$$U_*^2 = C_d U_{10}^2$$

$$C_d = \begin{cases} 1.2875 \times 10^{-3} & for\ U_{10} < 7.5\dfrac{m}{s} \\ (0.8 + 0.065 \times U_{10}) \times 10^{-3} & for\ U_{10} \geq 7.5\dfrac{m}{s} \end{cases}$$

(2)

in which U_{10} is wind speed at an elevation of 10 m above sea level, ρ_a and ρ_w are air and wind density respectively, θ_w is wind direction, c is phase speed and β is Mile parameter (see SWAN Manual for more details)

Several other types of dissipation formulae based on wave steepness or saturated level are also available and linear wave growth can be considered. Quadruplet wave-wave interaction is implemented in both exact (WRT) and approximate (DIA) methods. Besides shallow water processes, such as wave breaking and wave setup, there are several formulae for bed friction and triad wave-wave interactions. Diffraction and the effects of obstacles can be taken into account also.

Moreover, SWAN has the ability to calculate wave information at its boundary from deep water wave models, such as WAM or WAVEWATCH-III.

5.4. METHODOLOGY

WAVEWATCH-III is used to hindcast wave spectra for the entire Gulf of Mexico domain. Figure 5.1 shows the grid used for this simulation. The grid resolution for the rectangular grid is 0.125° in both latitude and longitude. Magenta lines along the northwestern corner of the domain show the boundary of the coastal model (see Figure 5.2) nested with this regional model. Hourly directional wave spectra computed for each grid points along these lines were used as open boundary conditions for the coastal SWAN model. Bathymetry data were downloaded from the National Geophysical Data Center (NGDC) online database for each grid point.

Coastal wave simulations were performed using an unstructured SWAN model which designates a mesh file used for computing the wave fields along the Louisiana-Texas coast. Since our interests were primarily in simulating the wave transformation due to shoals, finer-mesh elements were assigned around Sabine Bank as well as the location of NDBC buoy 42035 (see Figure 5.2). Very high resolution bathymetry data was downloaded from NGDC webpage and imported into the SWAN model.

5.4.1. Wind data

To enhance the accuracy and resolution of the wind data we have blended National Oceanic and Atmospheric Administration (NOAA) Hurricane Research Division (HRD) high-resolution analyzed wind data with the North American Regional Re-analyzed (NARR) wind. The latter has a coarser resolution of approximately 32 km (19.88 mi) as opposed to the higher resolution grid of HRD wind data (~6 km [3.73 mi]). The HRD wind data analysis uses all available surface weather platforms, aviation reports, and reconnaissance aircraft data adjusted to the surface and is gridded in a 1000 km x 1000 km "moving box" centered around the hurricane's track. From the HRD wind data, storm centers are first linearly interpolated to three hourly interval locations and consecutive HRD maps are then overlapped at the three hourly locations and linearly interpolated. The three hourly HRD winds are then merged with NARR winds using a weight that retains the HRD wind data within its data boundary and smoothly transits into the NARR wind beyond that boundary. Figure 5.3 illustrates a snapshot of the HRD wind during the approaching phase of Hurricane Ike.
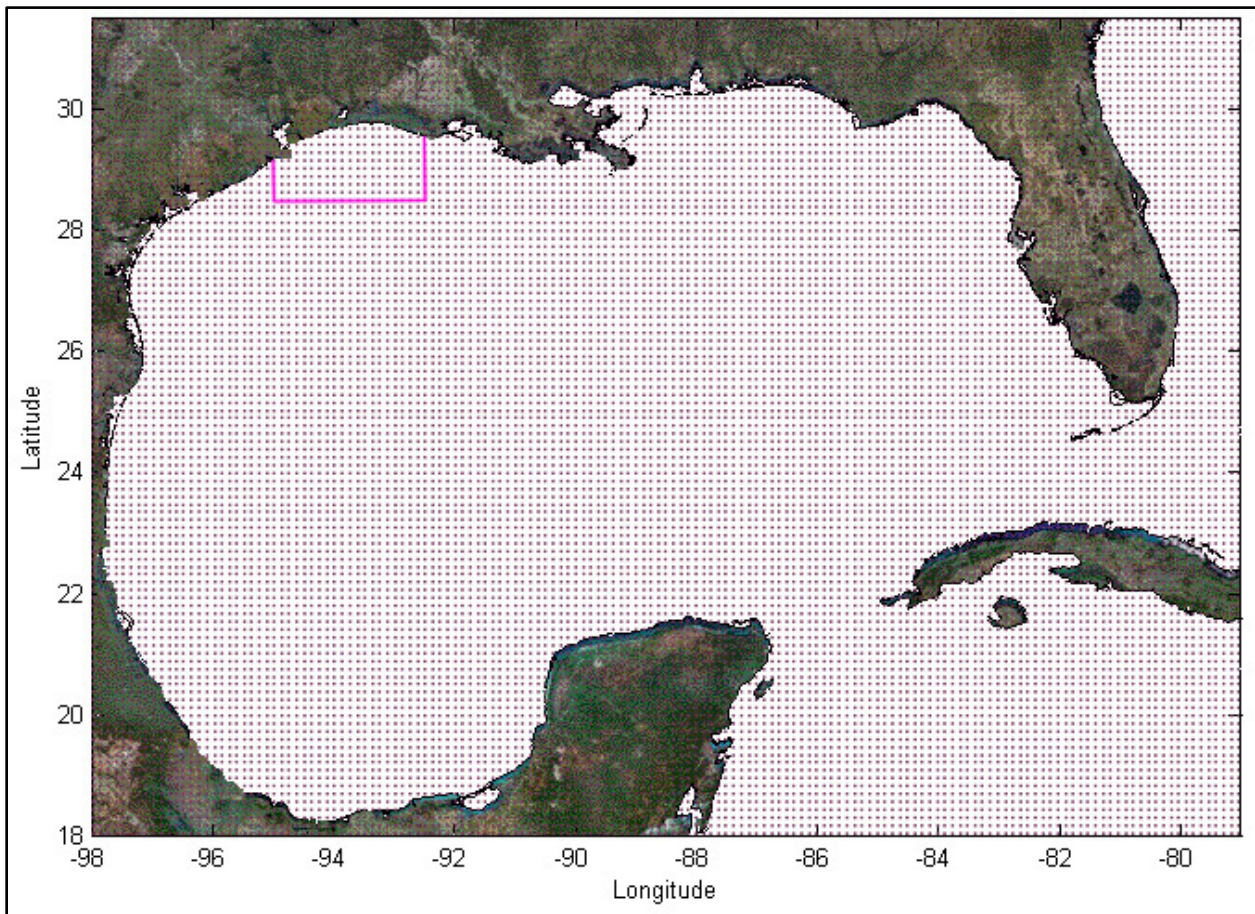
Figure 5.1   WAVEWATCH-III computational grid and output boundaries for the local model.
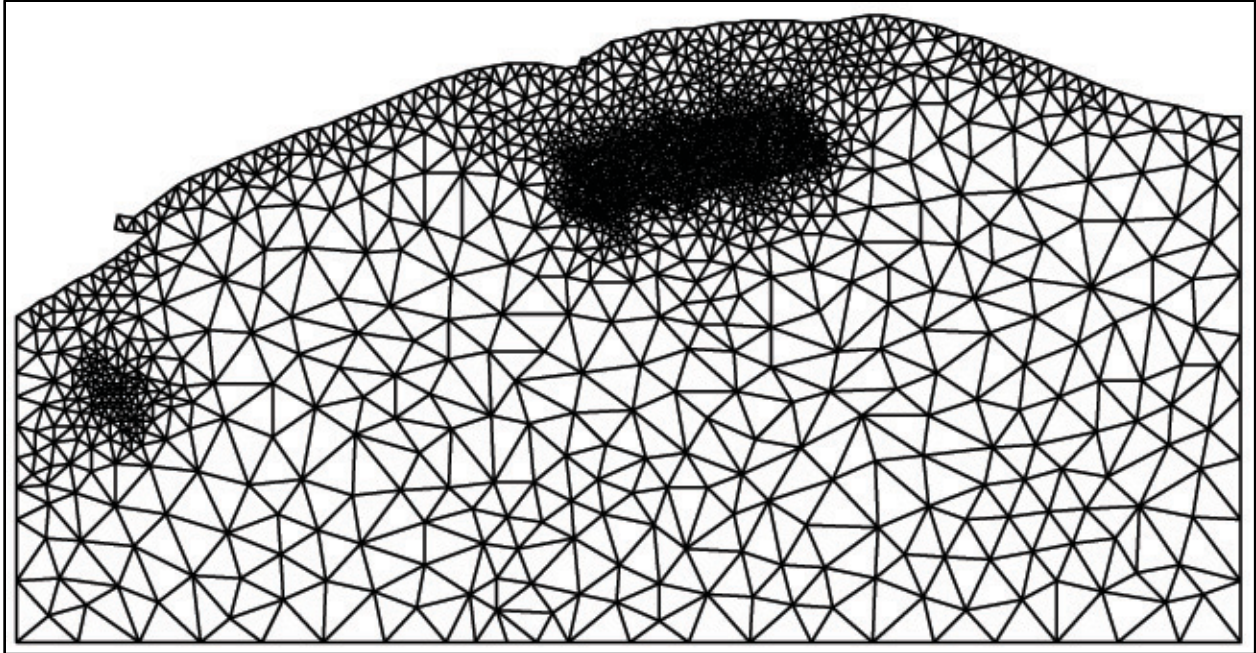
Figure 5.2   Unstructured SWAN Mesh used for the coastal wave hindcasting.

High resolution mesh grid was used for Sabine Bank for resolving the complex wave transformation processes over the shoal. Also, a high resolution grid was used for the model validation site, NDBC 42035.
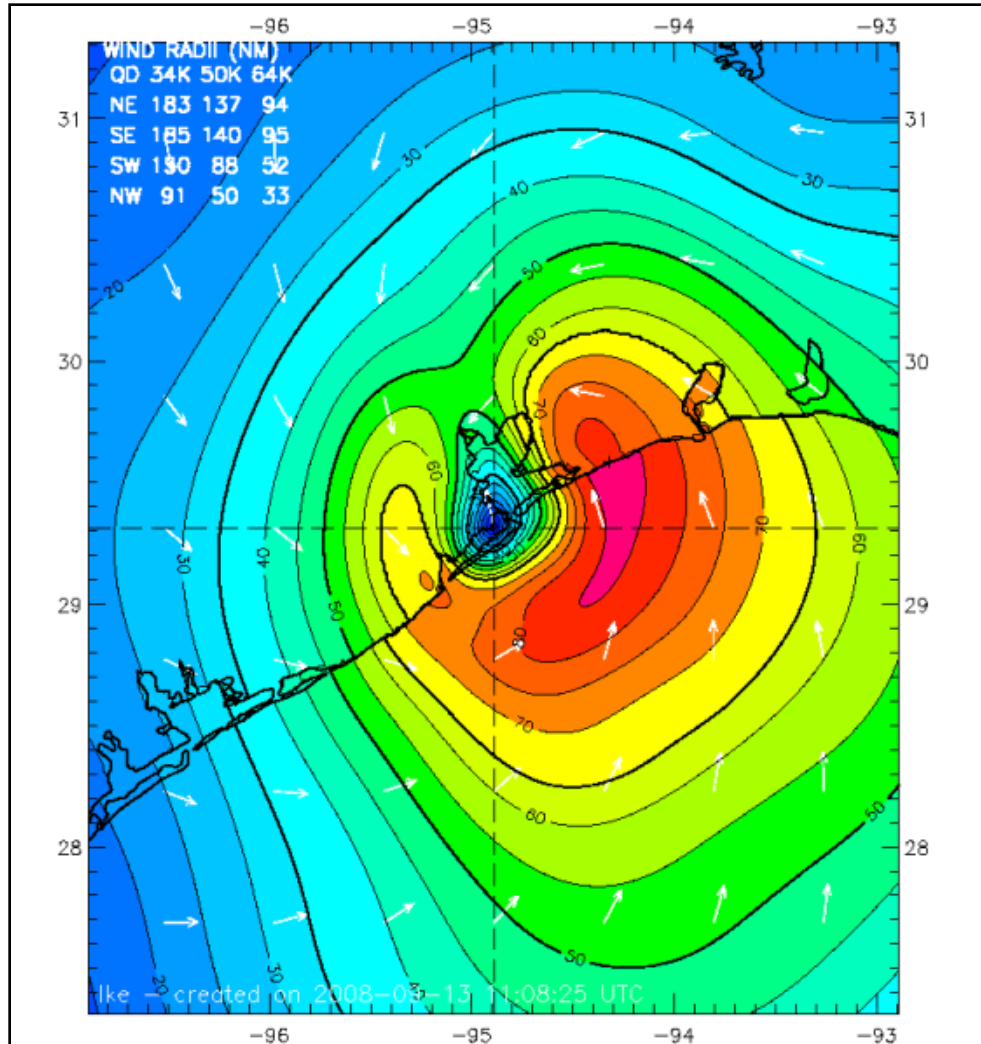
Figure 5.3   Hurricane Ike on the September 13, 2008, 07:30 UTC. High resolution (~6 km) wind data is provided by NOAA/Atlantic Oceanographic and Meteorological Laboratory.

5.4.2. Details of dredging

Since the objective of the study is to estimate the effect of the shoal on coastal wave transformation, we have computed the wave fields using two bathymetries. One computation was run with the shoal present and the other computation with partial removal of the west and east shoal crests for a cumulative dredging scenario. The location and the volume of sand estimated for this dredging project were discussed in Chapter 4. For each scenario, wave parameters were computed for the entire domain. Moreover, for comparison, time series distribution of bulk wave parameters was computed for five stations along the coast. The station locations are given in Figure 5.4.
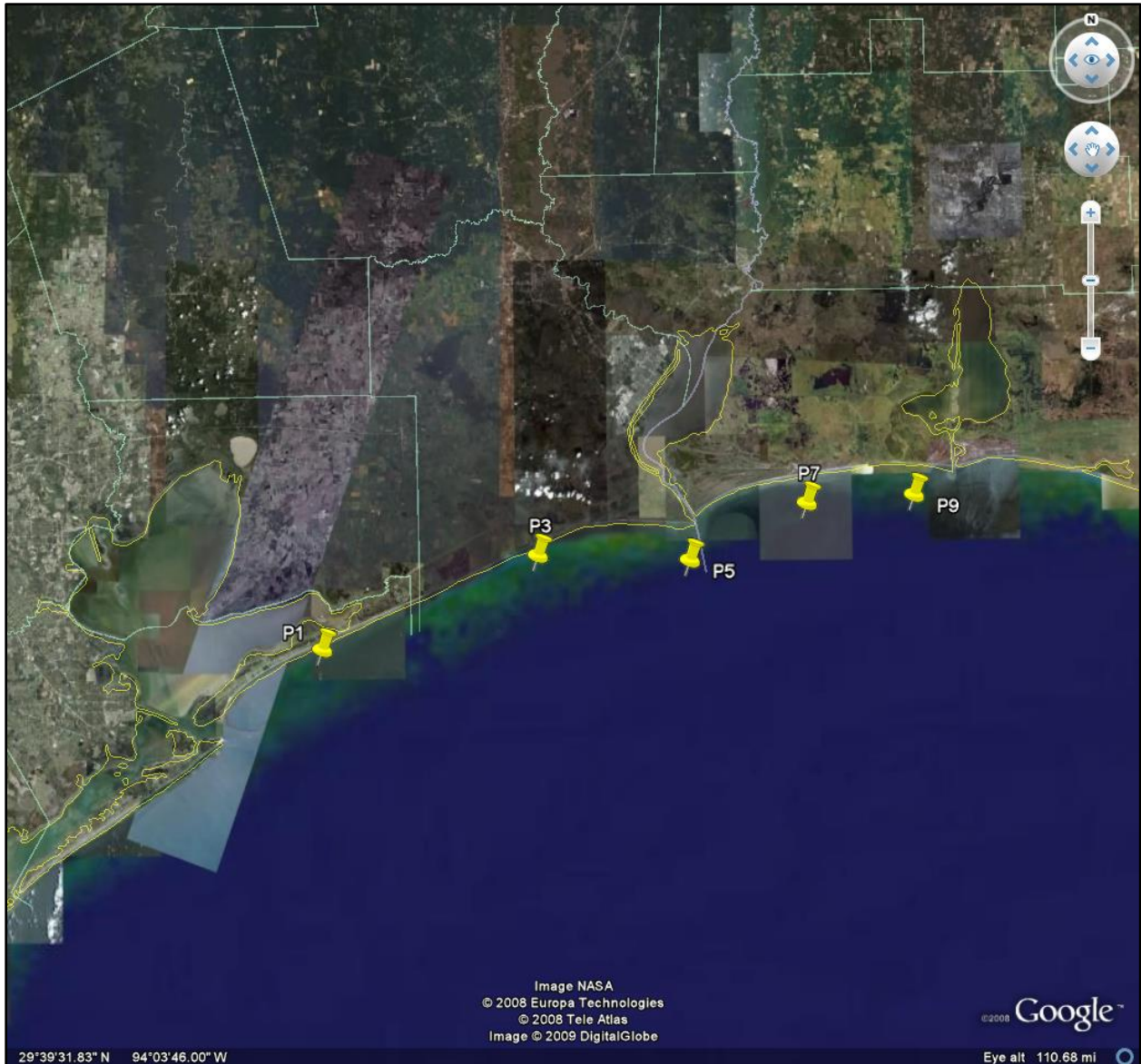
Figure 5.4   Stations selected along the coast to compute the bulk wave parameters.

The stations were selected along the 8 m isobaths, considering the uncertainties in the nearshore bathymetry.

5.4.3 Model Skill Assessment

In order to skill assess the model, computations were conducted for a winter storm season from December 5, 2006 to January 5, 2007. The NCEP and NARR wind data were used for this model. Archived wind data were downloaded from the NCEP archives and re-formatted according to the input specifications for the WAVEWATCH III model, using Matlab routines. Simulations were conducted and the bulk wave parameters were plotted against *in situ* observations from NDBC buoys, viz., NDBC 42001, NDBC 42002 and NDBC 42007; the results are provided in Figures 5.5–5.14. The simulated wave fields are generally in good agreement with the *in situ* observations from the offshore buoys. The under-prediction of wave

heights by the model can be attributed to the limitation of the wind data. Similar observations were reported by Jose and Stone (2006) and Jose et al., (2007), based on their wave modeling studies for the Gulf of Mexico, using MIKE 21. Figures 5.15 – 5.16 provide the validation of the SWAN model using both *in situ* as well as WAVEWATCH III-generated wave parameters. Significant wave height simulated with the SWAN model also was in good agreement with the other two data sets.
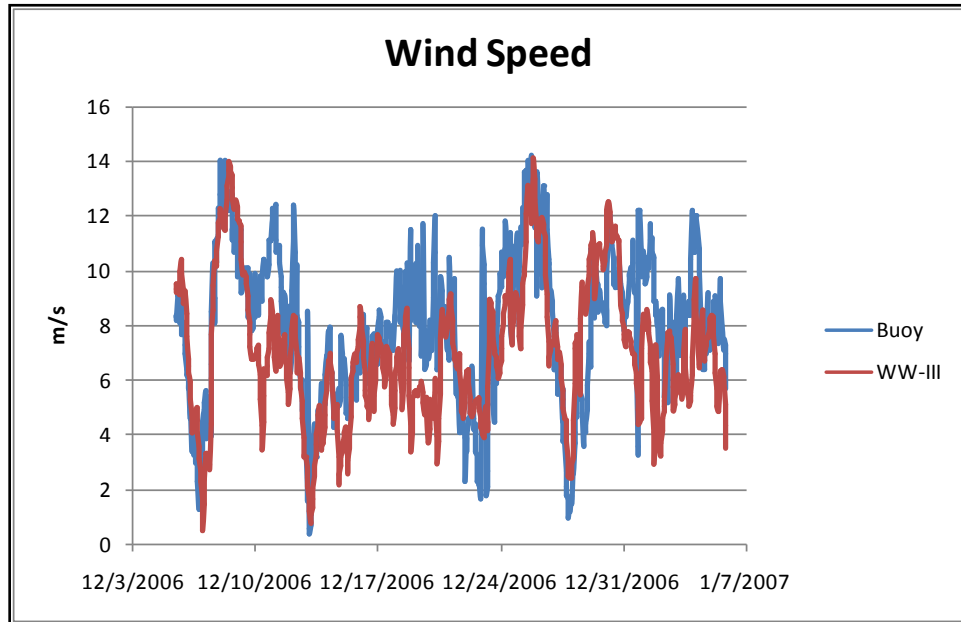
Figure 5.5   Wind speed from NDBC 42001 and reanalyzed wind data used for wave hindcasting.
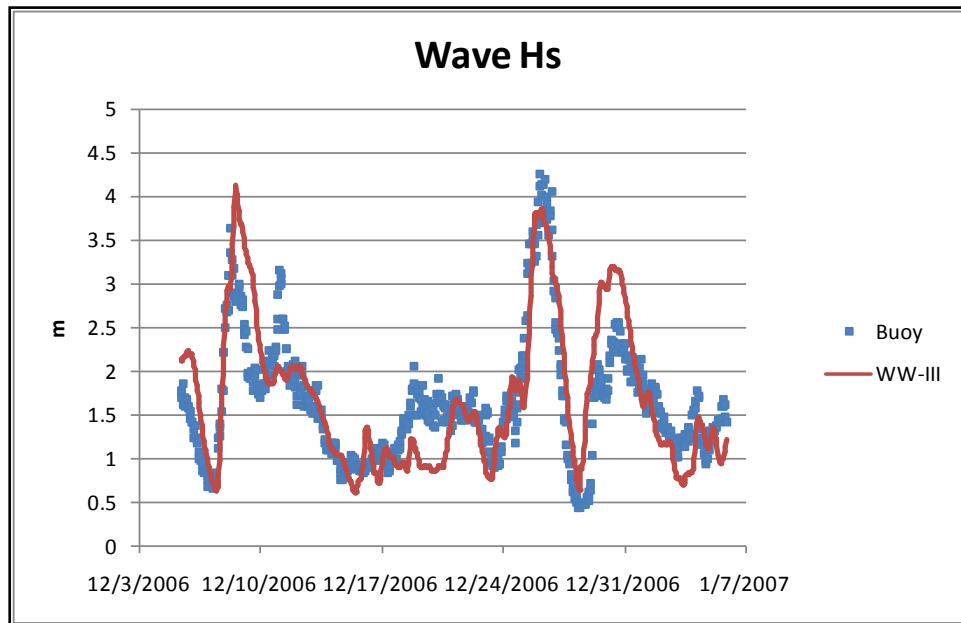
Figure 5.6   NDBC 42001 measured significant wave height and WW-III simulation results for this station.

93
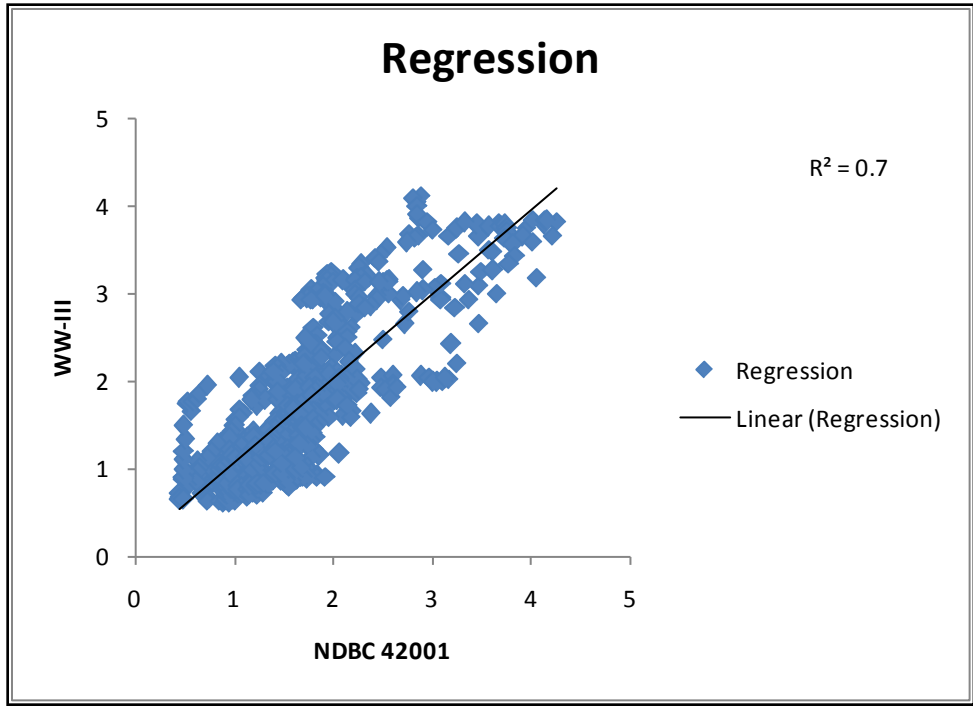
Figure 5.7   Regression between WW-III simulation results and NDBC 42001 measured data.
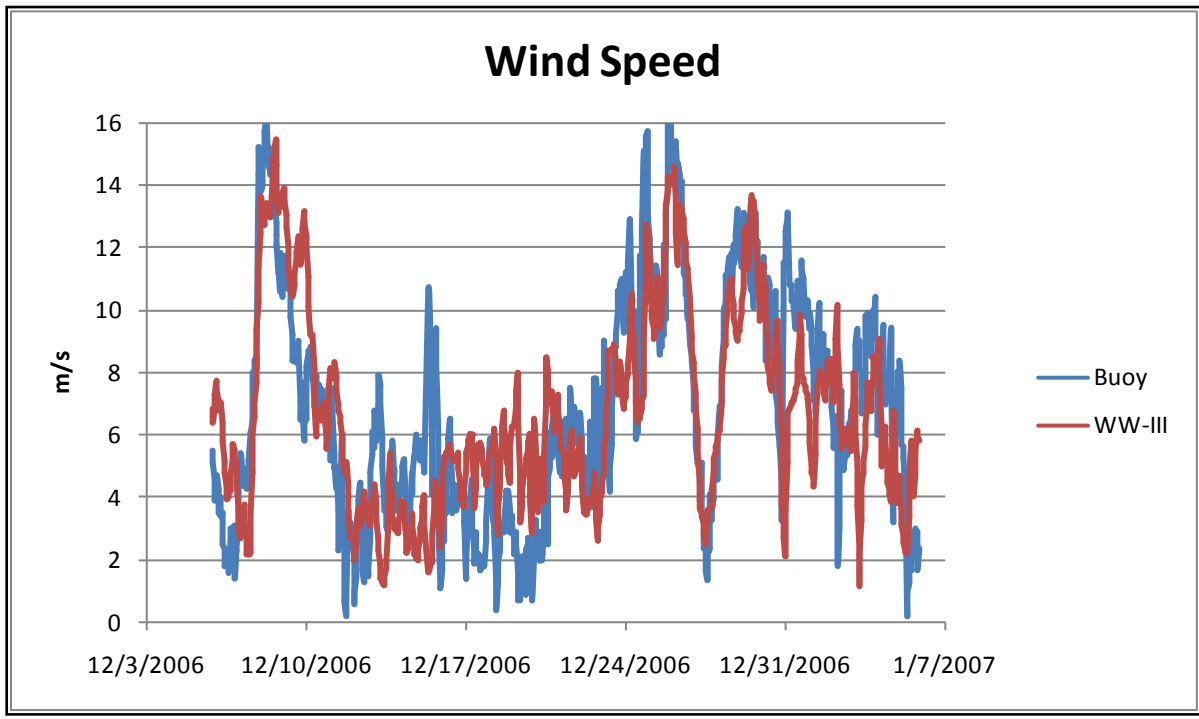
Figure 5.8   Wind speed from NDBC 42002 and reanalyzed wind data used for wave hindcasting.

94
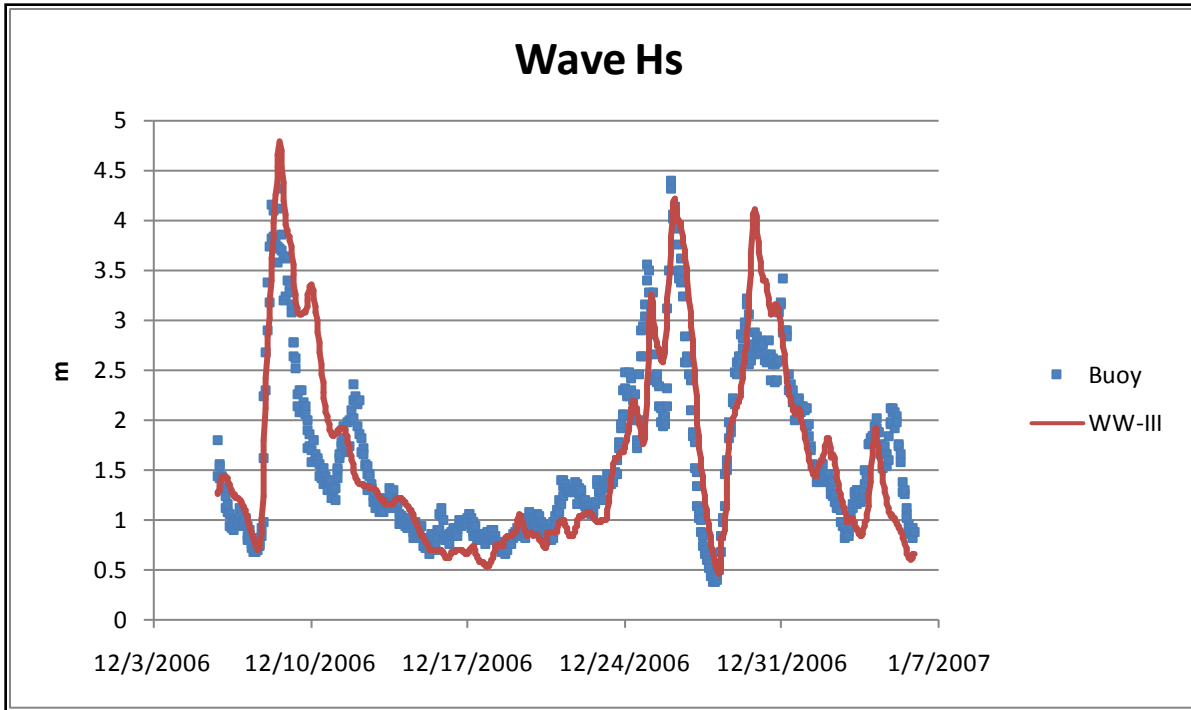
Figure 5.9   NDBC 42002 measured significant wave height and WW-III simulation result for this station.
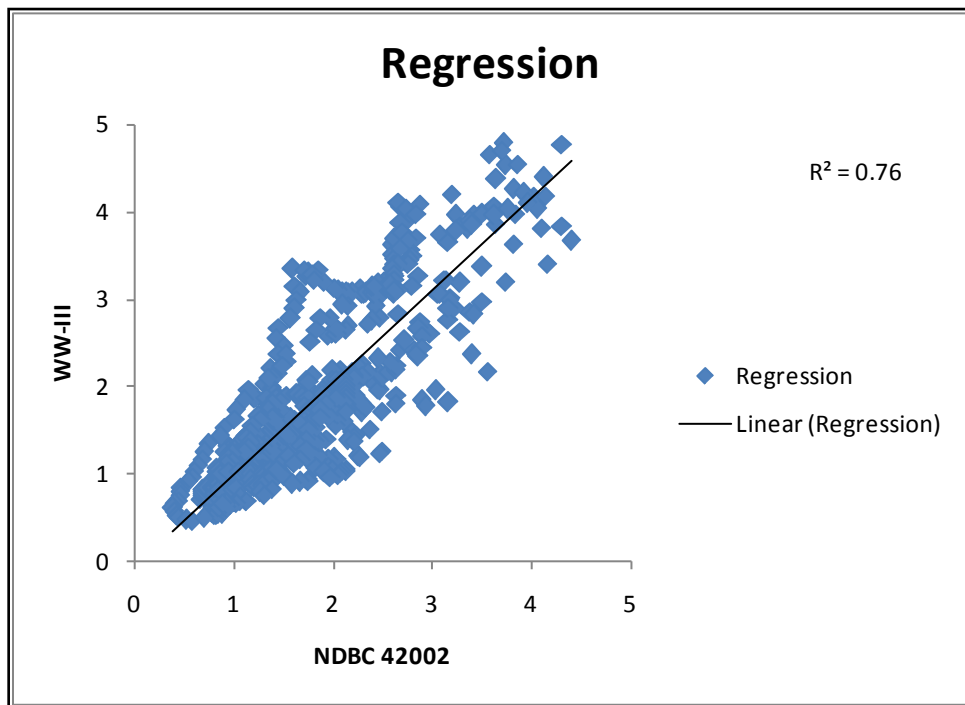
Figure 5.10   Regression between WW-III simulation results and NDBC 42002 measured data.

95
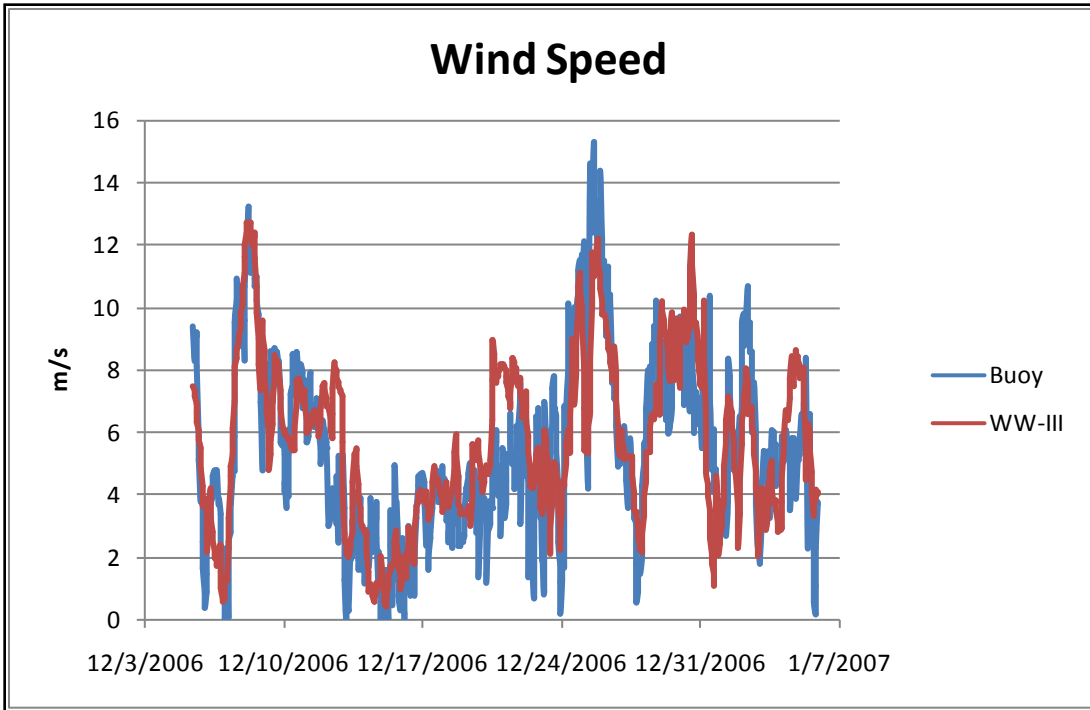
Figure 5.11   Wind speed from NDBC 42007 and reanalyzed wind data used for wave hindcasting.
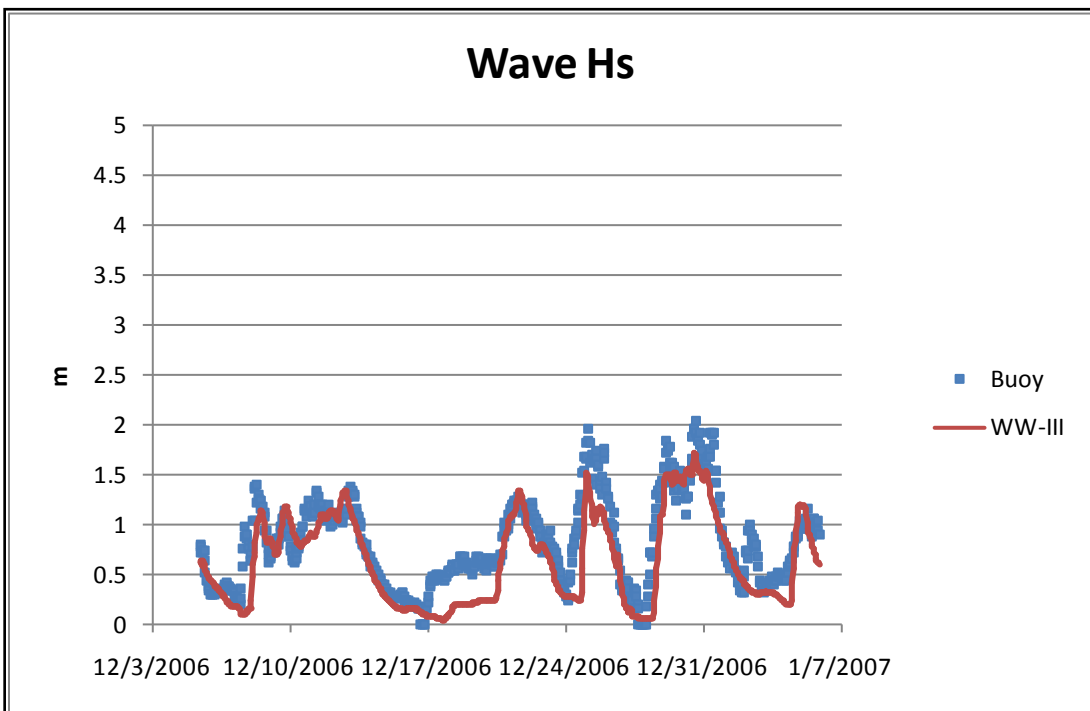
Figure 5.12   NDBC 42007 measured significant wave height and WW-III simulation result for this station.
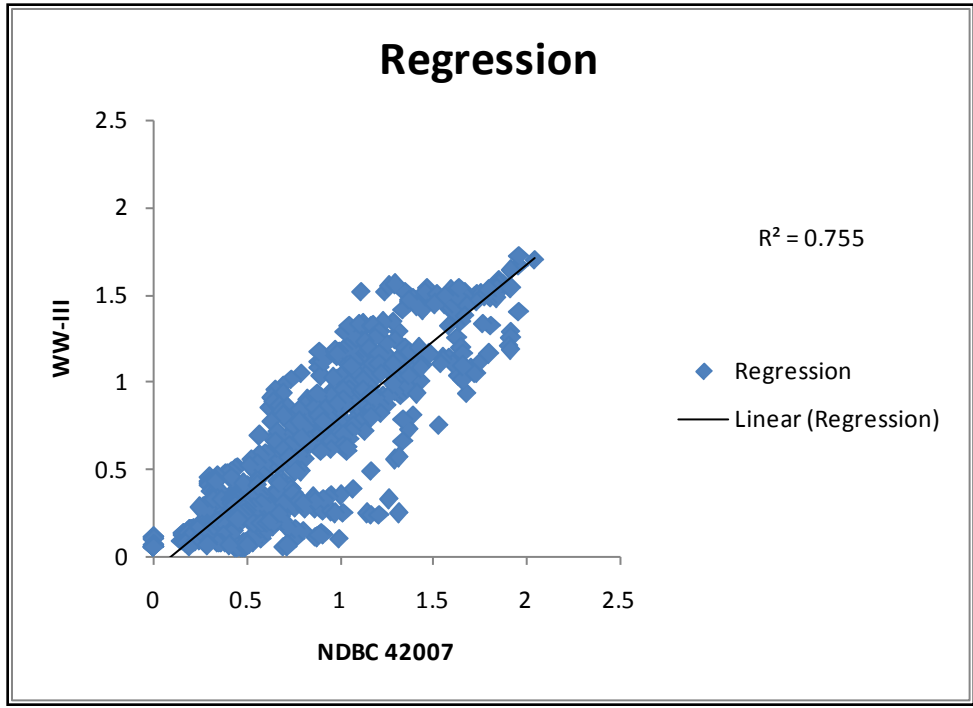
Figure 5.13   Regression between WW-III simulation results and NDBC 42007 measured data.
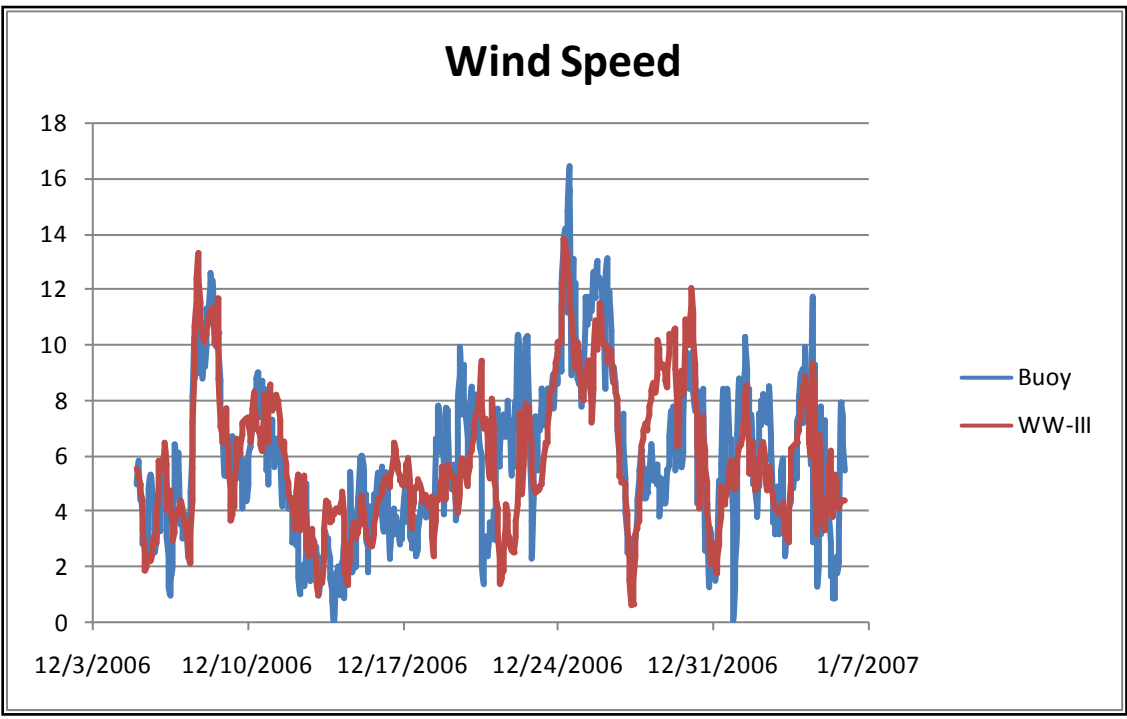
Figure 5.14   Wind speed from NDBC 42035 and reanalyzed wind data used for wave hindcasting.
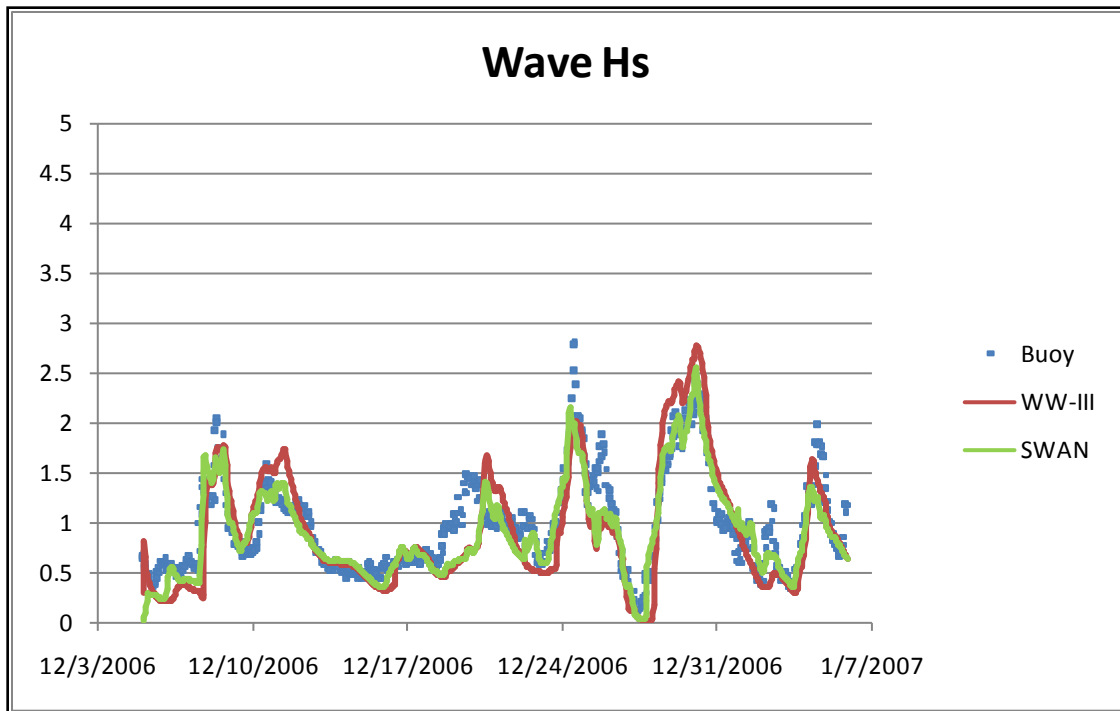
Figure 5.15   NDBC 42035 measured significant wave height, SWAN and WW-III simulation result for this station.
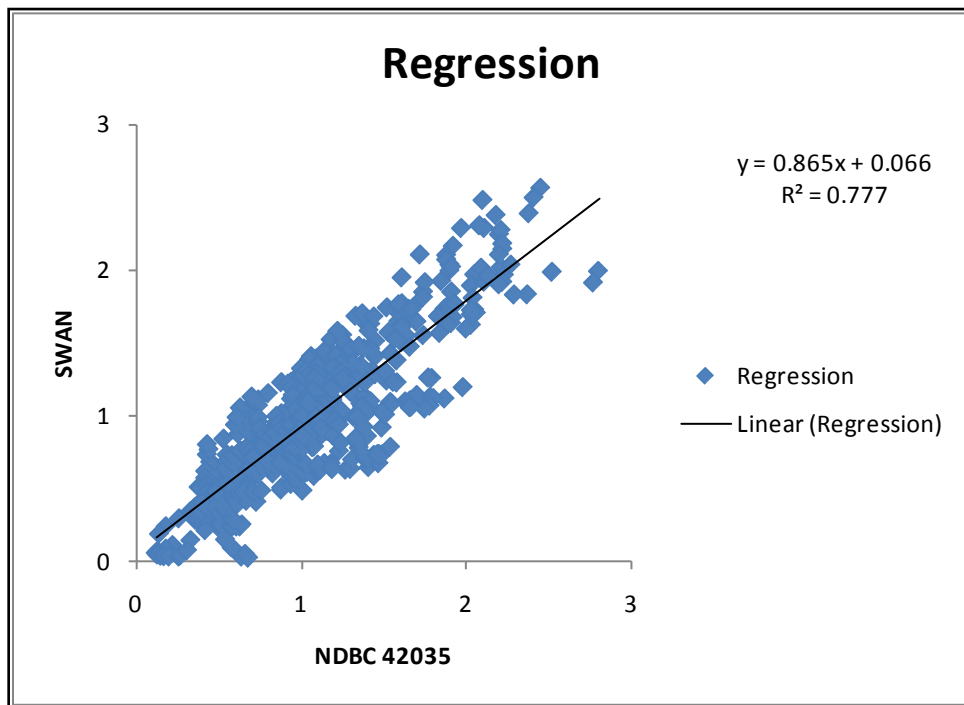
Figure 5.16   Regression between SWAN simulation results and NDBC 42035 measured data.

5.5. RESULTS AND DISCUSSION

Bulk wave parameters generated by hurricane force winds were simulated using WAVEWATCH III and SWAN simulations. Significant wave height distribution maps are provided in Figures 5.17–5.26, for the two scenarios, viz., with shoal and with partial removal of the shoal. It is observed that even during the landfall of Hurricane Gustav, which made landfall farther east of the study area, the shoal sheltered the coast to some extent by attenuating long period swells. During the approaching phase and during landfall of Hurricane Ike the dissipation of wave energy over the shoal was conspicuous. However, insignificant modification in wave pattern was observed in the scenario considering partial removal of the shoal crests (Figures 5.18, 5.20, 5.22, 5.24 and 5.26). Wave fields with the complete removal of the shoal have not yet been computed. Kobash et al. (2009b) conducted a similar study for Ship Shoal, incorporating a scenario of complete removal of the shoal and the alterations in the wave patterns were profoundly evident. It is concluded that the proposed selective mining of the western and eastern shoals of Sabine Bank would not significantly affect the coastal wave regime landward of the 8 m isboath.
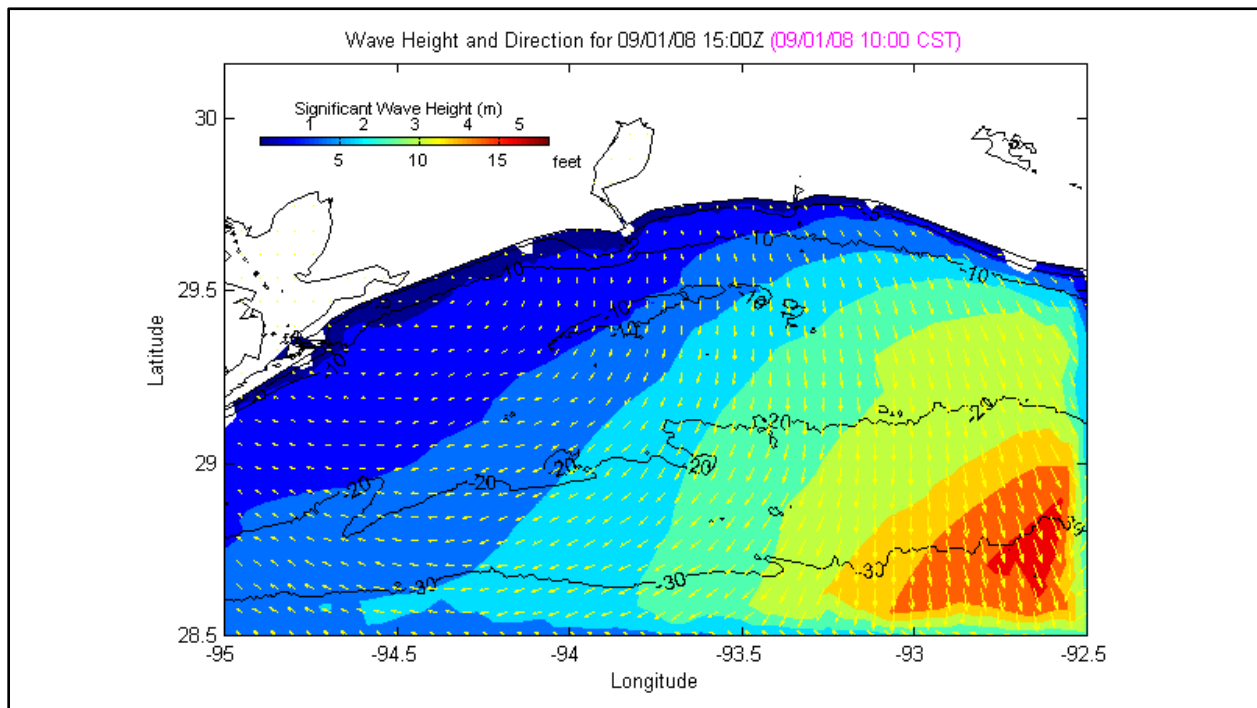
Figure 5.17   Wave field along the study area when Hurricane Gustav made landfall.

Bathymetry corresponds to the pre-dredging scenario.
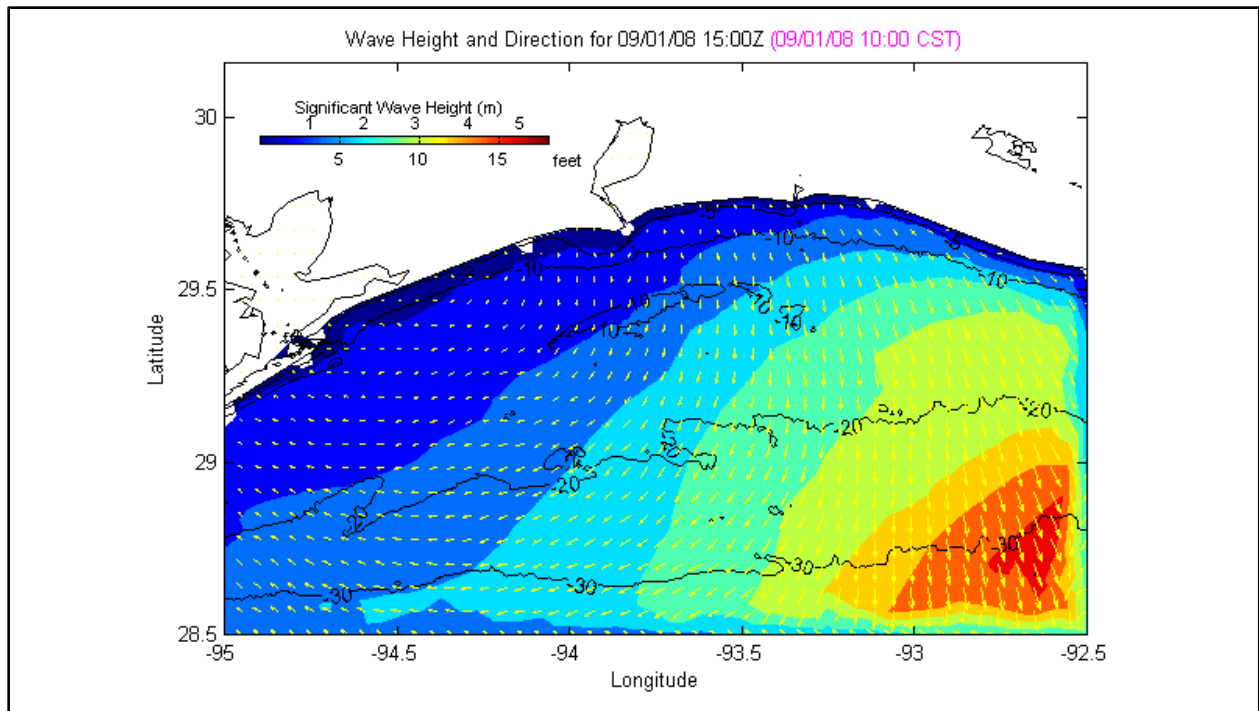
Figure 5.18   Wave field along the study area when Hurricane Gustav made landfall.

Bathymetry reflects partial removal of the western and eastern shoal.
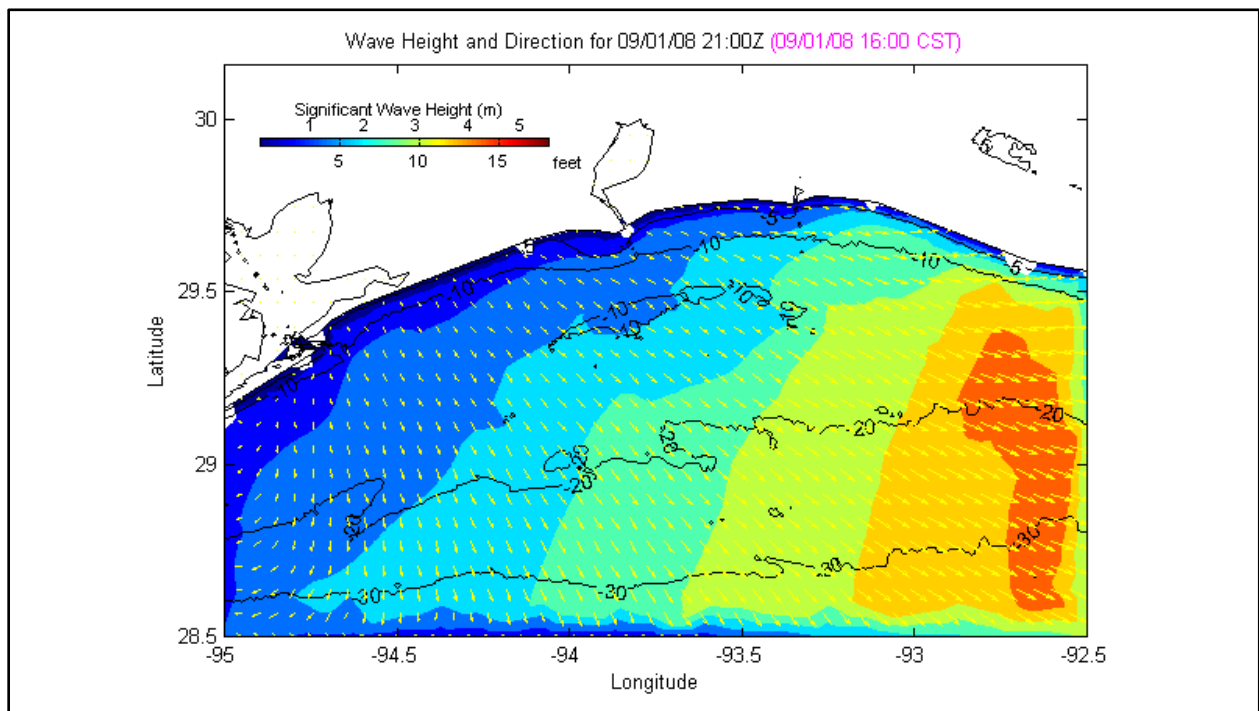
Figure 5.19   Wave field along the study area six hours after Hurricane Gustav made landfall.

Bathymetry corresponds to pre-dredging scenario.
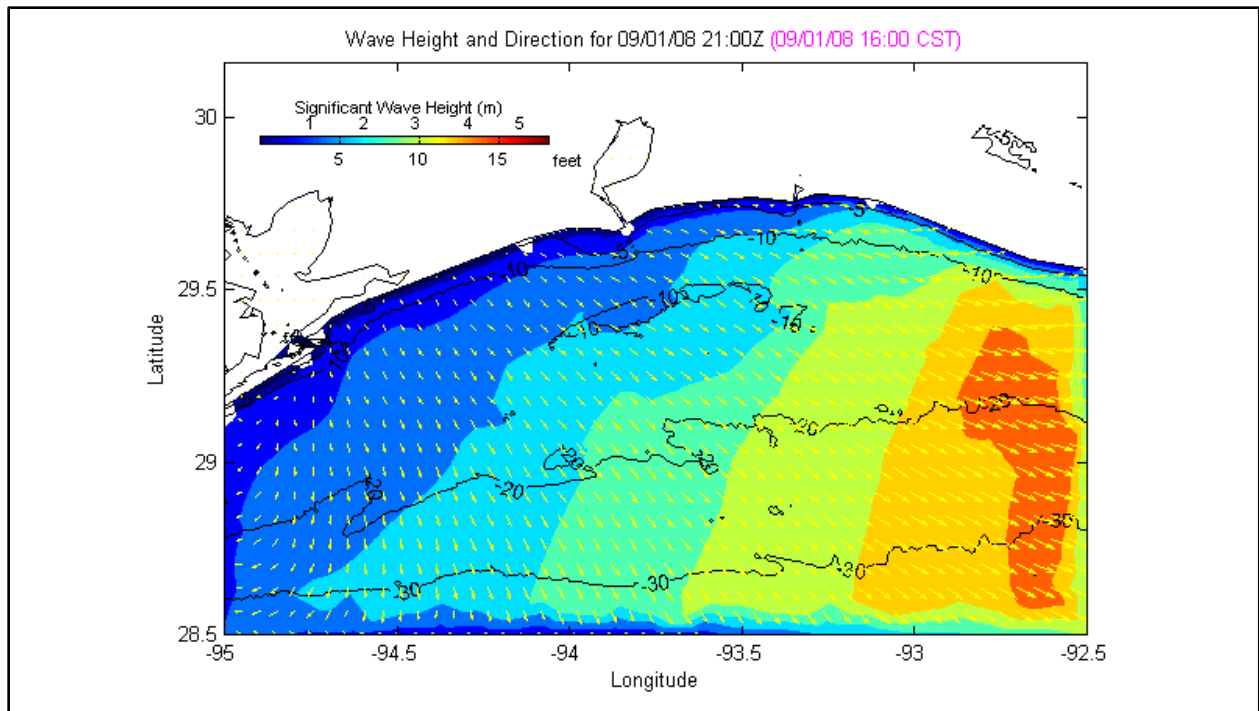
Figure 5.20   Wave field along the study area six hours after Hurricane Gustav made landfall.

Bathymetry reflects partial removal of the crest from the west and east shoals.
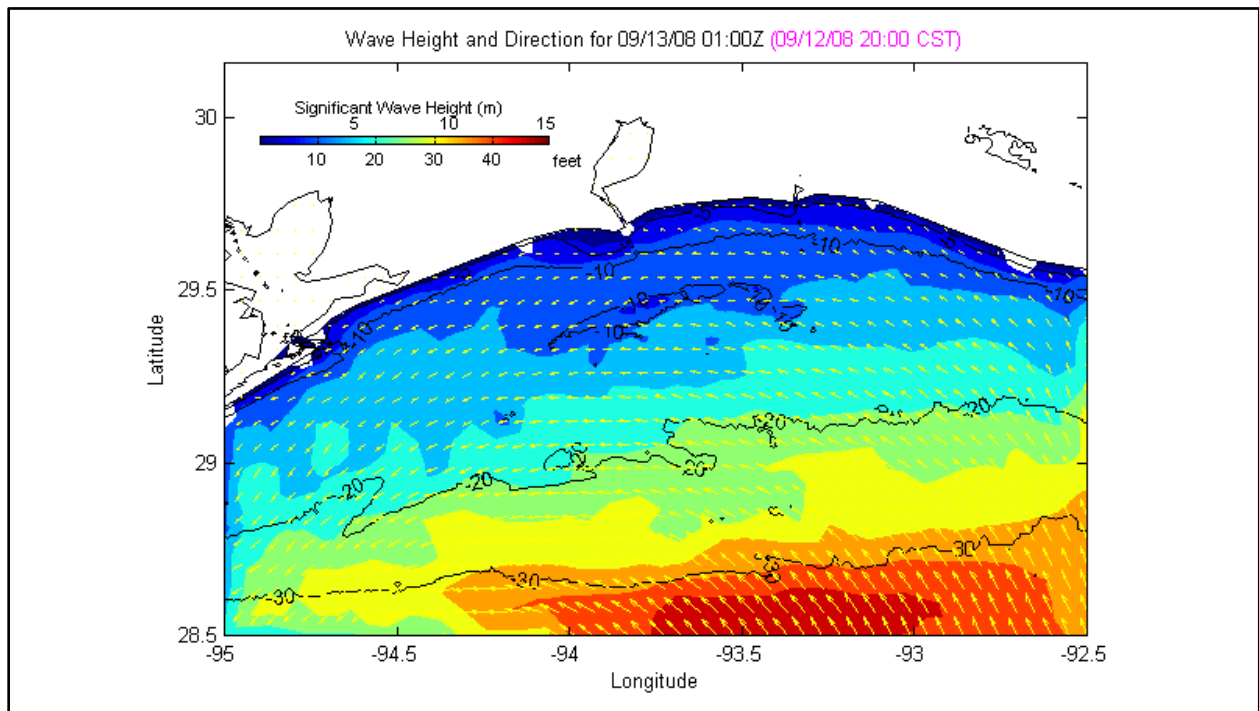
Figure 5.21   Wave field along the study area six hoursbefore the landfall of Hurricane Ike.

Bathymetry corresponds to pre-dredging scenario.

101
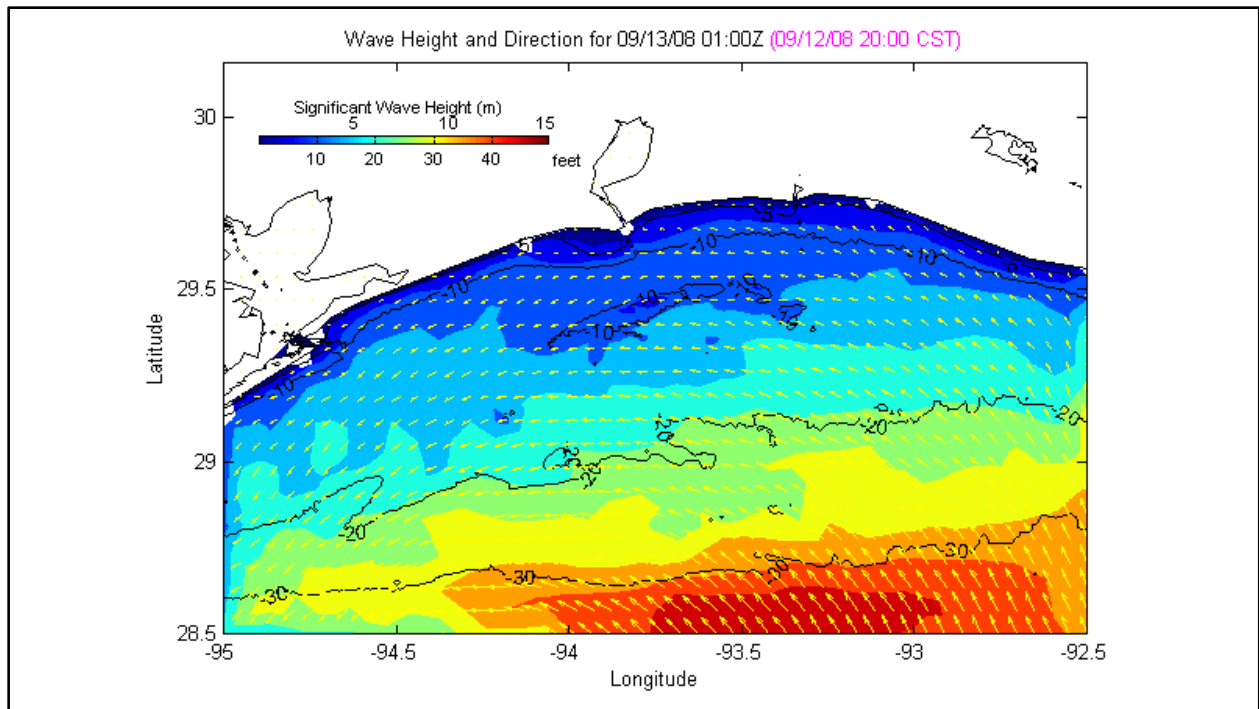
Figure 5.22   Wave fields along the study area six hours before the landfall of Hurricane Ike.

Bathymetry reflects the partial removal of crests from the western and eastern shoals.
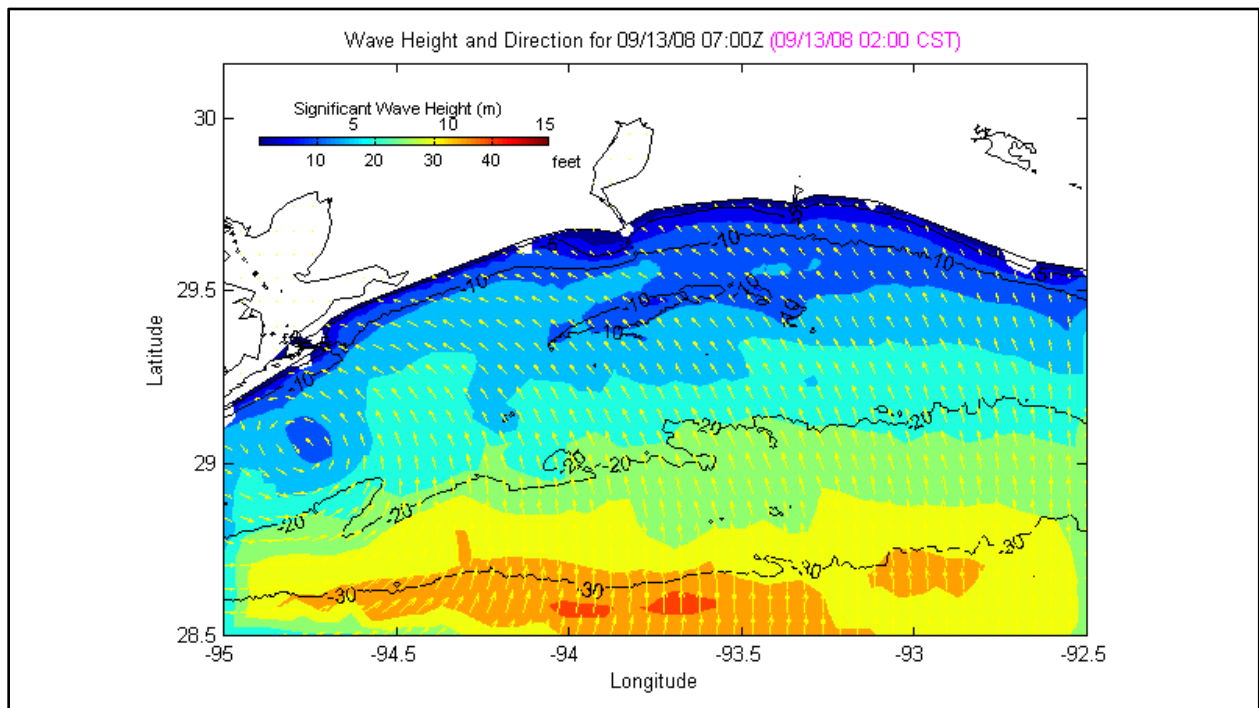
Figure 5.23   Wave field along the study area when Hurricane Ike made landfall.

Bathymetry corresponds to the pre-dredging scenario.
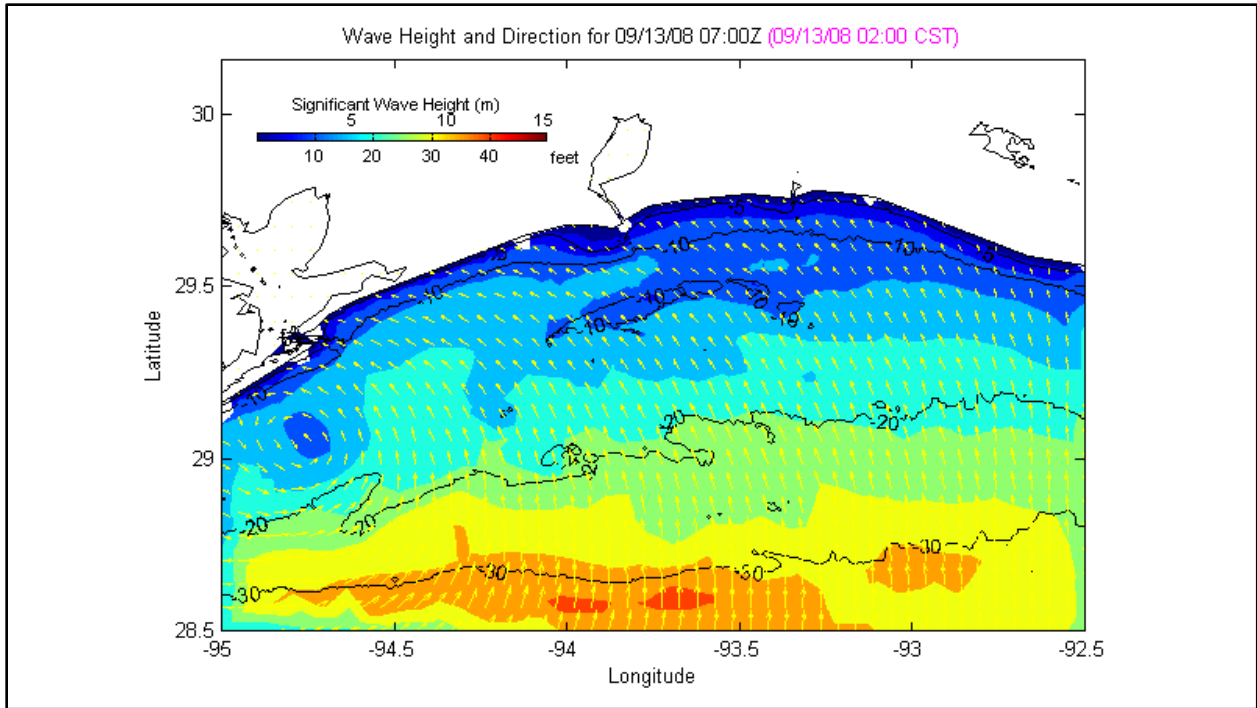
Figure 5.24   Wave field along the study area when Hurricane Ike made landfall.

Bathymetry reflects partial removal of the crests from the western and eastern shoals.
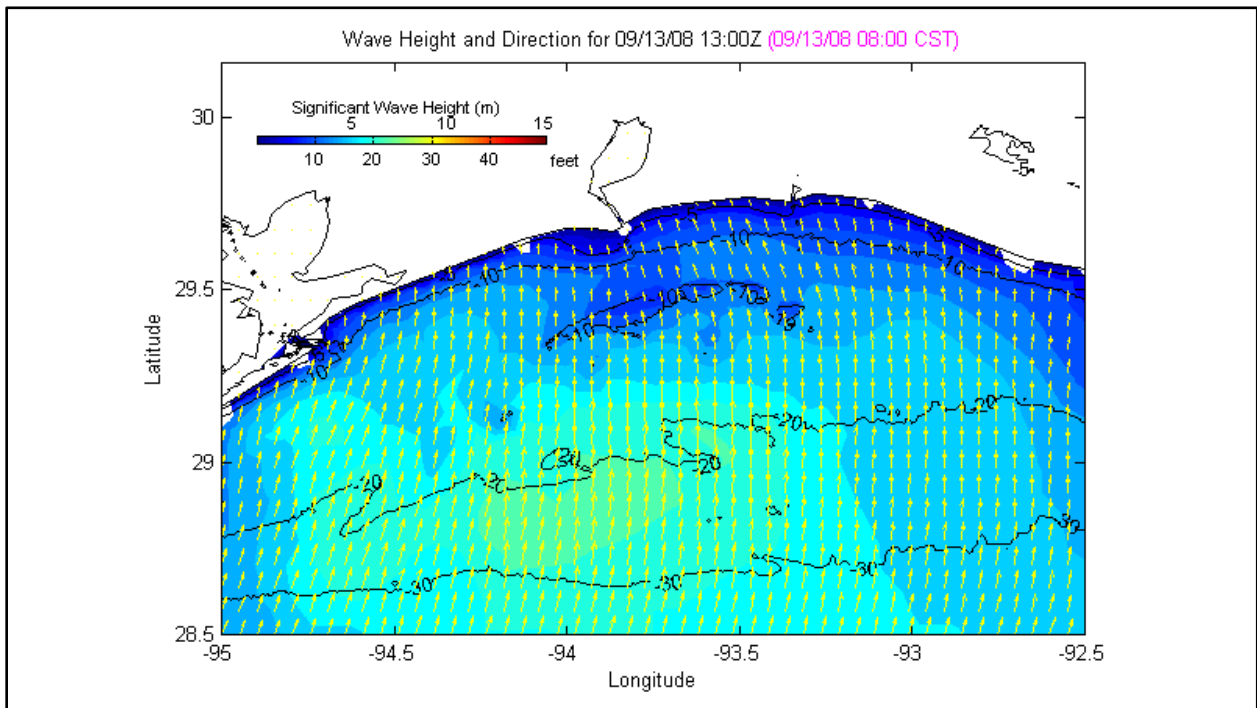
Figure 5.25   Wave field along the study area six hours after the landfall of Hurricane Ike.

Bathymetry corresponds to pre-dredging scenario.
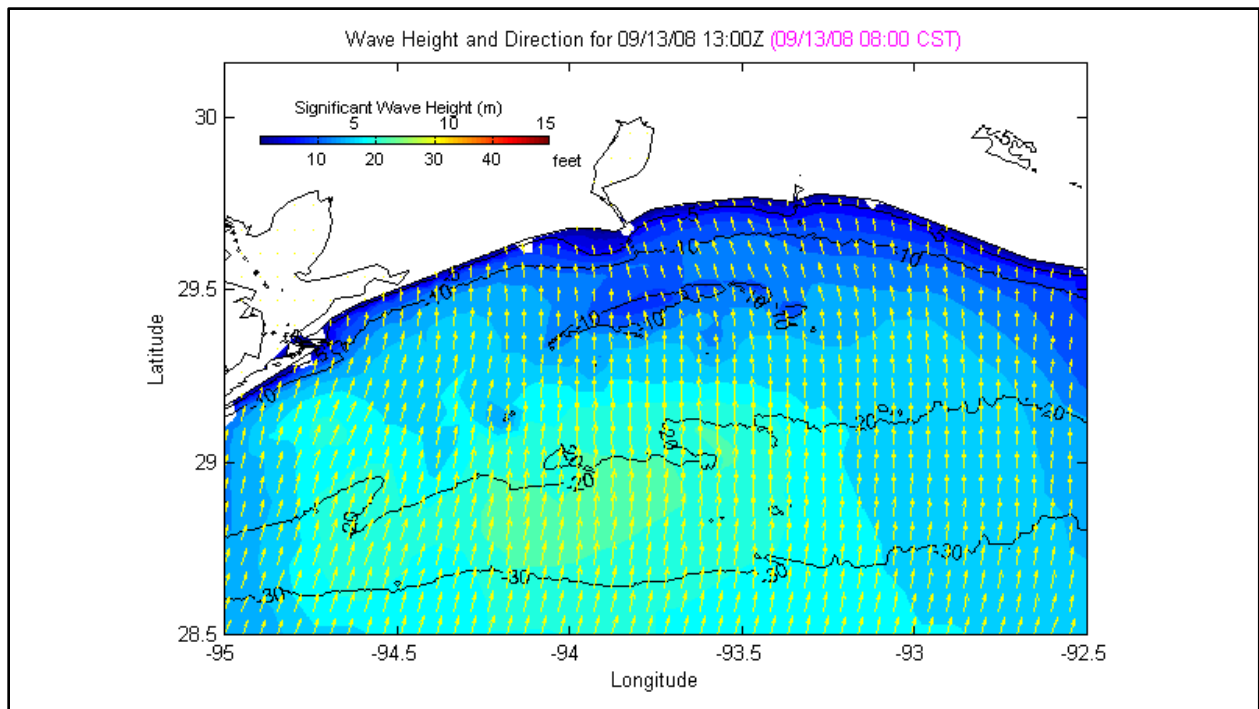
Figure 5.26   Wave fields along the study area six hours after the landfall of Hurricane Ike.

Bathymetry reflects partial removal of the crests from the west and east shoals.

To further investigate this finding, we have compared the time series of significant wave height from five locations along the coast (see Figure 5.4 for the locations). The comparison plots are given in Figures 5.27–5.31. It is observed that the variation (often time increase) in wave height is remarkably insignificant, of the order of less than 2%. Among the five stations, the highest variability is observed for the easternmost station, which in fact was not sheltered by the offshore bank. It is therefore concluded that partial removal of the crest from western and eastern shoals of Sabine Bank will not affect the coastal or inner shelf wave fields.
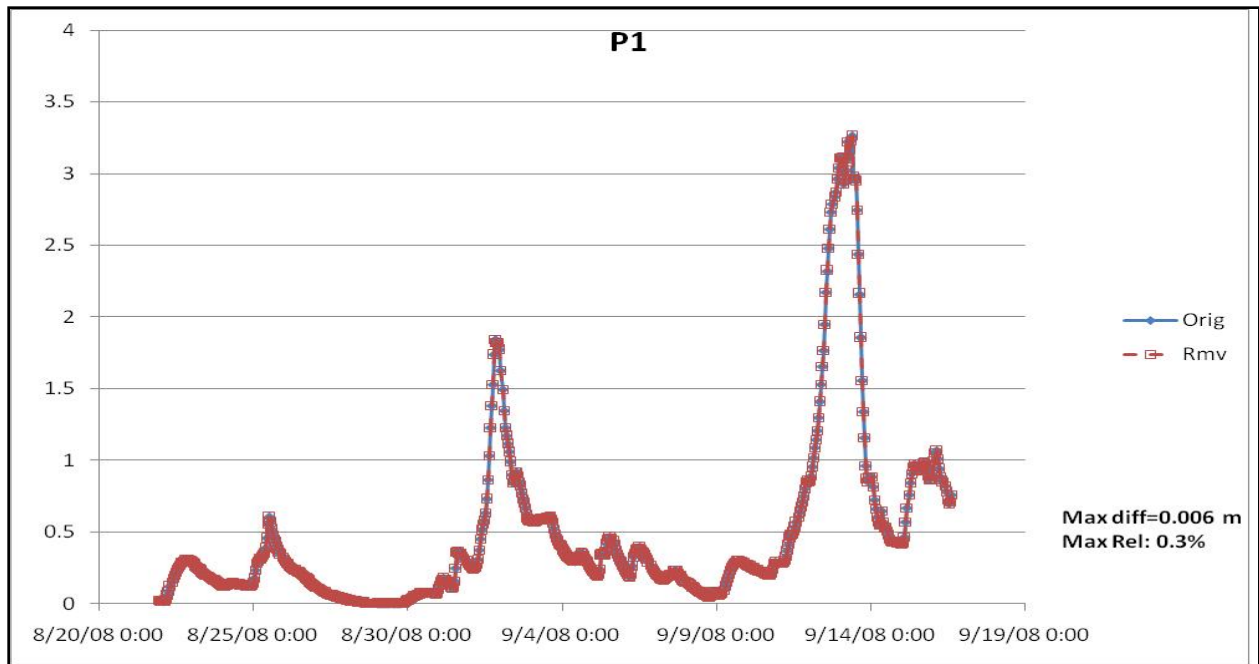
Figure 5.27   Time series plots of significant wave height from coastal station P1.

The red curve indicates pre-mining conditions and the blue curve represents partial removal of the crests from the western and eastern shoals. The highest peak in wave height corresponds to Ike and the second highest to Gustav.
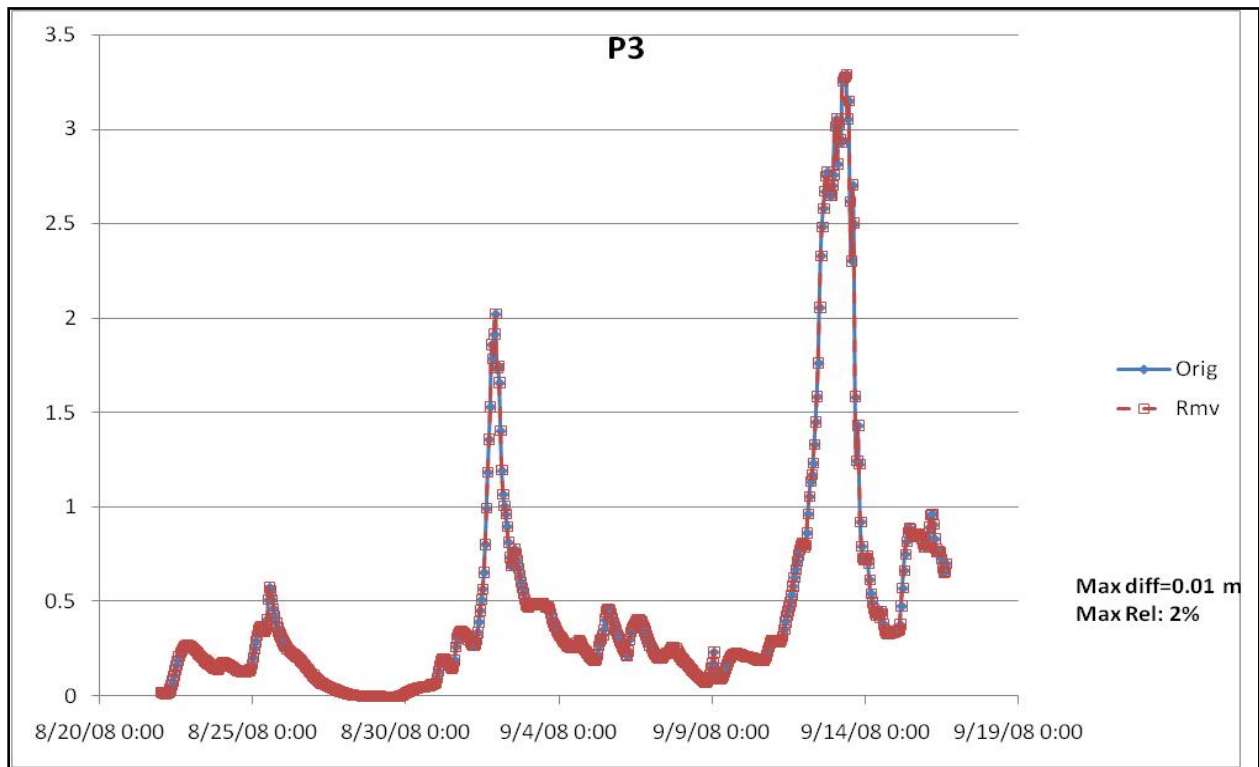
Figure 5.28   Time series plots of significant wave height from coastal station P3.

The red curve indicates pre-mining conditions and the blue curve represents partial removal of the crests from the western and eastern shoals. The highest peak in wave height corresponds to Ike and the second highest of Gustav.
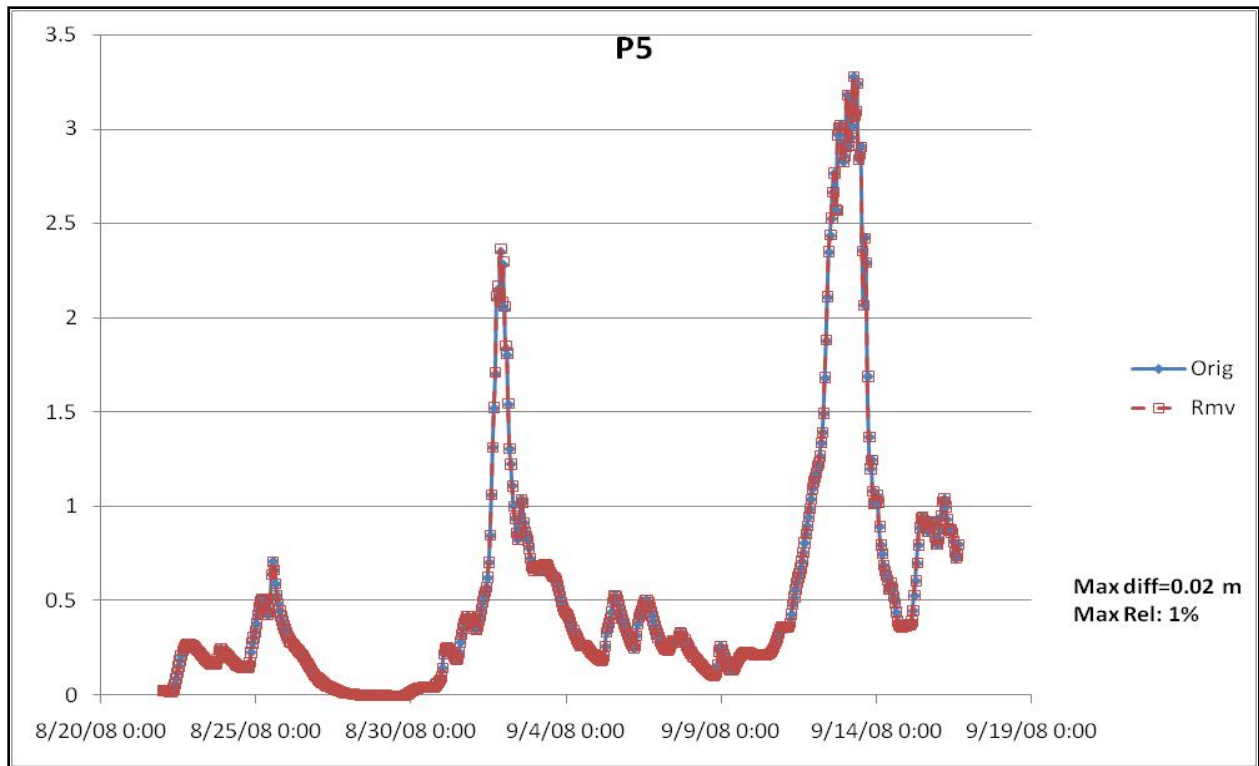
Figure 5.29   Time series plots of significant wave height from coastal station P5.

The red curve indicates pre-mining conditions and the blue curve represents partial removal of the crests from the western and eastern shoals. The highest peak in wave height corresponds to Ike and the second highest corresponds to Gustav.
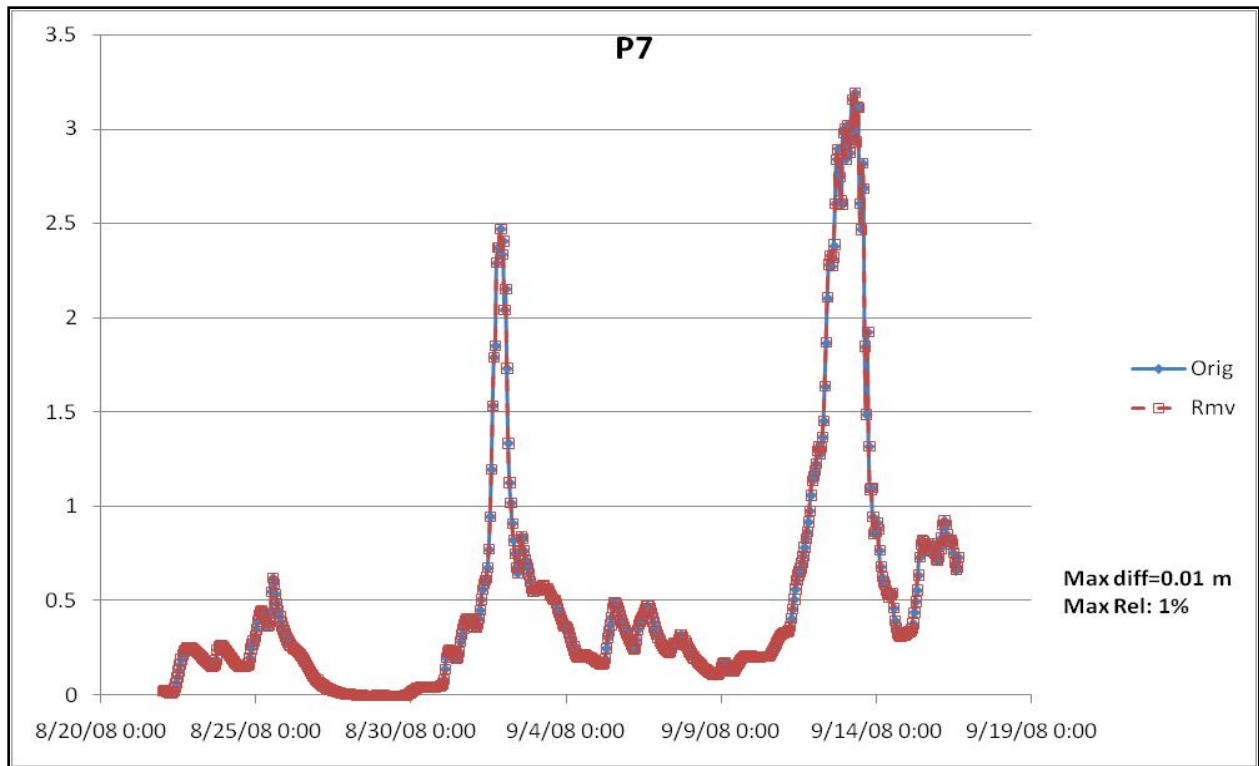
Figure 5.30   Time series plots of significant wave height from coastal station P7.

The red curve indicates pre-mining conditions and the blue curve represents partial removal of the crests from the western and eastern shoals. The highest peak in wave height corresponds to Ike and the second highest corresponds to Gustav.
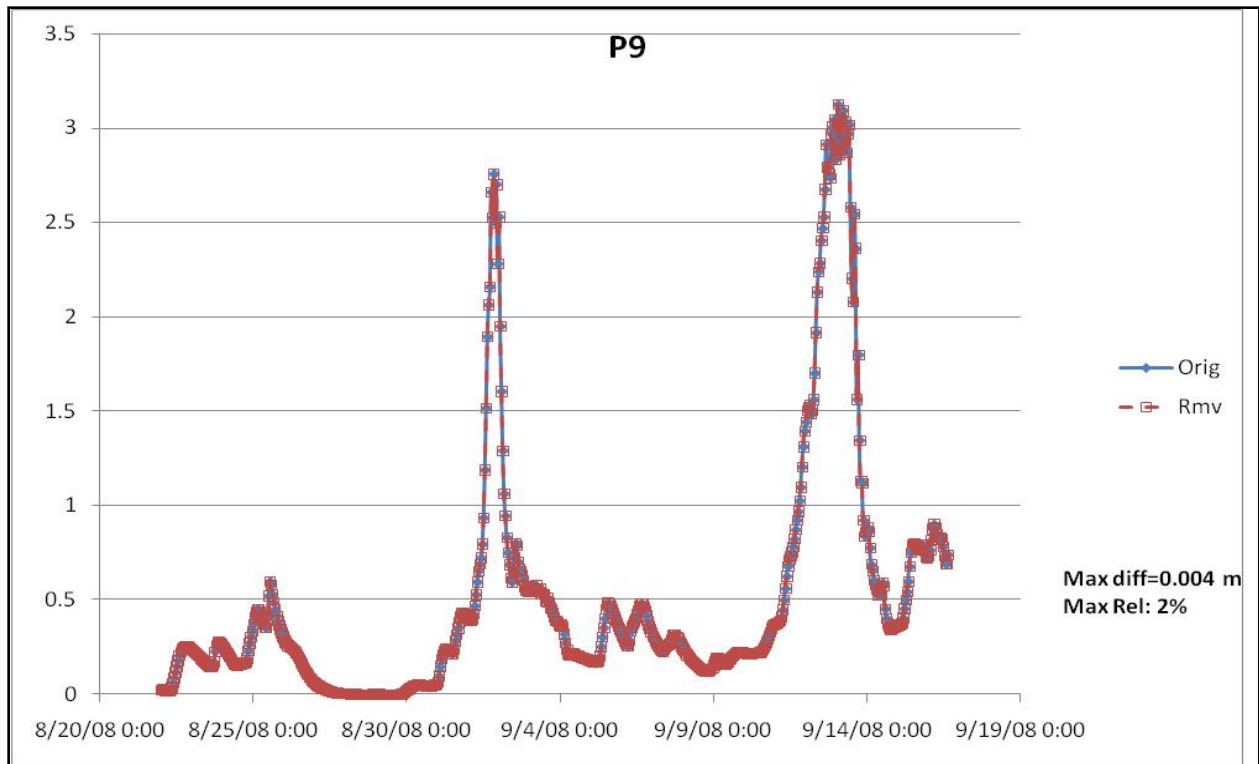
Figure 5.31   Time series plots of significant wave height from coastal station P9.

The red curve indicates pre-mining conditions and the blue curve represents partial removal of the crests from the western and eastern shoals. The highest peak in wave height corresponds to Ike and the second highest corresponds to Gustav.

CHAPTER 6: CONCLUSIONS

This study examined wave bottom interaction and bottom boundary layer dynamics for Sabine Bank. The objective this research was to evaluate the impact of targeted sand mining from the western and eastern shoals on the hydrodynamics and sediment transport characteristics of the region. Previous studies (e.g., Underwood et al. 1999) showed that Sabine Bank has an important effect on shoreward propagating waves in fair weather conditions, as well as on mitigating the wave field during storms. Based on our extensive field surveys, met-ocean data analysis, and numerical modeling studies, we present the following conclusions.

6.1. *IN SITU* OBSERVATIONS

To fully understand the wave characteristics and bottom boundary layer dynamics of Sabine Bank, three extensive field deployments were conducted during spring 2004, winter 2006, and summer 2008. The *in situ* measurements from these deployments include time series of waves, currents (horizontal and vertical), water level, suspended sediment concentration, bottom elevation change, and time series of temperature and salinity at the bottom. In addition, surface sediments were collected during the deployment and retrieval of the tripods. The computed parameters, based on *in situ* observations were wave and current-induced shear stress at the bottom, shear velocity, re-suspension intensity, and sedimentological parameters of the bottom sediments. The following conclusions were drawn based on the bottom boundary layer studies;

- Waves were weak and did not re-suspend sediment during fair weather conditions.
- Currents were sufficiently strong to re-suspend sediment during the entire period except for during fair weather conditions.
- Wave and bottom boundary layer interactions were strongly associated with the passage of cold fronts across the region. Strong southerly/southeasterly wind regimes also affected the wave and the bottom boundary layer interactions during the observation period.
- During summer 2008, bottom boundary layer dynamics were significantly influenced by the high wind regime associated with high pressure covered over the eastern Gulf and U.S. East Coast. The high wind regime, during fair weather, accompanied high wave height and relatively strong currents over the bank. Frequencies associated with this high wind regime were approximately every 2 to 3 weeks.
- During the summer, except for the periods of the high wind regime, waves and currents were weak, and therefore bottom sediment re-suspension was insignificant. The turbidity data during the 2008 summer deployment imply that bottom boundary layer dynamics may be controlled by sediment supply from outside Sabine Bank, perhaps by fluvial sediment from the Atchafalaya River or Sabine Pass.

In summary, it is evident that while waves are not an important factor for sediment transport during fair weather conditions, waves generated during cold fronts and strong southerly/southeasterly wind regimes affect sediment transport significantly. Currents are effectively strong enough to re-suspend sediment for the entire period, except during fair-weather. Therefore, it is evident that the cold fronts and strong wind regimes are important to the

bottom boundary layer dynamics of Sabine Bank. In summer, the strong wind regime seems to be a dominant force for bottom boundary layer dynamics and sediment transport.

6.2 . NUMERICAL MODELING

We have implemented a suite of state-of-the-art, third-generation, numerical models to quantify modifications in wave and sediment re-suspension parameters at Sabine Bank, associated with the proposed sand mining projects for the nourishment of beaches and barrier islands along the Louisiana and Texas coasts. The MIKE 21 Spectral Wave (SW) model and MIKE 3 Hydrodynamic models were implemented to examine the wave and current regime over the shoal and its modifications due to targeted mining. The SWAN model, coupled with WAVEWATCH III, was implemented to quantify the hurricane-generated wave fields along the Louisiana and Texas coast and its modifications due to partial removal of sand from Sabine Bank.

6.2.1. Shoal Hydrodynamics Modeling

The wave and hydrodynamic modeling studies provide the following conclusions:
- The spectral wave model (MIKE 21 SW) performed well for the study area; however the hydrodynamic model needs further calibration for the shoal environment. Inaccuracy in the shoal bathymetry may be a plausible reason for the erratic behavior of the hydrodynamic model.
- Variations in bulk wave parameters, due to modified bathymetry, two mining scenarios (cumulative and Holly Beach restoration) were not very significant.
- Sediment re-suspension intensity (RI) was high over the inner shelf and shoal during severe and strong storms. During moderate storm conditions, the RI decreases from the shallowest western flank of the shoal to the deeper eastern portion of this deposit; the RI off the shoal was significantly lower than on the shoal. The RI with partial mining was insignificantly lower than with the shoal present.

6.2.2. Hurricane Simulations

The following conclusions were drawn from the study of wave fields associated with Hurricanes Gustav and Ike:

- The shoal acts as a submerged breakwater against hurricane-generated waves and effectively protects the coast from higher energy waves that are potentially destructive and erosional to the coast. The level of energy dissipation over the shoal depends on the height and wavelength of the incoming waves. Although wind stress and regenerated waves were accounted for in the modeling domain, the dynamic effects of wind on waves landward of Sabine Bank were beyond the scope of this proposal. However, given subsequent hurricanes and their impacts as evidenced after the inception of this work, such an investigation is worthy.
- No significant modification in wave/current hydrodynamics pattern was observed when the partial removal of the shoal crests scenario was simulated. Wave fields with the complete removal of the shoal have not yet been computed. However, Kobashi et al. (in prep) conducted a similar study for Ship Shoal, with a scenario involving complete

removal of the shoal for which the alteration in the wave pattern was substantial. This approach, as stated earlier, should be conducted for future dredging on Sabine Bank.

- Variation in wave heights along the coast, due to partial removal of the shoal crests, was remarkably insignificant, of the order of less than 2%. Among the five stations selected for coastal monitoring, the highest variability was observed for the easternmost station, which, in fact, was not sheltered by the offshore bank.

6.3. OVERALL CONCLUSIONS

The data presented here allow us to conclude that large-scale sand mining (entire removal of the shoal) would significantly change hydrodynamics over the shoal, particularly waves and associated wave-induced sediment re-suspension and currents. Therefore, LARGE-SCALE dredging is not recommended. For SMALL-SCALE dredging projects, such as those which were already proposed by BOEM (then MMS), such changes were minimal. Thus, the small-scale dredging should have minimal impacts and those impacts are expected to be recovered within several years. Post-Rita side scan sonar survey by Dellapenna et al. (2006) confirmed the rapid recovery of the shoal from extreme energetic events. Depth changes were a significant factor for changes in waves and wave-induced sediment re-suspension, but did not yield abrupt changes in current distribution. More details on the hydrodynamics will be included based on the MIKE 3 model implementation. Simulation of the hurricane wave fields associated with Hurricanes Gustav and Ike also demonstrated that partial removal of the crest from western and eastern shoals of Sabine Bank would not significantly affect the coastal or inner shelf wave fields.

REFERENCES

Adams, C.E., D.J. Swift and J.M. Coleman. **1987**. Bottom currents and fluviomarine sedimentation on the Mississippi prodelta shelf: February-May 1984. Journal of Geophysical Research 92(C.13):14595-14609.

Andersen, O.B. **1995**. Global ocean tide from ESR-1 and TOPEX/POSEIDON altimetry. Journal of Geophysical Research 100(C12):25249-25259.

Anderson, J. and J.S. Wellner. **2002**. Evaluation of Beach Nourishment Sand Resources along the East Texas Coast. Unpublished manuscript. Available at <http://gulf.rice.edu/coastal/>.

Brooks, R.A., T. Dellapenna, A. Quaid and K.J. Sulak. **2004**. Assessment of fish communities associated with offshore sand banks and shoals in the northwestern Gulf of Mexico. Interim report submitted to United States Geological Survey. 6 pp.

Brooks, R.A. and A. Quaid. **2003**. Assessment of fish communities associated with offshore sand banks and shoals in the northwestern Gulf of Mexico. USGS Cruise Sabine 2003-01 Report submitted to Minerals Management Service. 20 pp.

Byrnes, M.R., R.M. Hammer, B.A. Vittor, S.W. Kelley, D.B. Snyder, J.M. Cote , J.S. Ramsey, T.D. Thibaut, N.W. Phillips and J.D. Wood. **2003**. Collection of Environmental Data Within Sand Resource Areas Offshore North Carolina and the Implications of Sand Removal for Coastal and Beach Restoration. U.S. Department of the Interior, Minerals Management Service, Leasing Division, Sand and Gravel Unit, Herndon, VA. OCS Report MMS 2000-056. Volume I: Main Text 257 pp, Volume II: Appendices 70 pp.

Byrnes, M.R., R.M. Hammer, B.A. Vittor, J.S. Ramsey, D.B. Snyder, K.F. Bosma, J.D. Wood, T.D. Thibaut and N.W. Phillips. **1999**. Environmental Survey of Identified Sand Resource Areas Offshore Alabama: Volume I: Main Text, Volume II: Appendices. U.S. Department of Interior, Minerals Management Service, International Activities and Marine Minerals Division (INTERMAR), Herndon, VA. OCS Report MMS 99-0052. 326 pp. + 132 pp. appendices pp.

Chan, A.W. and M.D. Zoback. **2007**. The role of hydrocarbon production on land subsidence and fault reactivation in the Louisiana coastal zone. Journal of Coastal Research 23(3):771-786. doi: Doi 10.2112/05-0553.

Cochrane, J.D. and F.J. Kelly. **1986**. Low-Frequency Circulation on the Texas-Louisiana Continental-Shelf. Journal of Geophysical Research 91(C9):10645-10659.

Condrey, R. and C. Gelpi. **2008**. Blue crab use of the Ship/Trinity/Tiger shoal complex as a nationally important spawning/hatching/foraging ground: Discovery, evaluation, and sand mining recommendations. Final report submitted to U.S. Minerals Management Service. 34 pp.

Crout, R.L. and R.D. Hamiter. **1981**. Response of Bottom Waters on West Louisiana Shelf to Transient Wind Events and Resulting Sediment Transport. Proceedings of Transaction, Gulf Coast Association of Geological Societies. Pp 273-278.

Dalrymple, R.A. and J.T. Kirby. **1991**. REFDIF 1 Version 2.3. Documentation Manual. Report No. CACR 91-2. Center for Applied Coastal Research, Deptartment of Civil Engineering, University of Delaware, Newark. 19 pp.

Dean, R.G. and R.A. Dalrymple. **2000**. Water wave Mechanics for Engineers and Scientists, Advanced Series on Ocean Engineering, Vol. 2, World Scientific. 353 pp.

Dellapenna, T.M., S. Hiller, B. Fielder, E. Majzlik and C.J. Noll, Jr. **2006**. Sabine Bank side scan investigation. Report submitted to USGS. 27 pp.

DHI. **2005**. MIKE21&3 Flow Model FM. Hydrodynamics and Transport Module, Scientific Documentation. 42 pp.

Drake, D.E. and D.A. Cacchione. **1992**. Wave Current Interaction in the Bottom Boundary-Layer during Storm and Nonstorm Conditions - Observations and Model Predictions. Continental Shelf Research 12(12):1331-1352.

Drucker, B.S., W. Waskes and M.R. Byrnes. **2004**. The US Minerals Management Service Outer Continental Shelf Sand and Gravel program: Environmental studies to assess the potential effects of offshore dredging operations in federal waters. Journal of Coastal Research 20(1):1-5.

Earle, M.D. **1996**. Nondirectional and Directional Wave Data Analysis Procedures. NDBC Technical Document 96-01, National Data Buoy Center, NOAA. 37 pp.

Friedrichs, C.T., L.D. Wright, D.A. Hepworth and S.C. Kim. **2000**. Bottom-boundary-layer processes associated with fine sediment accumulation in coastal seas and bays. Continental Shelf Research 20(7):807-841.

Georgiou, I.Y., D.M. Fitzgerald and G.W. Stone. **2004**. Louisiana coastal area, Ecosystem restoration study, Appendix D. Louisiana Gulf shoreline restoration report, Louisiana Department of Natural Resources. 13-40 pp.

Georgiou, I.Y., D.M. FitzGerald and G.W. Stone. **2005**. The impact of physical processes along the Louisiana coast. Journal of Coastal Research 44:72-89.

Grant, W.D. and O.S. Madsen. **1986**. The Continental-Shelf Bottom Boundary-Layer. Annual Review of Fluid Mechanics 18:265-305.

Green, M.O. **1992**. Spectral Estimates of Bed Shear-Stress at Subcritical Reynolds-Numbers in a Tidal Boundary-Layer. Journal of Physical Oceanography 22(8):903-917.

Guinasso, N.L.J., J. Yip, R.O. Reid, L.C. Bender, III., M. Howard, L.L. Lee, III., J.N. Walpert, D.A. Brooks, R.D. Hetland and R.D. Martin. **2001**. Observing and forecasting coastal currents: Texas automated buoy system (TABS). Oceans 2001, Vol. 2. 1318-1322 pp.

Harper, D.E., L.D. McKinney, R.R. Salzar and R.J. Case. **1981**. The occurance of hypoxic bottom water off the upper Texas coast and its effect on the benthic biota. Contributions in Marine Science 24:53-79.

Hasselmann, K. **1974**. On the spectral dissipation of ocean waves due to whitecapping. Boundary-Layer Meteorology 6(1-2):107-127.

Hasselmann, S. and K. Hasselmann. **1985**. Computations and Parameterizations of the Nonlinear Energy-Transfer in a Gravity-Wave Spectrum .1. A New Method for Efficient Computations of the Exact Nonlinear Transfer Integral. Journal of Physical Oceanography 15(11):1369-1377.

Horikawa, K., T. Sasaki and H. Sakuramota. 1977**.** Mathematical and laboratory models of shoreline changes due to dredged holes. Journal of Faculty of Engineering, the University of Tokyo, Japan XXXIV(1):47-57.

Hsu, S.A. **1988**. Coastal Meteorology. San Diego: Academic Press. 260 pp.

Hunt, J.N. **1979**. Direct Solution of Wave Dispersion-Equation. Journal of the Waterway Port Coastal and Ocean Division-Asce 105(4):457-459.

Janssen, P.A.E.M. **1989**. Wave-Induced Stress and the Drag of Air-Flow over Sea Waves. Journal of Physical Oceanography 19(6):745-754.

Janssen, P.A.E.M. **1991**. Quasi-linear theory of wind-wave generation applied to wave forecasting. Journal of Physical Oceanography 21:1631-1642.

Johnson, H.K., T.V. Karambas, I. Avgeris, B. Zanuttigh, D. Gonzalez-Marco and I. Caceres. **2005**. Modelling of waves and currents around submerged breakwaters. Coastal Engineering 52(10-11):949-969. doi: DOI 10.1016/j.coastaleng.2005.09.011.

Jose, F., D. Kobashi and G.W. Stone. **2007**. Spectral wave transformation over an elongated sand shoal off south central Louisiana, USA. Journal of Coastal Research SI 50:757-761.

Jose, F. and G.W. Stone. **2006**. Forecast of nearshore wave parameters using MIKE 21 spectral wave model. Transactions, Gulf Coast Association of Geological Societies 56:323-327.

Keim, B.D., R.A. Muller and G.W. Stone. **2007**. Spatiotemporal patterns and return periods of tropical storm and hurricane strikes from Texas to Maine. Journal of Climate 20:3498-3508.

Kelley, S.W., J.S. Ramsey and M.R. Byrnes. **2004**. Evaluating shoreline response to Offshore Sand mining for beach nourishment. Journal of Coastal Research 20(1):89-100.

Khalil, S.M., C. Finkl, J. Andrew and C.P. Knotts. **2007**. Restoration-quality sand from Ship Shoal, Louisiana: Geotechnical investigation for sand on a drowned barrier island. Proceedings of Coastal Sediments '07. New Orleans, Louisiana. Pp 685-698.

Kim, S.C., C.T. Friedrichs, J.P.Y. Maa and L.D. Wright. **2000**. Estimating bottom stress in tidal boundary layer from Acoustic Doppler Velocimeter data. Journal of Hydraulic Engineering 126(6):399-406.

Kjerfve, B. **2003**. Book Review of "Muddy Coast Dynamics and Resource Management". EOS Transactions of the American Geophysical Union 84(22):99.

Kobashi, D., F. Jose, Y. Luo and G.W. Stone. **2009a**. Wind-driven dispersal of fluvial fine sediments for two contrasting storms: extra-tropical and tropical storms, Atchafalaya Bay-Shelf, Louisiana. Marine Geology:In Review.

Kobashi, D., F. Jose and G.W. Stone. **2005**. Hydrodynamics and sedimentary responses within bottom boundary layer: Sabine Bank, western Louisiana. Transaction, Gulf Coast Association of Geological Societies 55:392-399.

Kobashi, D., F. Jose and G.W. Stone. **2007a.** Heterogeneity and dynamics of sediments on a shoal during spring-winter storm season, south-central Louisiana, USA. Proceedings of Coastal Sediments '07. Pp 921-934.

Kobashi, D., F. Jose and G.W. Stone. **2007b**. Impacts of fluvial fine sediments and winter storms on a transgressive shoal, off south-central Louisiana, U.S.A. Journal of Coastal Research SI 50:858-862.

Kobashi, D. and G.W. Stone. **2008a**. Two contrasting morpho-hydrodynamics over recurring sandy and muddy bottoms of a shore-parallel Holocene transgressive shoal, south-central Louisiana, USA. Continental Shelf Research In Review

Kobashi, D. and G.W. Stone. **2008b**. Variability of Surface Water Level and Current Profiles associated with Varying Storm Winds over the Louisiana Inner Shelf and a Holocene Transgressive Shoal, Louisiana, USA: In-Situ Observations and Numerical Model Analyses. In Preparation

Kobashi, D., G.W. Stone, S.M. Khalil and D.R. Kerper. **2009b**. Impacts of sand removal from a shore-parallel Holocene transgressive shoal on hydrodynamics and sediment transport, south-central Louisiana, USA. In Preparation

Komar, P.D. **1976**. The transport of cohesive sediments on continental shelves. In: Stanley, D.J. and D.J.P. Swift, eds. Marine Sediment Transport and Environmental Management. New York: Wiley. Pp 107-125.

Komen, G.J., L. Cavaleri, M. Donelan, K. Hasselmann, S. Hasselmann and P.A.E.M. Janssen. **1994**. Dynamics and Modelling of Ocean Waves. Cambridge: Cambridge University Press. 532 pp.

Komen, G.J., S. Hasselmann and K. Hasselmann. **1984**. On the Existence of a Fully-Developed Wind-Sea Spectrum. Journal of Physical Oceanography 14(8):1271-1285.

Kraus, N.C., K.J. Gingerich and J.D. Rosati. **1988**. Toward an improved empirical formula for longshore sand transport. Proceedings of 21st Coastal Engineering Conference, American Society of Civil Engineers. Pp 1183-1196.

Lacy, J.R. and C.R. Sherwood. **2004**. Accuracy of a pulse-coherent acoustic Doppler profiler in a wave-dominated flow. Journal of Atmospheric and Oceanic Technology 21(9):1448-1461.

Lhermitte, R. and R. Serafin. **1984**. Pulse-to-Pulse Coherent Doppler Sonar Signal Processing Techniques. Journal of Atmospheric and Oceanic Technology 1(4):293-308.

Li, M.Z., C.L. Amos and D.E. Heffler. **1997**. Boundary layer dynamics and sediment transport under storm and non-storm conditions on the Scotian Shelf. Marine Geology 141:157-181.

Liu, H.Q., L. Xie, L.J. Pietrafesa and S.W. Bao. **2007**. Sensitivity of wind waves to hurricane wind characteristics. Ocean Modelling 18(1):37-52. doi: DOI 10.1016/j.ocemod.2007.03.004.

Maa, J.P.Y., C.H. Hobbs, S.C. Kim and E. Wei. **2004**. Potential impacts of sand mining offshore of Maryland and Delaware: Part I - Impacts on physical oceanographic processes. Journal of Coastal Research 20(1):44-60.

Madsen, O.S. **1976**. Wave climate of the continental margin: Elements of its mathematical description. In: Stanley, D.J. and D.J. Swift, eds. Marine Sediment Transport and Environmental Management. New York: Wiley. Pp 65-87.

Mesinger, F., G. DiMego, E. Kalnay, K. Mitchell, P.C. Shafran, W. Ebisuzaki, D. Jovic, J. Woollen, E. Rogers, E.H. Berbery, M.B. Ek, Y. Fan, R. Grumbine, W. Higgins, H. Li, Y. Lin, G. Manikin, D. Parrish and W. Shi. **2006**. North American regional reanalysis. Bulletin of the American Meteorological Society 87(3):343-360. doi: Doi 10.1175/Bams-87-3-343.

Michel, J., R. Nairn, J.A. Johnson and D. Hardin. **2001**. Development and design of biological and physical monitoring protocols to evaluate the long-term impacts of offshore dredging operations on the marine environment. U.S. Department of Interior, Minerals Management Service. OCS Study MMS 2001-089. 116 pp.

Morton, R.A. and J.C. Gibeaut. **1995**. Physical and environmental assessment of sand resources, Sabine and Heald Bank, Second Phase 1994-1995. Final Report prepared for United States Department of Interior, Mineral Management Service. 244 pp.

National Research Council. **2006**. Driving Louisiana's New Map, Addressing Land Loss in Coastal Louisiana. Washington, DC: National Academies Press. 190 pp.

Nielsen, P. **1979**. Some basic concepts of wave sediment transport. Series paper 20 Institute of Hydrodynamics and Hydraulic Engineering, Technical University of Denmark. 160 pp.

NOAA. **2004**. Meteorological Data at SRST2 station, National Data Buoy Center. Available at http://www.ndbc.noaa.gov/index.shtml.

O'Connel, M.T., C.D. Franze, E.A. Spalding and M.A. Poirrier. **2005**. Biological resources of the Louisiana coast: part 2. Coastal animal and habitat associations. Journal of Coastal Research SI 44:146-161.

Penland, S., R. Boyd and J.R. Suter. **1988**. Transgressive depositional systems of the Mississippi delta plain: A model for barrier shoreline and shelf sand development. Journal of Sedimentary Petrology 58(6):932-949.

Penland, S., P.F. Connor, A. Beall, S. Fearnley and S.J. Williams. **2005**. Changes in Louisiana's shoreline: 1855-2002. Journal of Coastal Research 44:7-39.

Pepper, D.A. **2000**. Hydrodyanmics, Bottom Boundary layer processes and sediment transport on the south-central Louisiana inner shelf: The influence of extra-tropical storms and bathymetric modification. Ph.D. Dissertation. Louisiana State University, Baton Rouge, LA. 159 pp.

Pepper, D.A. and G.W. Stone. **2002**. Atmospheric forcing of fine-sand transport on a low-energy inner shelf: south-central Louisiana, USA. Geo-Marine Letters 22(1):33-41. doi: DOI 10.1007/s00367-002-0094-x.

Pepper, D.A. and G.W. Stone. **2004**. Hydrodynamic and sedimentary responses to two contrasting winter storms on the inner shelf of the northern Gulf of Mexico. Marine Geology 210(1-4):43-62. doi: DOI 10.1016/j.margeo.2004.05.004.

Rabalais, N.N., R.E. Turner and D. Scavia. **2002**. Beyond science into policy: Gulf of Mexico hypoxia and the Mississippi River. Bioscience 52(2):129-142.

Roberts, H.H. **1997**. Dynamic changes of the holocene Mississippi River delta plain—the delta cycle. Journal of Coastal Research 13:605-627.

Roberts, H.H., O.K. Huh, S.A. Hsu, L.J. Rouse and D.A. Rickman. **1989**. Winter storm impacts on the Chenier Plain coast of southwestern Louisiana. Gulf Coast Association of Geological Societies Transactions 34:515-522.

Rodriguez, A.B., J.B. Anderson, F.P. Siringan and M. Taviani. **1999**. Sedimentary facies and genesis of Holocene sand banks of the east Texas inner continental shelf. In: Snedden, J. and K. Bergman, eds. Isolated Shallow Marine Sand Bodies: Sequence Stratigraphic Analysis and Sedimentological Interpretation. SEPM Special Publication 64. Pp 165-178.

Sarkar, R.K.A., V.K. Aggarwal, V. Bhatt, P.K. Bhaskaran and S.K. Dube. **2000**. Ocean wave model- sensitivity experiments. Proceedings of International Conference PORSEC-2000 NIO. Goa, India. Vol. II, Pp 621-627.

Sheremet, A. and G.W. Stone. **2003**. Observations of nearshore wave dissipation over muddy sea beds. Journal of Geophysical Research-Oceans 108(C11):3357. doi: 10.1029/2003JC001885, 2003.

Smith, J.M., A.R. Sherlock and D.T. Resio. **2001**. STWAVE: Steady-state spectral wave model. User's manual for STWAVE, version 3.0. ERDC/CHL SR-01-1. Coastal and Hydraulic Laboratory, US Army Corps of Engineers. 81 pp.

Snedden, J.W. and R.W. Dalrymple. **1999**. Modern shelf sand ridges: From historical perspective to unified hydrodynamic and evolutionary model. SEPM Special Publication 64. Pp 13-28.

Snyder, R.L., F.W. Dobson, J.A. Elliott and R.B. Long. **1981**. Array Measurements of Atmospheric-Pressure Fluctuations above Surface Gravity-Waves. Journal of Fluid Mechanics 102(Jan):1-59.

SonTek Inc. **1996**. Acoustic Doppler velocimter principles of operation. SonTek Technical Notes, San Diego, California. 15 pp.

SonTek Inc. **1997a**. Pulse-coherent Doppler processing and the ADV correlation coefficient. SonTek Technical Notes.San Diego, CA. 5 pp.

SonTek Inc. **1997b**. SonTek Doppler Current Meters – Using Signal Strength Data to monitor Suspended Sediment Concentration. SonTek Application Notes.San Diego, California. 7 pp.

SonTek Inc. **2004**. PC-ADP - Read Me First! SonTek PC-ADP manual, San Diego, California. 28 pp.

Sorensen, O.R., H. Kofoed-Hansen, M. Rugbjerg and L.S. Sorensen. **2004**. A third-generation spectral wave model using an unstructured finite volume technique. Proceedings of International Conference on Coastal Engineering 29. Pp 894-906.

Spaziani, A.L., Jose, F. and Stone, G.W. **2009**. Sediment dynamics on an innershelf shoal during storm events in the northeastern Gulf of Mexico. Journal of Coastal Research Submitted

Sternberg, R.W. **1972**. Predicting Initial Motion and Bedload Transport of sediment particles in the shallow marine environment. In: Swift, D.J.P., D.B. Duane and O.H. Pilkey, eds. Shelf sediment transport: Process and Pattern. Stroudsburg, PA: Dowden, Hutchinson, and Ross, Inc. Pp 61-82.

Stone, G.W. **2000**. Wave climate and bottom boundary layer dynamics with implications for offshore sand mining and barrier island replenishment in south-central Louisiana. U.S. Dept. of the Interior, Minerals Management Service, Gulf of Mexico OCS Region, New Orleans, LA. OCS Study MMS 2000-53. 90 pp.

Stone, G.W., R. Condrey and J. Fleeger. **2009**. Environmental investigation of the long-term use of Ship Shoal sand resources for large-scale beach and coastal restoration in Louisiana. Report in preparation for U.S. Dept. of the Interior, Minerals Management Service, Gulf of Mexico OCS Region, New Orleans, LA.

Stone, G.W., D. Kobashi and F. Jose. **2005**. Sabine Bank field survey report. 25 pp.

Stone, G.W., B.Z. Liu, D.A. Pepper and P. Wang. **2004**. The importance of extratropical and tropical cyclones on the short-term evolution of barrier islands along the northern Gulf of Mexico, USA. Marine Geology 210(1-4):63-78. doi: DOI 10.1016/j.mangeo.2004.05.021.

Stone, G.W. and J.P. Xu. **1996**. Wave climate modeling and evaluation relative to sand mining on Ship Shoal, offshore Louisiana, for coastal and barrier island restoration. U.S. Dept. of the Interior, Minerals Management Service, Gulf of Mexico OCS Region, New Orleans, LA. OCS Study MMS 96-0059. 170 pp.

Stone, G.W., X. Zhang, J. Li and A. Sheremet. **2003**. Coastal Observing Systems: Key to the future of coastal dynamics investigation. GCAGS/GCSSEPM Transactions 53:783-799.

Stone, G.W., X.P. Zhang, W. Gibson and R. Frederichs. **2001**. A new wave-current online information system for oil spill contigency planning (WAVCIS). Proceedings of 24th Arctic and Marine Oil spill Program Technical Seminar. Edmonton, Alberta, CANADA. Pp 401-425.

Swift, D.J.P. **1985**. Response of the shelf floor to flow. In: Tillman, R.W., D.J.P. Swift and R.G. Wlaker, eds. Shelf Sands and Sandstone Reservoirs. SEPM Short Course Notes 13. Pp 135-241.

Tolman, H.L. and D. Chalikov. **1996**. Source terms in a third-generation wind wave model. Journal of Physical Oceanography 26(11):2497-2518.

Underwood, S.A., R. Chen, G.W. Stone, X.P. Zhang, M.R. Byrnes and R.A. McBride. **1999**. Beach response to a segmented breakwater system, southwest Louisiana, USA. Proceedings of Coastal Sediments' 99. Pp 2042-2056.

U.S. Geological Survey. **1995**. Louisiana coastal wetlands: A resource at risk. Fact sheet. Available at http://marine.usgs.gov/fact-sheets/LAwetlands/lawetlands.html.

Voulgaris, G. and J.H. Trowbridge. **1997**. Evaluation of the Acoustic Doppler Velocimeter (ADV) for turbulence measurements. Journal of Atmospheric and Oceanic Technology 15:272-289.

Walker, N.D. and A.B. Hammack. **2000**. Impacts of Winter Storms on Circulation and Sediment Transport: Atchafalaya-Vermilion Bay Region, Louisiana, U.S.A. Journal of Coastal Research 16(4):996-1010.

Walker, N.D., R. Jarosz and S.P. Murray. **2001**. An investigation of pressure and pressure gradients along the Louisiana/Texas inner shelf and their relationships to wind forcing and current variability. U.S. Dept. of the Interior, Minerals Management Service, Gulf of Mexico OCS region, New Orleans, LA. OCS Study MMS2001-057. 40 pp.

Wang, D.W., D.A. Mitchell, W.J. Teague, E. Jarosz and M.S. Hulbert. **2005**. Extreme waves under Hurricane Ivan. Science 309(5736):896-896. doi: DOI 10.1126/science.1112509.

Wells, J.T. and P. Kemp. **1981**. Atchafalaya mud stream and recent mudflat progradation: Louisiana chenier plain. Transaction, Gulf Coast Association of Geological Society 31:409-416.

Wright, L.D., C.R. Sherwood and R.W. Sternberg. **1997**. Field measurements of fairweather bottom boundary layer processes and sediment suspension on the Louisiana inner continental shelf. Marine Geology 140(3-4):329-345.

The Department of the Interior Mission

As the Nation's principal conservation agency, the Department of the Interior has responsibility for most of our nationally owned public lands and natural resources. This includes fostering sound use of our land and water resources; protecting our fish, wildlife, and biological diversity; preserving the environmental and cultural values of our national parks and historical places; and providing for the enjoyment of life through outdoor recreation. The Department assesses our energy and mineral resources and works to ensure that their development is in the best interests of all our people by encouraging stewardship and citizen participation in their care. The Department also has a major responsibility for American Indian reservation communities and for people who live in island territories under US administration.

The Bureau of Ocean Energy Management

The Bureau of Ocean Energy (BOEM) promotes energy independence, environmental protection, and economic development through responsible, science-based management of offshore conventional and renewable energy resources.

The BOEM Environmental Studies Program

The mission of the Environmental Studies Program (ESP) is to provide the information needed to predict, assess, and manage impacts from offshore energy and marine mineral exploration, development, and production activities on human, marine, and coastal environments.